Universiteit Utrecht

Study on the preparation of Highly Active and Stable Cobalt on Carbon Nanotubes Catalysts for the Fischer-Tropsch reaction

Thesis for the degree of

Master in Science
Nanomaterials: Chemistry & Physics

René Manchester
Utrecht, November 2012
Supervisors: Krijn de Jong and Thomas Eschemann
Debye Institute for Nanomaterials Science – Inorganic Chemistry and Catalysis
Utrecht University

Contents

Chapter One
Introduction

The Fischer-Tropsch synthesis is the heterogeneously catalysed conversion of synthesis gas - a mixture of carbon monoxide (CO) and hydrogen (H_2) - into hydrocarbon chains.[1] Synthesis gas is mainly produced from methane, coal or biomass.

History and drivers

In the beginning of the 20th century the first experiments on the catalytic hydrogenation of carbon monoxide were carried out. Sabatier and Senderens described the conversion of carbon monoxide and carbon dioxide over nickel catalysts[2] and within decades after this discovery the production of e.g. ammonia and methanol were invented and commercialised. Mittasch and Schneider were the first to patent the synthesis of liquid hydrocarbons by the conversion of mixtures of carbon monoxide and hydrogen in the presence of supported metal heterogeneous catalysts. They e.g. report supported cobalt oxide.[3,4,5] But it was until 1923 that Hans Fischer and Franz Tropsch reported the Synthol process: carbon monoxide and hydrogen reacted with alkalized iron chips which gave a mixture of aliphatic oxygenated compounds.[6,7,8,9,10]

In the preparations for World War II Germany was producing synthetic fuels and lubricants on a large scale. These synthetic oil products were mainly produced from coal and to a small extent from other raw materials. By September 1939 the production of synthetic oil products reached an annual rate of 2.3 million tons, which was ~ 30% of its total production and imports of oil products and liquid fuels. From the latter figure, 1.3 million tons were produced from hydrogenation processes and 0.2 million by the Fischer-Tropsch (FT) synthesis. The remainder was produced by coal tar distillation and carbonization, and of benzol for admixtures with gasoline.[11] The production of synthetic oil products could be used to ensure Germany of a supply of liquid fuels during World War II, being of great strategic importance since they hardly had any oil supply. Despite the fact that these plants ceased to operate after the Second World War, interest in the FT process continued because of the perception that the crude oil supplies were very limited.[12]

During the 50s the FT process became economically less viable, mainly due to discoveries of large crude oil reserves in the Middle East and advances in drilling and refining of crude oil. Nevertheless scientific and industrial interest remained in South Africa due to their large coal reserves - coal can be

converted to a mixture of carbon monoxide and hydrogen - and the surge to become energy independent. The first South-African coal based FT plant was built in the mid 50s.[13]

Nowadays the FT process has regained global interest again. Various drivers are responsible for this renewed interest: depleting oil reserves, environmental demands, geopolitical reasons and high oil prices. Estimations of the worldwide crude oil reserves in combination with our growing world population and fuel use are an important driver for the search for alternative routes to transportation fuels. The current known natural gas reserves are more abundant than crude oil, however, these gas fields are often located in remote areas lacking pipelines or other infrastructure for transportation to the main markets.[14] The gas-to-liquid conversion technology - conversion of natural gas via steam cracking and subsequent FT synthesis into synthetic fuels - is an interesting option for making these remote gas reserves commercially attractive. Mainly because the liquids produced in this process are easily transportable as opposed to natural gasses. Also stricter emission standards for transportation fuels give the FT industry a boost. Synthetic fuels offer environmental benefits as opposed to transportation fuels produced from crude oil. These synthetic fuels are essentially free of nitrogen, sulphur, aromatics and metals and thus produce less NO_x, SO_x and soot during combustion. Often these FT fuels are used as fuels or blended with lower-quality fuels produced from crude oil. Geopolitical factors also play a significant role in the interest in the FT process. The opportunity to produce transportation fuels from other carbon sources e.g. methane, biomass or coal make countries less dependent on oil exporting countries. This factor will possibly catalyse the quest for alternative routes to transportation fuels in the near future. Of course financial incentives play an important role as well. For the FT synthesis different estimates have been made for which crude oil price per barrel the construction of a FT plant would become economically viable. In some reports it is estimated that the build and the exploitation of a FT plant would become economically competitive with a sustained crude oil price[§] above US $ 40 per barrel.[15,16] Since 1974 the price of crude oil has risen and dropped above and below US $ 40 per barrel, as can be seen in figure 1.

[§] Assuming a required return on investment of 10 %.

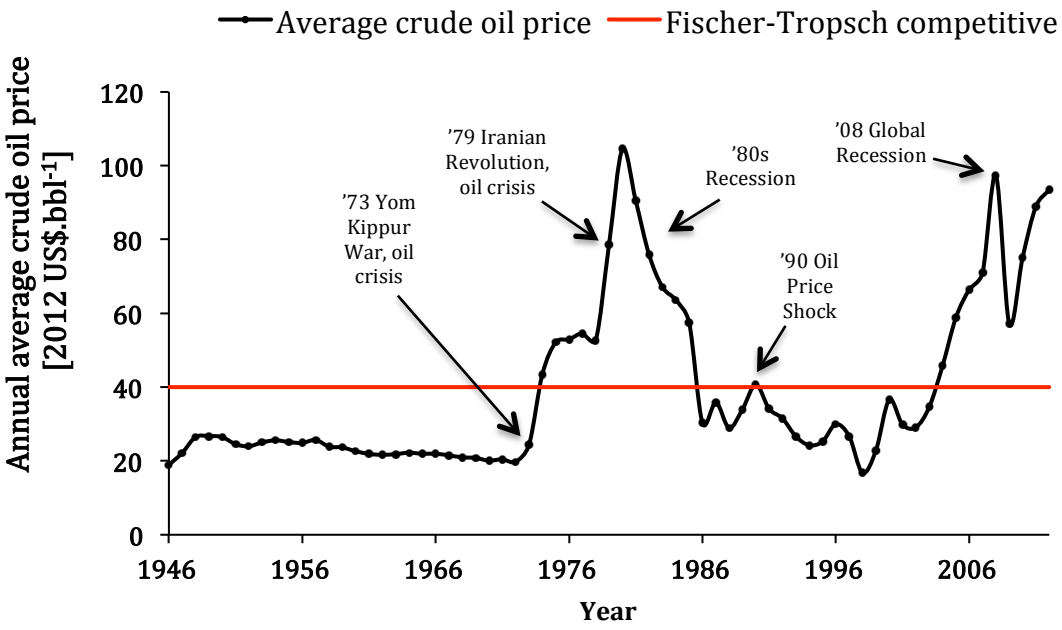

Figure 1. Historical development of the crude oil price corrected for inflation to June 2012 in US $.bbl^{-1}.[17]

The current production of transportation fuels by the FT process is ~ 270 thousand barrels per day[18], as opposed to the world's use of 85 million barrels per day.[14] Nevertheless the FT process is growing in importance and might contribute more to the global oil production in the upcoming years.

Fischer-Tropsch process

The gas-to-liquids process comprises three main elements: the synthesis gas production, the Fischer-Tropsch synthesis and the upgrade of products produced during the FT synthesis. In the cobalt based FT synthesis, syngas is mainly produced from methane. The different technologies that are used for the syngas production are: steam reforming, partial oxidation and autothermal reforming,[19,20] with the latter being considered to be the economically most viable process.[21] The next step in the FT process is the catalytic conversion of syngas into paraffins and olefins of varying chain lengths. In the literature there is no general consensus on the FT reaction mechanism. Various mechanisms have been postulated for the initiation, propagation and termination of the Fischer-Tropsch reaction. One possible mechanism states that the reaction chain is initiated by CO dissociation at the catalyst surface, also known as the carbide mechanism. The chain growth reaction is not a single elementary reaction step in which a C-C bond is

formed, but also hydrogen addition steps are involved. Adsorbed hydrogenated single carbon atom CH_x intermediates self-organize into adsorbed linear hydrocarbon chains, which desorb from the surface as paraffins or olefins by reaction with hydrogen atoms or as aldehydes or alcohols by insertion of CO.[22,23,24,25,26,27] In equation [1] the exothermic hydrogenation of carbon is shown in the polymerization reaction resulting in hydrocarbon chains over a cobalt catalyst.[14,28,29]

$$n\,CO + (2n+1)\,H_2 \longrightarrow C_nH_{2n+2} + n\,H_2O \qquad \Delta H^o_{298} = -165\,kJ.mol^{-1} \qquad [1]$$

The product distribution ranges from methane to hard waxes. Also a small fraction of oxygenates is present in the mixture. The last step in the FT process is the upgrading of the different products, varying from chemical building blocks, lubricants to transportation fuels. The cold flow properties of diesel are improved by hydrocracking and hydroisomerisation reactions. The various products go through a distillation column and are separated into fractions of naphtha, diesel, kerosene and residue. The residue can be run through the hydrocracking or hydroisomerisation reactor to improve the product quality or be used as an oil precursor.[30]

Fischer-Tropsch catalysis

In the hydrogenation of carbon monoxide to hydrocarbons, all group VIII metals have noticeable activity. From these metals only ruthenium, iron, cobalt and nickel have features allowing them to be used for FT synthesis.[31] However, ruthenium is too expensive; moreover, its worldwide reserves are insufficient for large-scale industry and nickel catalysts lead to the formation of too much methane. High methane selectivity is undesirable because this is a very expensive way of recycling syngas. FT catalysts based on iron are less expensive as compared to cobalt, but are less active and show significant activity in the water-gas shift reaction, presented in equation [2]. For this reason they are mainly used for coal-based FT plants where the hydrogen to carbon ratio is lower as compared to natural gas based FT.[1]

$$CO + H_2O \longrightarrow CO_2 + H_2 \qquad \Delta H^o_{298} = -41\,kJ.mol^{-1} \qquad [2]$$

Cobalt-based catalysts have been the preferred candidate to catalyse the FT reaction based on natural gas because of their high selectivity to linear

hydrocarbons, their high stability towards deactivation by water and their low activity for the competing water-gas-shift reaction.[32] Parameters such as cost, availability, desired product stream, reactant feed, catalyst lifetime and activity are considered when selecting the optimal catalyst.[33] Due to the relative high price of cobalt compared to iron, Co FT catalyst need to have a long lifetime in order to offer a good balance between cost and performance.[12]

Support material

Industrial catalysts are generally supported on an appropriate support in order to achieve metal particles with a high dispersion enhancing catalytic activity. The main function of the support is to increase the surface area of the active component, thermal stabilization of the metal against sintering, increase mechanical strength, facilitate heat transfer in an exothermic reaction and introduce porosity to facilitate mass transfer.[34] The support could also influence the structure and electronic properties of small cobalt metal particles.[35] In the FT synthesis different support materials have been used in industry: mainly SiO_2, Al_2O_3 and TiO_2.[36,37,38,39] A drawback of using these metal oxides as support is that they can interact strongly with the support material forming mixed compounds that are only reducible at high temperatures.[35,40] These mixed oxides are not active in the FT synthesis.[37,41] One way to overcome this difficulty is by using an inert support e.g. carbon materials. Different carbon supports have been used to prepare FT catalyst e.g. activated carbon, carbon spheres, carbon nanofibers (CNF) and carbon nanotubes (CNT).[40,42,43,44] CNT exhibit a variety of interesting properties for support materials, including high mechanical strength, high thermal conductivity and good chemical stability in aggressive media.[45,46,47] But also, the expensive metal can be recovered from spent catalysts by a controlled combustion of the carbon material. In this thesis the sharp structures of CNT, figure 2, might simplify taking edge-on images with transmission electron microscopy (TEM) and could facilitate the study of sintering.

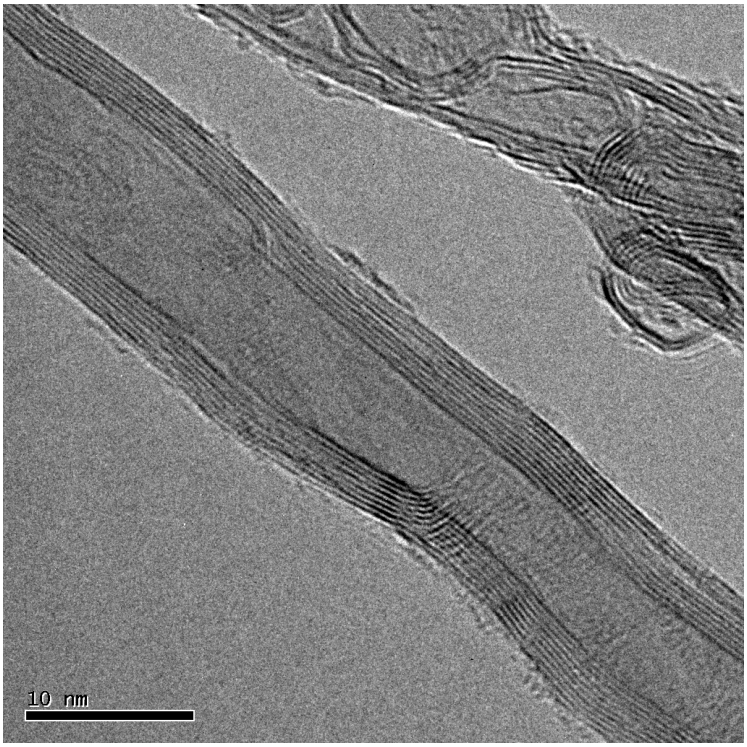

Figure 2. TEM-image of CNT as received from Bayer Material Science.

Previous work

Various research groups have undertaken attempts to increase the cobalt FT catalyst effectiveness. A rational strategy in the search for an even more active catalyst is to improve the cobalt dispersion by decreasing the cobalt particle size.[1] In this group catalytic performance, physical and chemical properties, promoter and particle size effects of Co FT catalysts have been studied extensively before.[48,49,50,51] Bezemer et al.[51] identified ideal cobalt particle sizes between 6-8 nm. For smaller particle sizes a lower FT synthesis turn over frequency (TOF) was reported. The lower activity is ascribed to blocking of edge/corner sites and lower intrinsic activity at the small terraces. In previous research, catalysts have been developed with high activity for the FT synthesis.[48, 52] Nevertheless, these catalysts undergo deactivation when exposed to industrially relevant conditions.[53]

Deactivation

The main causes of catalyst deactivation in cobalt-based FT synthesis as they appear in the literature are poisoning, re-oxidation of cobalt active sites, formation of surface carbon species, carbidization, surface reconstruction, metal-support solid state reactions, attrition and sintering of cobalt particles.[54]

Previous research in this group has shown that the cobalt particle size has a strong impact on the catalytic activity,[51] hence the abatement of sintering is particularly important and will be studied in this thesis. Sintering is a thermodynamically driven process favoured because of the energy minimization of the cobalt crystallites. This leads to a reduction of the active surface area, and thus to a loss of catalytic activity. Sintering is generally accelerated by hydrothermal conditions, which are present at industrial FT conditions.[55] Besides temperature and chemical environment, several other parameters including metal, promoters and support material affect the sintering rate. Two main mechanisms of sintering are known, figure 3: (A) Ostwald ripening or coarsening (atomic migration) and (B) coalescence (crystallite migration).[56] The mobility of the crystallites might be also be affected by the crystal structure with low coordinated atoms being more mobile.[57,58]

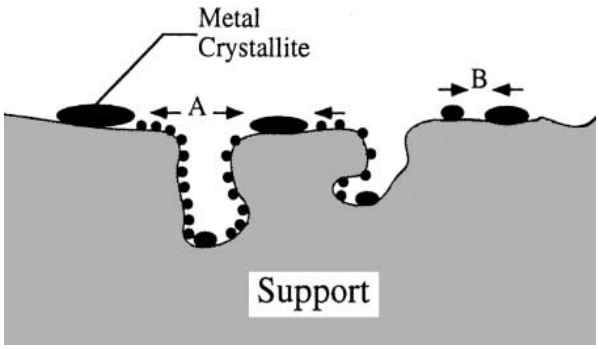

Figure 3. Sintering mechanisms (image obtained from reference 56).

Abatement of sintering

One method to prevent sintering is making use of promoters.[59] A drawback of using promoters is that the preparation and characterization of these systems is not a straightforward task, which makes the understanding of the sintering mechanism significantly more complicated. Other approaches to prevent sintering rely on the physical separation of the active metal particles.[60] This

can be for instance in the concept of embedded phases,[61] a permeable shell that protects the active metal.[62] In a study conducted by Xiong et al. cobalt particles are reported to being embedded in cavities produced by the removal of surface carbon that was in contact with the cobalt oxide species prior to autoreduction by CNT.[63,64] During the heat treatment step of the cobalt particles in an inert atmosphere CNT are reported to act as reducing agent, reducing Co_3O_4 to metallic cobalt accompanied by the consumption of carbon in the CNT. Xiong et al. report good stability of the FT catalyst and enhanced FT performance, which can possibly be attributed to the limited mobility of embedded cobalt particles. The embedding of cobalt particles by autoreduction of CNT might be a new way of protecting nanoparticles from sintering.

Another approach in the abatement of sintering might lie in the roughening of the CNT surface by oxidation. The introducing of functional oxygen groups by gas phase oxidation or liquid phase oxidation is accompanied with disruption of the outer CNT surface.[65,66] The mobility of cobalt particles is possibly reduced by the roughened surface and hence sintering is possibly reduced.

Scope of this thesis

The aim of this project is to prepare highly active cobalt on carbon nanotubes Fischer-Tropsch catalyst with low methane selectivity and a high C_{5+} selectivity, and to study the effects of surface roughening and heat treatment on the activity and stability Co on CNT FT catalysts.

In *chapter 2* carbon nanotubes catalyst support is characterized and the effects of surface roughening by gas phase oxidation and liquid phase oxidation on the CNT support are studied with TEM, N_2 physisorption and titration. In *chapter 3 a* series of Co on CNT catalysts were prepared by incipient wetness impregnation (IWI) using cobalt nitrate or cobalt acetate as precursors dissolved in water or ethanol, thermally treated in N_2 or 1 % v/v NO/N_2. The effects of different drying atmospheres, as well as solvent and precursor are studied with TEM, H_2 chemisorption and XRD. Furthermore, the prepared catalysts were subjected to atmospheric pressure catalytic testing to study the effects of the different preparation measures on catalytic

performance. *Chapter 4* builds further on the knowledge obtained in chapter three on the preparation of Co/CNT catalysts with cobalt particles well distributed on the surface. A series of Co on CNT catalysts were prepared by impregnation of the support with a cobalt nitrate precursor dissolved in ethanol and thermally treated in N_2, 1 % v/v NO/N_2 or air, varying the heating rate between 2 $K \cdot min^{-1}$, 0.5 $K \cdot min^{-1}$ or instantaneous drying. The possible autoreduction of the CNT was studied with TEM, TGA and XRD. Furthermore, the effects of stabilizing measures by means of surface roughening and heat treatment were also investigated with TEM and XRD and the prepared catalysts were at industrially relevant Fischer-Tropsch conditions. In *chapter 5* a summary of the results of the previous chapters is given and some concluding remarks and suggestions are made for future research.

[1] Khodakov, A.Y., Chu, W., Fongarland, P., Chemical reviews 107 (2007) 1692.
[2] Sabatier, P., Senderens, J.B., Comptes Rendus de l'Académie des Science Paris 134 (1902) 514.
3 Mittasch, A., Schneider, C.,BASF, German patent DRP 293, 787, (1913).
[4] Mittasch, A., Schneider, C.,BASF, German patent DRP 295, 202 (1914).
[5] Mittasch, A., Schneider, C.,BASF, German patent DRP 295, 203 (1914).
[6] Fischer, F., Tropsch, H., Brennstoff-Chemie 4 (1923) 276.
[7] Fischer, F., Tropsch, H., Brennstoff-Chemie 5 (1924) 201.
[8] Fischer, F., Tropsch, H., Brennstoff-Chemie 7 (1926) 97.
[9] Fischer, F., Tropsch, H., Berichtte der Deutschen Chemischen Gesellschaft 59 (1926) 830.
[10] Fischer, F., Tropsch, H., Brennstoff-Chemie 13 (1932) 61.
[11] United States Strategic Bombing Survey, The Effects of Strategic Bombing on the German War Economy (Washington, 1945) p. 73.
[12] Dry, M.E., Catalysis Today 71 (2002) 227.
[13] Bukur, D.B., Sivaraj, C., Applied Catalysis A: General 231 (2002) 201.
[14] de Jong, K.P, Lectures course: Adsorption Kinetics and Catalysis; Hydrogen and Synthesis Gas, Utrecht University (2012).
[15] Andrews, A., Logan, J., CRS Report for Congress: Fischer-Tropsch Fuels from Coal, Natural Gas, and Biomass, Background and Policy, 27 march 2008.
[16] Bezemer, G.L., PhD thesis, Utrecht University (2006).
[17] InflationData.com. Histrorical Crude Oil Prices. InflationData.com 19 June 2012.
[18] Moodley, D.Z., PhD Thesis, Technische Universiteit Eindhoven (2008).
[19] Rostrup-nielsen, J.R., Catalysis Today 71 (2002) 243.
[20] Vosloo, A.C., Fuel Processing Technology 71 (2001) 149.
[21] Bakkerud, P.K., Catalysis Today 106 (2005) 30.
[22] Biloen, P., Sachtler, W.M.H., Advances in Catalysis 30 (1981) 165.
[23] Bell, A.T., Catalysis Reviews, Science and Engineering 23 (1981) 203.
[24] van Santen, R.A., Ciobica, I.M., van Steen E., Ghouri, M.M., Advances in Catalysis 54 (2011) 127.
[25] van Santen, R.A., Ghouri, M.M., Shetty, S., Hensen, E.J.M., Catalysis Science & Technology 1 (2011) 891.
[26] Schulz, H., Catalysis Today 84 (2003) 67.
[27] Ciobica, I.M., Kramer, G.J., Ge, Q., Neurock, M., van Santen, R.A., Journal of Catalysis 212 (2002) 136.
[28] Schulz, H., Topics in Catalysis 26 (2003) 73.
[29] van Santen, R.A., Ghouri, M.M., Shetty, S., Hensen, E.M.H., Catalysis Science & Technology 1 (2011) 891.
[30] Chorkendorff, I., Niemandsverdriet, J.W.; Concepts Of Modern Catalysis and Kinetics, 2nd reprint Wiley-VCH (2011) ch. 9.
[31] Vannice, M.A., Journal of Catalysis 461 (1975) 449.
[32] Iglesia, E., Applied Catalysis A: General 161 (1997) 59.
[33] Dry, M.E., Catalysis Letters 7 (1990) 241.
[34] Zhang, Q., Kang, J., Wang, Y., ChemCatChem 2 (2010) 1030.
[35] Ishihara, T., Eguchi, K., Arai, H., Journal of Molecular Catalysis, 72 (1992) 253.
[36] Jacobs, G., Das, T.K., Zhang, Y., Li, J., Racoillet, G., Davis, B. H., Applied Catalysis A: General 233 (2002) 263.
[37] van Berge, P. J.,van de Loosdrecht, J., Barradas, S., van der Kraan, A. M., Catalysis Today 58 (2000) 321.

[38] Tavasoli, A., Mortazavi, Y., Khodadi, A., Abbas, A., Mousavian, M. A., Iranian Journal of Chemistry and Chemical Engineering 24 (2005) 9.
[39] Bartholomew, C.H., Reuel, R.C., Journal of Catalysis 88 (1984) 78.
[40] Bezemer, G.L., Laak, A.V., Dillen, A.J.V., de Jong, K.P., Studies in Surface Science and Catalysis 147 (2004) 259.
[41] Jacobs, G., Patterson, P.M., Das, T.K., Luo, M., Davis, B.H., Applied Catalysis A : General 270 (2004) 65.
[42] Serp, P., Corrias, M., Kalck, P., Applied Catalysis A : General 253 (2003) 337.
[43] Chen, A.A., Kaminsky, M., Geffroy, G.L., Vannice, M.A., Journal of Physical Chemistry 90 (1986) 4810.
[44] Moyo, M., Motchelaho, M.A.M., Xiong, H., Jewell, L.L., Coville, N.J., Applied Catalysis A: General 413-414 (2012) 223.
[45] Becker, M. J., Xia, W., Tessonnier, J. P., Blume, R., Yao, L., Schlögl, R., Muhler, M., Carbon 49 (2011) 5253.
[46] Tessonnier, J.P., Rosenthal, D., Hansen, T.W., Hess, C., Schuster, M.E., Blume, R., Girgsdies, F., Carbon 47 (2009) 1779.
[47] de Jong, K. P., Geus, J. W., Catalysis Reviews 42 (2000) 481.
[48] Prieto, G., Martínez, A., Concepción, P., Moreno-Tost, R., Journal of Catalysis 266 (2009) 129.
[49] den Breejen, J.P., Sietsma, J.R.A., Friedrich, H., Bitter, J.H., de Jong, K.P., Journal of Catalysis 270 (2010) 146.
[50] den Breejen, J.P., Radstake, P.B., Bezemer, G.L., Bitter, J.H., Frøseth, V., Holmen, A., de Jong, K. P., Journal of the American Chemical Society 131 (2009) 7197.
[51] Bezemer, G.L., Bitter, J.H., Kuipers, H.P.C.E., Oosterbeek, H., Holewijn, J.E., Xu, X., Kapteijn, F., van Dillen, A.J., de Jong, K.P., Journal of the American Chemical Society 128 (2006) 3956.
[52] Yu, Z., Borg, Ø., Chen, D., Enger, B.C., Frøseth, V., Rytter, E., Wigum, H., Holmen, A., Catalysis Letters 109 (2006) 43.
[53] Saib, A., Moodley, D.J., Ciobîcă, I.M., Hauman, M.M., Sigwebela, B.H., Weststrate, C.J., Niemantsverdriet, J.W., van de Loosdrecht, J., Catalysis Today 154 (2010) 271.
[54] Tsakoumis, N.E., Rønning, M., Borg, Ø., Rytter, E., Holmen, A., Catalysis Today 154 (2010) 162.
[55] Bezemer, G.L., Remans, T.J., van Bavel, A.P., Dugulan, A.I., Journal of the American Chemical Society 132 (2010) 8540.
[56] Bartholomew, C.H., Applied Catalysis A : General 212 (2001) 17.
[57] Das, T.K., Jacobs, G., Patterson, P.M., Conner, W.A, Li, J., Davis, B.H., Fuel 82 (2003) 805.
[58] Palasantzas, G., Vystavel, T., Koch, S.A., de Hosson, J.T.M., Journal of Applied Physics 99 (2006) 024307.
[59] Morales, F., Weckhuysen, B.M., Catalysis (Royal Society of Chemistry) 19 (2006) 1.
[60] Prieto, G., Zečević, J., Friedrich, H., de Jong, K.P., de Jongh, P.E., Nature Materials, Published Online: 11 November (2012) 1.
[61] de Rogatis, L., Cargnello, M., Gombac, V., Lorenzut, B., Montini, T., Fornasiero, P., ChemSusChem 3 (2010) 24.
[62] Dai, Y., Lim, B., Yang, Y., Cobley, C.M., Li, W., Cho, E.C., Grayson, B., Fanson, P.T., Campbell, C.T., Sun, Y., Xia, Y., Angewandte Chemie (International edition) 49 (2010) 8165.
[63] Xiong, H., Moyo, M., Rayner, M.K., Jewell, L.L., Billing, D.G., Coville, N.J., ChemCatChem 2 (2010) 514.
[64] Xiong, H., Motchelaho, M.A.M., Moyo, M., Jewell, L.L., Coville, N.J., Journal of Catalysis 278 (2011) 26.
[65] Xia, W., Jin, C., Kundu, S., Muhler, M., Carbon 47 (2009) 919.
[66] Toebes, M.L., Ph.D.thesis, Utrecht University (2004).

Chapter Two

Characterization of the untreated and oxidized Carbon Nanotubes Catalyst Support

Research and industrial application on Co FT catalysts is mainly confined to cobalt on oxidic supports.[1,2,3,4] As mentioned in chapter 1, a difficulty with using these metal oxides as support is that they can form strong metal-support interactions. These metal-support interactions can lead to the formation of mixed compounds that are only reducible at high temperatures[5,6,7] and are not active in the FT synthesis.[2,8] One way to overcome this difficulty is by using an inert support. Different groups have used carbon materials as support to prepare FT catalysts.[9,10,11,12] In this thesis multiwall carbon nanotubes (CNT) are used as support material.

CNT are composed entirely of carbon-carbon bonds having sp^2 hybridization, similar to graphene.[13] In the literature there is no agreement on the definition of multiwall carbon nanotubes. CNT as discussed in this thesis are tubular graphene sheets, forming a multiple-shell structure of cylindrical tubes. The tubular graphene sheets have different chirality and are arranged coaxially along the tube axis in a Russian doll fashion.[14] This is illustrated in figure 1 where it can be seen that the distance between the sheets is ~ 0.34 nm.[15]

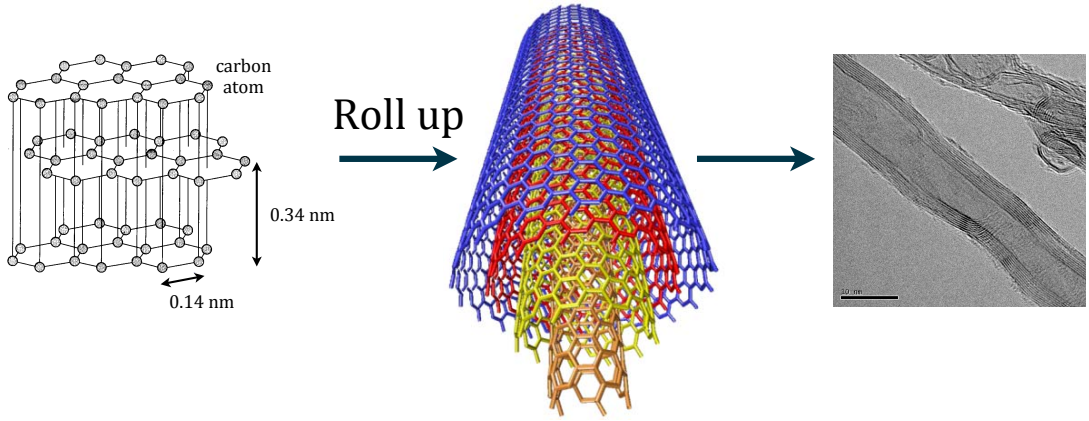

Figure 1. Illustration of multi wall carbon nanotube (the left two images are obtained from reference,[16] the right image is a TEM picture from this research).

CNT exhibit a variety of interesting properties for support materials.[17] The main advantages for using CNT in heterogeneous catalysis are their high surface area and their chemical inertness.[12] However the hydrophobic and inert nature of CNT can be unfavourable for some applications. To overcome this, CNT can be treated with nitric acid (HNO_3), introducing oxygen containing surface groups, enhancing the wettability for polar solvents and making the surface more reactive.[18,19] In this chapter the as received CNT and

surface treated CNT are characterized using different techniques. The surface treated CNT have been oxidized with HNO_3 in the gas or liquid phase. In the surface treatment the nitronium ion (NO_2^+) can attack aromatic compounds, which is probably the first step in the introduction of oxygen containing surface groups.[20]

Here, we report on the effects of surface oxidation of CNT by liquid phase oxidation and gas phase oxidation. TEM was used to study the graphite-like structure of untreated and surface treated CNT. N_2 physisorption was used to explore to possible changes in the texture. Titration was used to determine the number of acidic surface groups.

Experimental

Gas Phase Oxidation

CNT fabricated by chemical vapour deposition were acquired from Bayer material science.[21] The CNT (Baytubes® C150 HP) consist of high purity agglomerates with outer mean diameter of ~ 13 nm, inner mean diameter of ~ 4 nm and a typical length of ≥1 μm.[22] The set up used for the gas phase oxidation is shown in figure 2. In a typical experiment 0.5 g of CNT, dried overnight at 393 K, were loaded into a glass sample holder with a quartz frit allowing gas to flow through. Prior to oxidation the sample holder was dried for 2 h at 398 K. The round bottom flask was filled with 250 mL of concentrated nitric acid (HNO_3 65 % Merck) and heated for 2.5 h at 373 K. The reflux condenser was connected to an open-end exhaust line to air. After 2.5 h the heating mantle was switched off, the sample holder disconnected of the round bottom flask and heated for another 2 h at 373 K to dry the surface treated CNT.

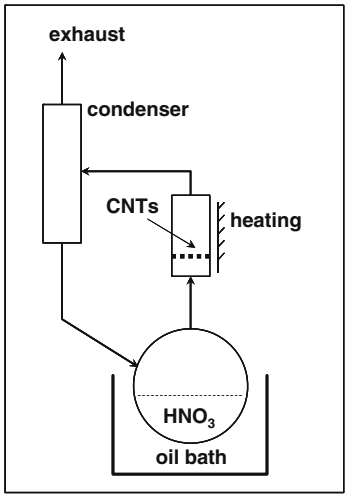

Figure 2. Illustration of the gas phase oxidation set-up used for the surface treatment of the CNT. The sample holder is heated by a heating trace (image obtained from Xia et al.[25]).

Liquid Phase Oxidation

The as received CNT were stirred under reflux conditions in concentrated nitric acid (HNO_3 65 % Merck) for 0.5-7h. In a typical experiment 2 g of CNT was refluxed in 40 mL solution. Subsequently the CNT were washed with demi-water until the filtrate had reached pH ~ 7. The surface treated CNT were dried in air at 393 K overnight. The carbon loss percentage - relative weight loss during oxidation and drying - was determined by weighing tubes, dried at 393 K, before and after GPO and LPO treatment.

Titration

The number of acid sites of the untreated and surface treated CNT were determined by performing direct acid-base titrations. Samples of 100 mg were stirred with 100 mL 0.1 M KCl. While stirring, nitrogen was flushed through the reactor in order to remove dissolved CO_2. Titration was performed with a Titralab TIM Titration Manager with 10 mM NaOH aqueous solution. Acid sites with a $pK_a < 7.5$ were measured.

N_2 physisorption

Specific surface areas were determined for the CNT supports from the N_2 adsorption-desorption isotherms at 77 K using a Micromeritics Tristar 3000 apparatus. Prior to measurements the samples were degassed at 498 K and 393 K, respectively, for 20h with a of ramp 10 $K \cdot min^{-1}$ to remove moisture from the CNT (the impact of pre-drying on the N_2 physisorption measurements is shown in appendix chapter 2 and 3 table 1). N_2 physisorption data were obtained from 0 to 0.995 $P \cdot P_0^{-1}$. Measurements were performed on typically 100 mg of sample. Data were analysed with the Micromeritics Tristar software. Total surface area was estimated using the B.E.T. approach. Average pore size distributions were determined from the desorption branches of the isotherms using the B.J.H. method. The micropore surface area was approximated using the t-plot method. The total pore volume was determined from the single point adsorption.

Transmission Electron Microscopy

TEM images were obtained with a FEI Tecnai 20 F TEM operating at 200 kV or a FEI Tecnai 12 TEM operating at 120 kV. The catalysts were crushed and suspended in ethanol under ultrasonic vibration. A droplet of this suspension was dispersed on a holey carbon film on a copper TEM grid.

Results and discussion

Characterization of the support

TEM images reveal that CNT show narrow tubular morphology with average inner and outer diameters of 4 nm and 13 nm, respectively. In figure 3 A and B an overview and a close up TEM image of an untreated CNT sample is seen. From image 3 B it can be seen that the graphene sheets are parallel to the main axis and appear to be well organized. Single graphene sheets can propagate over several hundreds of nanometers.[14] Nevertheless, most of the nanotubes exhibit disordered graphene-like deposits all over their inner and outer surfaces. The CNT form an interwoven matrix of tubes, figure 3 A, creating meso- and macropores. No micropores are present,[23] thus reducing diffusion limitations in catalytic reactions.[24] Also the tubes show inner walls that can partially close the inner channel, indicated with a black arrow in figure 3 B. However in many cases the inner channels are not completely blocked.

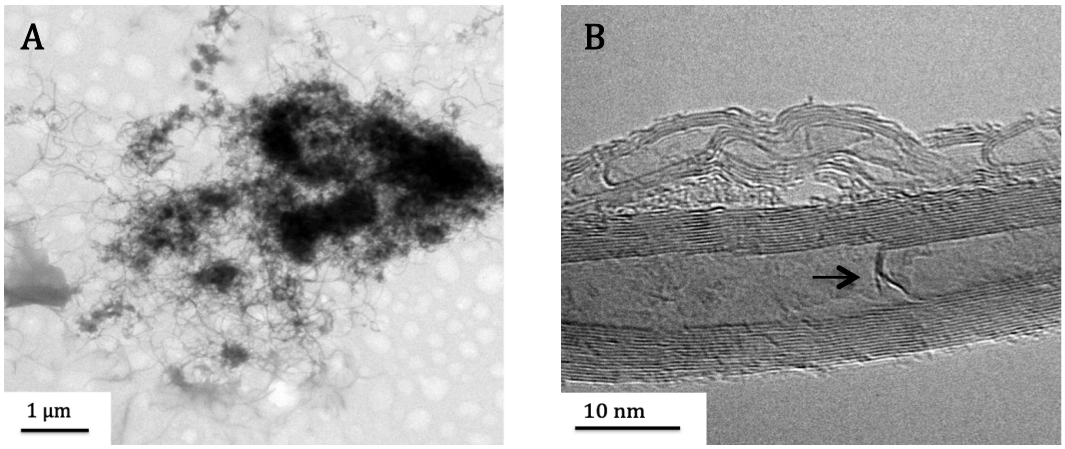

Figure 3. A: overview TEM image and B: HR-TEM image of as received CNT.

In the high angle annular dark field mode (HAADF) cobalt growth catalysts residues can be seen, these are the white elongated particle seen in figure 4 A and B. The particles have a diameter of ~ 4 nm matching the mean inner tube diameter. With Energy-dispersive X-ray spectroscopy (EDX) a lineprofile was obtained - the line indicated with red in figure 4 B and the accompanying EDX line profile is shown in appendix chapter 2 and 3, figure 3 - which confirmed the presence of cobalt particles in the tubes. This is also reported by Tessonier[14] who determined the inorganic growth catalysts impurities in Baytubes® C150 P to be cobalt (0.78 wt%) and manganese (0.75 wt%).

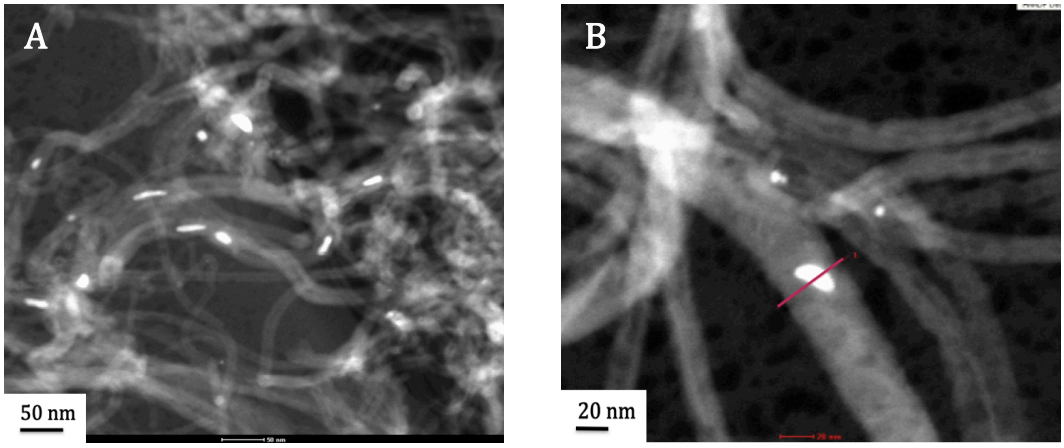

Figure 4. A: HDAAF-STEM overview image and, B: HAADF-STEM image of cobalt particles in as received CNT.

GPO and LPO were performed on the CNT, to introduce functional oxygen groups, which can be used as anchoring points for catalyst metal precursor complexes.[25] The effects of these surface treatment methods were studied with TEM. The oxidation treatment by acids in the stirred liquid phase under reflux conditions can be accompanied by structural damage to the CNT.[25] Figure 5 A is a TEM image taken after a LPO treatment illustrating that the graphite-like structure of the tubes can be altered. Overall the graphite-like structure remained intact, however severe disruption of the tubes can be seen, in some parts even the inner tubes seem to be interrupted.

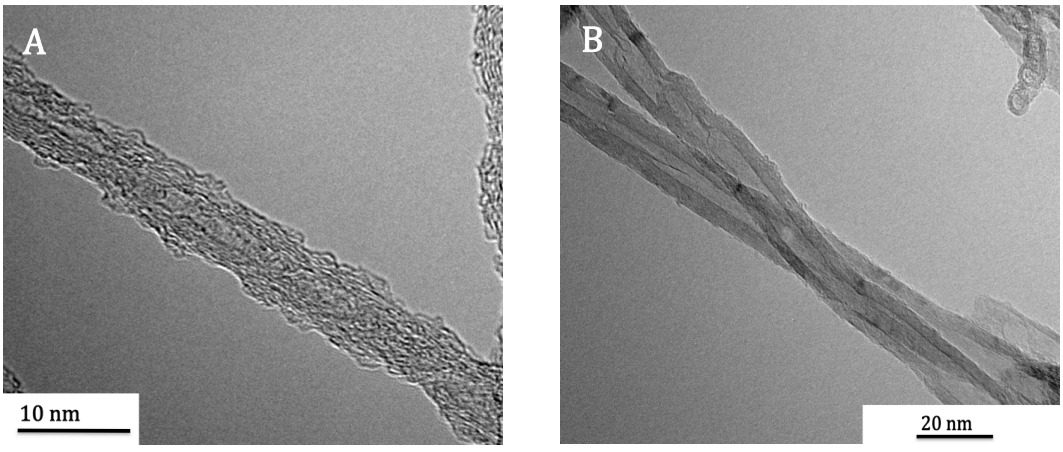

Figure 5. A: L-CNT 2h. B: G-CNT 2.5 h.

The separation of the treated CNT from the acids in the LPO method - which is in many cases carried out by filtration - appears to be challenging due to small diameter of the tubes. The filtration step is accompanied by a considerable loss of CNT. The carbon loss percentage was determined for the various treatments shown in table 1. The carbon loss percentages - relative weight loss during oxidation and drying - are comparable with the results reported by Toebes.[26] As can be seen in table 1 oxidizing the tubes for 7 h has a significant impact on the carbon loss percentage. Treatment of the tubes with a strong oxidizing agent can lead to complete oxidation, consumption and the breaking up of CNT.[27,28,29] Especially during the longer acid treatment the shorter nanotube fragments blocked the pores of the filter and could also be found in the filtrate. The tubes treated in the LPO method were strongly agglomerated possibly caused by the drying step.[25]

The GPO treatment appeared to be considerably milder than the LPO method causing less damage to the tubes. Disruption of the tubes can also be seen after the GPO method, figure 5 B, however the severe disruption as seen after the LPO method seems to be absent and the graphite-like structure seems to be unaffected. The GPO set-up illustrated in figure 2, in the experimental part, is designed to ensure that the surface treatment is under gas phase conditions. The set-up prevents that refluxed liquid HNO_3, collected by the reflux condenser is deposited on the CNT. Hence, wetting of CNT by HNO_3 is prevented and the treatment is completely under gas phase conditions. The vapour phase[1] flowing through the sample is a complex mixture of HNO_3, O_2, H_2O, N_2O, and NO_x.[25] A benefit of using the GPO treatment is that the separation by filtration step is not needed, thus minimizing the carbon loss as can be seen in table 1. Also the treatment is less harsh on the tubes than the LPO treatment.

Table 1. Carbon loss % due to different oxidation procedures.

Samples	Acid treatment	carbon loss %
G-CNT 2.5h	GPO 2.5h in 65% HNO_3	2.2
L-CNT 0.5h	LPO 0.5h in 65% HNO_3	6.1
L-CNT 2h	LPO 2h in 65% HNO_3	5.6
L-CNT 7h	LPO 7h in 65% HNO_3	27

[1] Under the applied conditions the decomposition products of HNO_3 e.g. NO_2 can also act as oxidizing agents.

N_2 physisorption was performed on the as received samples and the treated samples to obtain information on the textural properties of the different samples. The adsorption-desorption isotherms of representative samples are given in figure 6. The LPO treated sample shows a similar curve as the GPO treated sample and is for this reason not presented here. The tubes present a typical IUPAC type IV isotherm, with a hysteresis at high $P \cdot P_0^{-1}$.

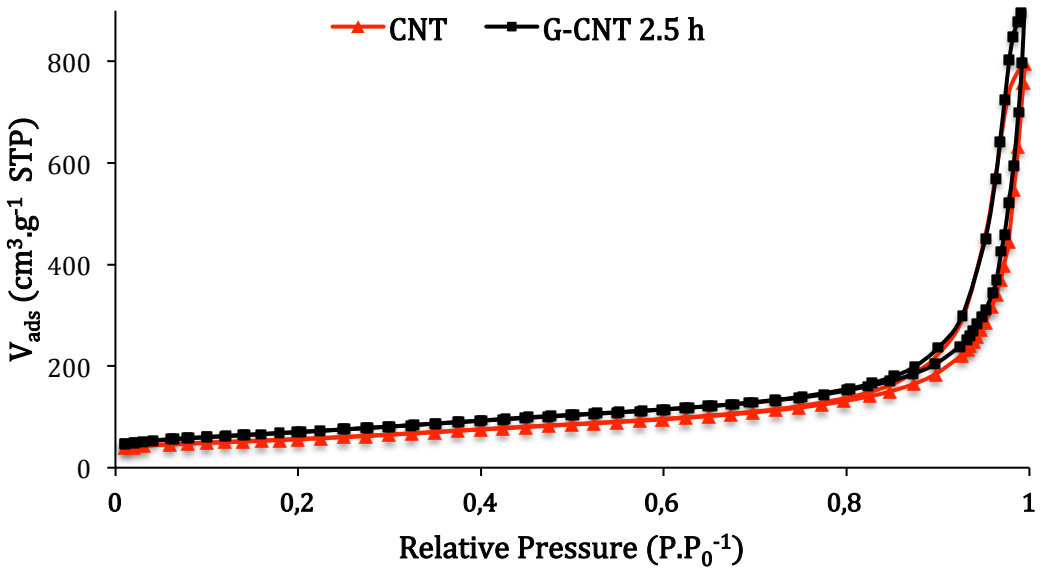

Figure 6. N_2 physisorptoin isotherms of as received CNT and G-CNT 2.5 h.

An increase in total surface area is noticed with an increase in duration of the oxidation treatment. The total surface area was determined from the B.E.T. equation and the micropore area was determined from the t-plot method, results given in table 2.

Table 2. Influence of the oxidation treatments on specific surface areas.

Support name	B.E.T. area $(m^2 \cdot g^{-1}) \cdot 10^2$	Micropore area $(m^2 \cdot g^{-1})$	Total pore volume $(mL \cdot g^{-1})$
CNT	2.0	24	1.2
G-CNT 2.5 h	2.5	18	1.4
L-CNT 0.5 h	2.4	16	1.4
L-CNT 2 h	2.7	14	1.1

The pore size distributions, calculated from the desorption branch of the isotherm using the B.J.H. method, have a bimodal distribution for the as received tubes and the surface treated tubes, figure 7. Small pores between 2 and 5 nm in diameter, corresponding to the inner channels of the tubes can be observed, but also larger pores between 6 and 150 nm in diameter, which are formed between the entangled nanotubes can be seen.[30] Tesonnier[14] reports a shift to smaller pore diameters after the nitric acid treatment. The shift to smaller pore sizes can be observed for the L-CNT 2.5 h sample however the opposite can be seen for the G-CNT 2.5 h sample, figure 7. The shift to smaller pore sizes can be interpreted as the tubes being more entangled. As mentioned earlier, agglomeration of the tubes is observed after the LPO treatment, which is probably caused by the drying step.[25] This could be a possible explanation for the shift to smaller pore sizes after the LPO treatment. Further research is recommended to explain the shift to larger pore diameters after the GPO treatment. Nitric acid is commonly used to open capped carbon nanotubes, consequently the total surface area increased from ~ 200 to ~ 250 nm. The tubes also show micropore area, which is unexpected, as the structure of the tubes should only show mesoporosity. The micropore area decreases after the acid treatment so these micropores probably arise from the carbon deposits or from remaining growth catalyst on the tubes. All the surface treatments led to an increase of specific surface area which can be ascribed to three effects: surface roughening, opening of the inner channels and fragmentation as can be seen in the TEM-images (not shown here).

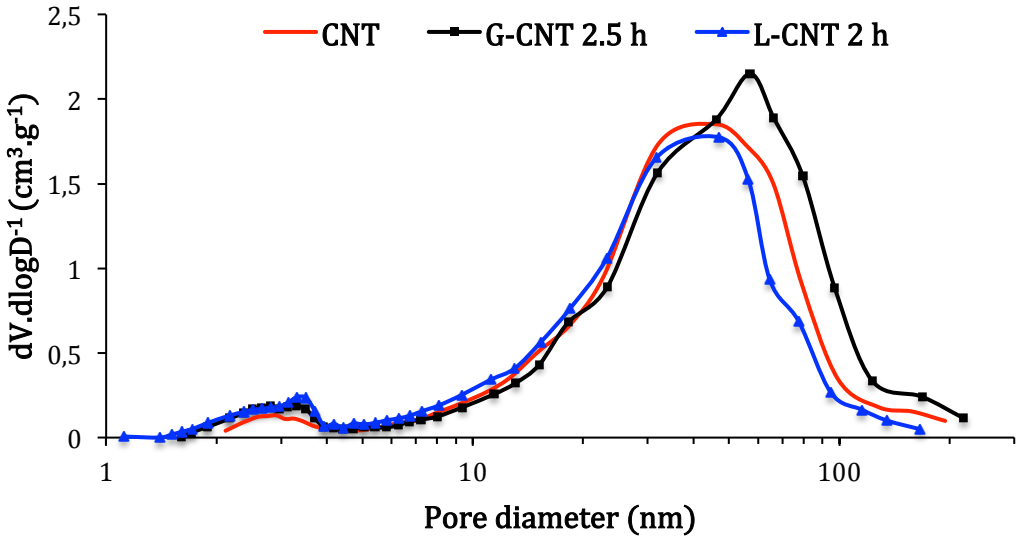

Figure 7. Pore size distributions of CNT, G-CNT 2.5 h and L-CNT 2.5 h.

To have an indication of the possible number of anchoring points a direct acid-base titration was performed. With the use of NaOH as titrant the number of accessible surface groups exhibiting a pK < 7.5 was determined. In table 3 the number of acidic oxygen-containing surface groups as measured by titration is given for the samples G-CNT 2.5 h and L-CNT 2h.
The number of acids groups found here are similar to the values reported in literature, where values ranging between 0.1 to 0.5 mmol acidic groups·g^{-1} are reported for the nitric acid LPO of CNF, depending on the treatment time and concentration used. [31, 32] In appendix chapter 2 and 3 figure 19 the accompanying titration curves of the samples are presented. Please note that by titration no distinction can be made between phenolic and carboxylic groups, however previous research has shown that for CNF, surface treatment with nitric acid, mainly leads to carboxylic groups.[33] Assuming similarity between CNT and CNF, the surface groups are mainly carboxylic.

Table 3. Number of acidic surface groups for surface treated CNT.

Support name	Acidic oxygen-containing surface groups.nm^{-2}	Acidic groups $mmol.g^{-1}$
G-CNT 2.5h	0.55	0.23
L-CNT 2h	0.90	0.40

Conclusions

The structure and texture of surface treated and untreated CNT as received by Bayer Material Science (Baytubes® C150 HP) were studied with TEM, N_2 physisorption, and titration. Results demonstrate that after the oxidation treatment by GPO and LPO in HNO_3, the graphite-like structure remained intact, however structural damage could be observed after the LPO treatment. The texture of the CNT was more noticeably modified after LPO treatment. During oxidation treatments, specific surface area increased, micropore area decreased and the number of acidic oxygen containing surface groups introduced, increased with the harshness of the treatment. The GPO method has shown to be a milder method in introducing functional groups into the CNT surface than the LPO method and is accompanied with less carbon loss due to the prevention of the filtration step.

[1] Jacobs, G., Das, T.K., Zhang, Y., Li, J., Racoillet, G., Davis, B. H., Applied Catalysis A: General 233 (2002) 263.

[2] van Berge, P.J., van de Loosdrecht, J., Barradas, S., van der Kraan, A.M., Catalysis Today 58 (2000) 321.

[3] Tavasoli, A., Mortazavi, Y., Khodadi, A., Abbas, A., Mousavian, M.A., Iranian Journal of Chemistry and Chemical Engineering 24 (2005) 9.

[4] Bartholomew, C.H., Reuel, R.C., Journal of Catalysis 88 (1984) 78.

[5] Khodakov, A.Y., Chu, W., Fongarland, P., Chemical reviews 107 (2007) 1692.

[6] Bezemer, G.L., Laak, A.V., Dillen, A.J.V., de Jong, K.P., Studies in Surface Science and Catalysis 147 (2004) 259.

[7] Jacobs, G., Das, T.K., Zhang, Y., Li, J., Racoillet, G., Davis, B. H., Applied Catalysis A: General 233 (2002) 263.

[8] Jacobs, G., Patterson, P.M., Das, T.K., Luo, M., Davis, B.H., Applied Catalysis A: General 270 (2004) 65.

[9] Moyo, M., Motchelaho, M.A.M., Xiong, H., Jewell, L.L., Coville, N.J., Applied Catalysis A: General 413-414 (2012) 223.

[10] Serp, P., Corrias, M., Kalck, P., Applied Catalysis A: General 253 (2003) 337.

[11] Chen, A.A., Kaminsky, M., Geffroy, G.L., Vannice, M.A., Journal of Physical Chemistry 90 (1986) 4810.

[12] de Jong, K.P., Geus, J.W., Catalysis Reviews 42 (2000) 481.

[13] Lijima, S., Nature 354 (1991) 56.

[14] Tessonnier, J.P., Rosenthal, D., Hansen, T.W., Hess, C., Schuster, M.E., Blume, R., Girgsdies, F., Carbon 47 (2009) 1779.

[15] Hou, P.X., Liu, C. Cheng, H.M., Carbon 46 (2008) 2003.

[16] Tessonnier, J.P., Lecture slides: carbon materials in catalysis, winter semester 2009-2010, Fritz Haber Institute of the Max Planck Society, Berlin (2009).

[17] Becker, M.J., Xia, W., Tessonnier, J.P., Blume, R., Yao, L., Schlögl, R., Muhler, M., Carbon 49 (2011) 5253.

[18] Rodriguez-Reinoso, F., Carbon 36 (1998) 159.

[19] Ros, T.G., van Dillen, A.J., Geus, J.W., Koningsberger, D.C., Chemistry a European Journal 8 (2002) 1151.

[20] Edwards, H.G.M., Fawcett, V., Journal of Molecular Structure 326 (1994) 131.

[21] www.baytubes.com.

[22] Avilés, F., Cauich-Rodríguez, J.V., Moo-Tah, L., May-Pat, A., Vargas-Coronado, R., Carbon 47 (2009) 2970.

[23] Serp, P., Castillejos, E., ChemCatChem 2 (2010) 41.

[24] Iglesia, E., Applied Catalysis A: General 161 (1997) 59.

[25] Xia, W., Jin, C., Kundu, S., Muhler, M., Carbon 47 (2009) 919.

[26] Toebes, M.L., Ph.D.thesis, Utrecht University (2004).

[27] Tsang, S.C., Chen, Y.K., Harris, P.J.F., Green, M.L.H., Nature 372 (1994) 159.

[28] Li, Y.H. Wang, S., Luan, Z., Ding, J., Xu, C., Wu., D., Carbon 41 (2003) 1057.

[29] Li, C.H., Yao, K.F., Liang, J., Carbon 41 (2003) 858.

[30] Peigney, A., Laurent, C., Flahaut, E., Bacsa, R. R., Rousset, A., Carbon, 39 (2001) 507.

[31] Lakshminarayanan, P.V., Toghiani, H., Pittman, C.U., Carbon 42 (2004) 2433.

[32] Li, J., Vergne, M.J., Mowles, E.D., Zhong, W.H., Hercules, D.M., Lukehart, C.M., Carbon 43 (2005) 2883.

[33] Plomp, A.J., Su, D.S., de Jong, K.P., Bitter, J.H., Journal of Physical Chemistry C 113 (2009) 9865.

Chapter Three

The preparation of Highly Active and well distributed Cobalt on Carbon Nanotubes Fischer-Tropsch Catalysts

Chapter Three

Incipient wetness impregnation (IWI) of a support with an aqueous solution of cobalt nitrate is a common way to produce FT catalysts. The main reasons for using a nitrate as precursor are high solubility enabling high loadings via single step impregnation, good availability, cost effectiveness and easy decomposition of the precursor. In the catalyst preparation procedure, IWI is followed by drying and a thermal treatment, to decompose the supported cobalt nitrate hydrate to supported cobalt oxide. Reduction transforms the inactive cobalt oxide to metallic cobalt prior to the FT reaction. Reduced catalysts prepared via an aqueous IWI show in general a broad particle size distribution and a low metal dispersion. The poor dispersion of supported catalysts prepared via nitrate precursors has been ascribed to redistribution of cobalt particles during drying or agglomeration during calcination. In this group it has been demonstrated that it is possible to prevent this redistribution by the use of a modified calcination treatment in a NO/He flow with cobalt on silica.[1]

Another approach to prepare cobalt catalysts with a high metal dispersion is with the use of cobalt acetate as precursor. Some early studies on the preparations of cobalt catalysts have shown that cobalt acetate can be used to prepare catalysts with highly dispersed cobalt particles using silica, titania or SBA-15 as support.[2,3,4]

This work presents a preliminary study on the effect of thermal treatment in different gas atmospheres, catalyst precursors and solvents, on the properties of CNT supported Co FT catalysts. A series of catalysts were prepared by IWI using cobalt nitrate or cobalt acetate as precursors dissolved in water or ethanol, thermally treated in N_2, 1 % v/v NO/N_2 or dried in static air. To our best knowledge we are the first to report the NO method performed on cobalt on carbon nanotubes catalysts and the application of the GPO treatment for Co/CNT catalysts. Characterization was performed with transmission electron microscopy (TEM), X-ray diffraction (XRD) and H_2 chemisorption. Catalytic testing was carried out in a fixed bed micro reactor at 493 K, atmospheric pressure and using a flow of H_2/CO v/v 2:1.

Experimental

Surface treatment

Pre-treatment in HNO_3 by Gas Phase Oxidation or Liquid Phase Oxidation as described in the experimental part of chapter two was performed on a selection of catalyst' CNT supports, before IWI was conducted.

Catalyst preparation

The catalysts were prepared by incipient wetness impregnation. Before impregnation the total catalyst pore volume was determined by adding demineralized water to degassed CNT with a syringe until the support had a sticky appearance, and by N_2 physisorption. Typically 1 g of CNT were degassed *in vacuo* under slight heating at ~ 348 K and stirring for ~ 1 h. The CNT were impregnated with 1.0 mL of aqueous solution, at room temperature containing cobalt nitrate hexahydrate (99 % Acros) or cobalt acetate tetrahydrate (98 % ABCR) as precursor. Another series of catalysts were prepared using cobalt nitrate as precursor and ethanol as solvent. To prevent evaporation of ethanol the impregnation of the degassed samples was performed at ~ 273 K using an ice bath. After impregnation the aqueous and ethanol samples were dried overnight in static air at 333 K and 393 K, respectively. The samples dried at 333 K were subjected to a thermal treatment for 4 h at 523 K in a fluidized bed with a ramp of 2 $K \cdot min^{-1}$ in a continuous flow of 1 $mL \cdot (mg^{-1} \cdot min^{-1})$ of N_2 and 1% v/v NO/N_2, respectively. The cobalt metal loadings varied from 6.0 to 18 wt%. The catalysts dried at 393 K were coded with four letters indicating surface treatment (when applied), method, precursor and solvent followed by the cobalt loading. The catalysts dried at 333 K with a subsequent thermal treatment were coded as mentioned above with an addition of used flow, e.g. G-INE8-NO referring to a catalyst that had been surface treated with a gas phase oxidation and prepared by incipient wetness impregnation with cobalt nitrate dissolved in ethanol with a 8 wt% cobalt loading subjected to a 1% v/v NO/N_2 flow. An example of the different designations possible is illustrated in figure 1. Furthermore, an overview of all the catalysts prepared with their designations and cobalt loadings is given in table 1.

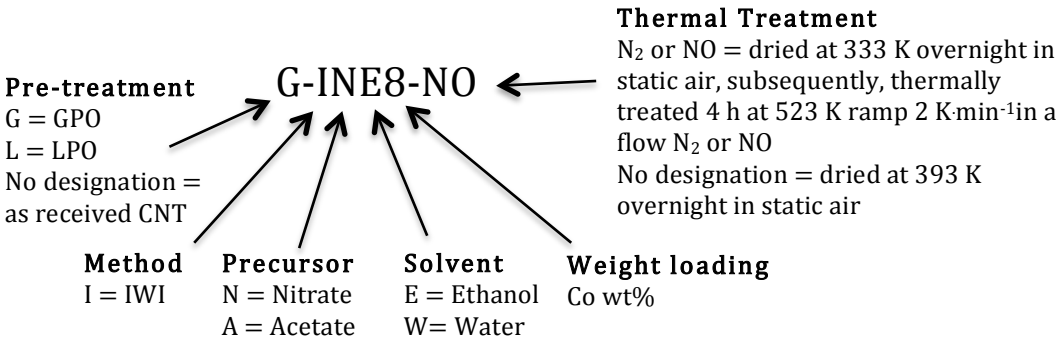

Figure 1. Illustration of the different catalyst designations.

H_2 chemisorption

Hydrogen chemisorption measurements were performed using a Micromeritics ASAP 2020 apparatus. Prior to chemisorption the samples were pre-treated in flowing He at 373 K for 1h. Next, typically 100 mg were heated in flowing H_2 with a heating rate of 5 K·min^{-1} to the reduction temperature of 623 K and held at this temperature for 2 h. After this the samples were degassed at the reduction temperature for 2h to remove chemisorbed hydrogen and water. The H_2 adsorption isotherms were measured at 423 K. A typical H_2 chemisorption isotherm is found in appendix chapter 2 and 3 figure 1. The H/Co ratios at zero pressure were found by extrapolation of the linear part of the isotherm. Metallic cobalt (Co^0) particle sizes were estimated from the total amount of (reversible + irreversible) amount of chemisorbed H_2, assuming: complete reduction, H/Co atomic ratio stoichiometry of 1 and a hemi-spherical particle size geometry. The formula in equation [1] was used with d the metallic cobalt particle diameter (nm), W the weight percentage of cobalt and X the total H_2 uptake in micromoles per gram of catalyst.[5]

$$d = 81.6 \cdot \frac{W}{X} \qquad [1]$$

Catalytic testing

The Fischer-Tropsch synthesis was performed at 493 K at atmospheric pressure in a plug-flow reactor with an H_2/CO v/v 2:1. Typically 50 mg of catalyst particles were diluted with 110 mg SiC (0.2 mm) in order to achieve isothermal plug-flow conditions. The thermal treated catalysts were reduced *in situ* for 2 h at 623 K, ramp 5 K·min^{-1} in a flow of 4 mL·min^{-1} H_2 and 36

mL·min^{-1} Ar. Online gas chromatography was on a Varian 3800 GC with a fused silica CP—Sil 5CB column and a FID to determine the hydrocarbon products (C_1-C_{18}) and CO conversions. The CO conversion, cobalt time yield (CTY), selectivity's (S_{C1} and S_{C5+}) and turn over frequency (TOF) were calculated according to equation [2] tot [6].

$$X_{CO} = \left(\frac{CO\ (mL{\cdot}s^{-1})}{H_2(mL{\cdot}s^{-1}) + CO\ (mL{\cdot}s^{-1})}\right) \cdot\ T\ V\ C_{C_1-C_{18}}\ \cdot\ 100\ \% \qquad [2]$$

$$CTY = \frac{CO\ (moles\cdot s^{-1}) \cdot X_{CO}}{mCo\ (g)} \qquad [3]$$

$$S_{C_1} = \frac{Concentration_{C_1}}{T\ V\ C_{C_1-C_{18}}} \cdot\ 100\ \% \qquad [4]$$

$$S_{C_{5+}} = \frac{(1-Concentration_{C_1-C_4})}{T\ V\ C_{C_1-C_{18}}} \cdot\ 100\ \% \qquad [5]$$

$$TOF = \frac{CO\ (moles\cdot s^{-1}) \cdot X_{CO}}{\left(\frac{mCo\ (g) \cdot Co_{surface\ area}(m^2{\cdot}g^{-1})}{S_{Co}(m^2) \cdot N_{av}}\right)} \qquad [6]$$

$T\ V\ C_{C_1-C_{18}} = Total\ Volume\ Concentration$

$N_{av} = 6.022\ \cdot 10^{23} \cdot mol^{-1}$

S_{Co} is a constant assuming one Co atom per 0.0628 nm^2.[21]

Selectivity of the catalyst was compared with the CO conversion in the range 1 – 3%, which was achieved by a flow 14 mL·min^{-1} H_2 and 7 mL·min^{-1} CO. The TOF was expressed in 10^{-3} s. The activity was expressed as CTY (CTY, 10^{-5} $mol_{CO}{\cdot}g_{Co}{\cdot}s^{-1}$). The reported CTY, selectivity and TOF are an average of initial activities in the first 16 h of the run, discarding the measurement in the first hour.

X-ray diffraction

X-ray diffraction patterns were acquired at room temperature with a Bruker-AXS D-8 Advance X-ray apparatus using monochomatised $Co_{K\alpha 1,2}$ radiation with λ= 1.79026 Å. The average particle sizes of Co_3O_4 were calculated from

the diffraction line broadening using the Scherrer equation[6] applied to the isolated Co_3O_4 (227) peak, 2Θ = 34°-38°. The mean Co° particle size in the prepared catalysts was obtained from the corresponding Co_3O_4 particle size by applying the molar volume correction, equation [7].[7]

$$d(Co) = \frac{3}{4} \cdot d(Co_3O_4) \qquad [7]$$

Transmission Electron Microscopy

The preparation of the TEM samples is described in the experimental part of chapter 2. The cobalt particle diameters of at least 200 particles for each sample were measured using the iTEM software, Soft Imaging Software GmbH. A sufficient number of particles used for particle size histogram analysis were picked randomly to give a good representation of the system. The oxidic cobalt diameters – Co_3O_4 for the aqueous and ethanol samples and CoO for the acetate samples, as determined with XRD, figure 6 - have been corrected according to equation 8 and 9, respectively.

$$d(Co) = \left(\frac{3 \cdot \rho\,(Co_3O_4) \cdot M_w(Co)}{\rho\,(Co) \cdot M_w(Co_3O_4)}\right)^{1/3} \cdot d(Co_3O_4) \qquad [8]$$

$$d(Co) = \left(\frac{\rho\,(\mathrm{CoO}) \cdot M_w(Co)}{\rho\,(Co) \cdot M_w(\mathrm{CoO})}\right)^{1/3} \cdot d(\mathrm{CoO}) \qquad [9]$$

$$d_{sw} = \left(\frac{\sum n_i d_i^2}{\sum n_i}\right)^{1/2} \qquad [10]$$

$$\sigma = \left(\frac{\sum (d_i - d_{sw})^2}{\sum n_i}\right)^{1/2} \qquad [11]$$

With the corrected sizes the surface-weighted average (d_{sw}) Co° particle sizes were calculated using equation [10][8]. The standard deviation (σ) was calculated assuming a Gaussian spread, equation [11]. In the histogram analysis the Co° particle sizes were distributed over bins sized 0.50 nm with a bin center ranging from 1.0, 1.5, 2.0 .... 20 nm.[1] The effect of binning was checked by varying the bin sizes and/or centers. Since the effect of varying these parameters hardly had any effect on the distributions, one bin size was chosen with accompanying bin center.

Results and discussion

Catalyst preparation

An overview of the IWI prepared catalysts and their properties is shown in table 1. In table 1 ST stands for surface treatment and TT for thermal treatment. The cobalt metal loadings varied from 6.0 to 18 wt%. The theoretical loadings were calculated from the cobalt intake, equation shown in appendix chapter 2 and 3 equation [1]. The cobalt particles sizes were determined with TEM, XRD and H_2 chemisorption.

Table 1. Catalyst codes, preparation procedures, cobalt loadings and cobalt metallic sizes as determined by TEM, XRD and H_2 chemisorption.

Catalyst	ST	Solvent	Precursor	TT	Co (wt %)[k]	TEM $d_{sw}(Co^0) \pm \sigma$[f](nm)	XRD $d(Co^0)$[g] (nm)	H_2 (nm)
INW18	-	Water	Nitrate	A	18	n.d.	7.4[i]	15
INW18-N2	-	Water	Nitrate	B	18	n.d.	4.7	9.4
INW18-NO	-	Water	Nitrate	B	18	3.9±1.3	4.1	8.3
INW11	-	Water	Nitrate	A	11	n.d.	8.5	32
INW10-N2	-	Water	Nitrate	B	10	5.6±1.7	6.1	5.6
INW10-NO	-	Water	Nitrate	B	10	3.2±0.8	2.9	8.3
INE7	-	Ethanol	Nitrate	A	7.2	n.d.	5.3	5.9
INE7-N2	-	Ethanol	Nitrate	B	7.2	6.5±1.8[e]	5.3	8.9
INE8-NO	-	Ethanol	Nitrate	B	7.9	3.6±0.9[e]	3.7	9.0
G-INE8-N_2	G	Ethanol	Nitrate	B[j]	8.3	n.d.	4.7	n.d.
G-INE8-NO	G	Ethanol	Nitrate	B	7.5	3.5±1.0	4.1[i]	n.d.
L-INE8-NO	L	Ethanol	Nitrate	B	8.4	3.4±1.3	3.8	n.d.
IAW6	-	Water	Acetate	A	6.0	n.d.	n.d	n.d.
IAW6-N2	-	Water	Acetate	B	6.0	7.7±3.2	8.2[h]	n.d.
IAW6-NO	-	Water	Acetate	B	6.0	n.d.	4.7[h]	n.d.

A Overnight 393 K in static air.
B Overnight 333 K in static air, subsequent thermal treatment 4 h 523 K ramp 2 K·min^{-1} fluidized bed in a continuous flow of N_2 or NO.

G Gas Phase Oxidation 2.5 h.

L Liquid Phase Oxidation 2 h.

e About 140 particles.

f Mean Co^0 particle size from the corresponding $d(Co_3O_4)$ by applying equation 7.

g Mean Co^0 particle size from the corresponding $d(Co_3O_4)$ by applying the molar volume correction equation 11.

h Used CoO peak 2Θ: 35^0-43^0 to determine crystallite size.

i Used Co_3O_4 peak 2Θ: 74^0-79^0 to determine crystallite size.

j Used a gas flow of 0.5 mL.(min^{-1}.mg^{-1}).

k Assuming cobalt to be in the form Co_3O_4.

TEM images revealed that aqueous impregnations were accompanied with increased clustering of the cobalt precursor on a macroscopic scale as compared to the ethanol impregnations. An aqueous and ethanol impregnation are shown in figure 2 A and B, respectively, dried in static air at 393 K overnight. The reduced clustering observed in the ethanol impregnations can be ascribed to the better wetting of the hydrophobic CNT surface by ethanol. For the aqueous impregnations for which carboxylic groups have been introduced on the CNT surface by liquid phase oxidation as described in chapter 2, a slight improvement on the decrease of clustering on a macroscopic scale can be observed, appendix chapter 2 and 3 figure 5. Nevertheless, the distribution of cobalt clusters is better for the ethanol impregnations as compared to the aqueous impregnated surface treated samples. This solvent effect is less pronounced on a macroscopic scale for the catalysts that have undergone a thermal treatment under N_2 at 523 K. The improved distribution of cobalt particles can be ascribed to redistribution during thermal treatment.[1]

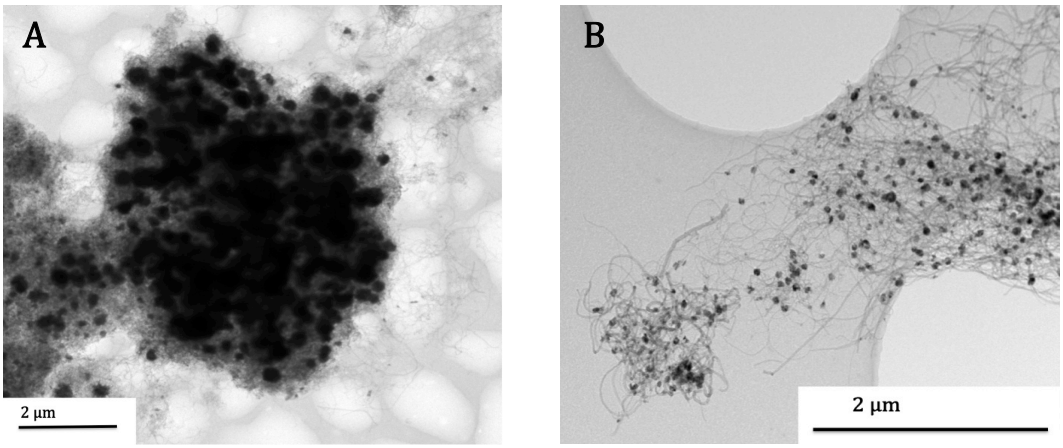

Figure 2. A: INW18. B: INE8.

The trends observed for the cobalt on carbon nanotubes catalysts, thermally treated at 523 K in a N_2 and NO/N_2 atmosphere, are in good accordance with what can be seen for cobalt on silica.[1] Thermal treatment in N_2 gives a broad particle size distribution and thermal treatment in a NO/N_2 atmosphere leads to smaller particles and a narrow particle size distribution, as presented in figure 3 and 4. The narrow particle size distribution is attributed to the prevention of redistribution of cobalt species during this drying procedure.[9, 10, 11]

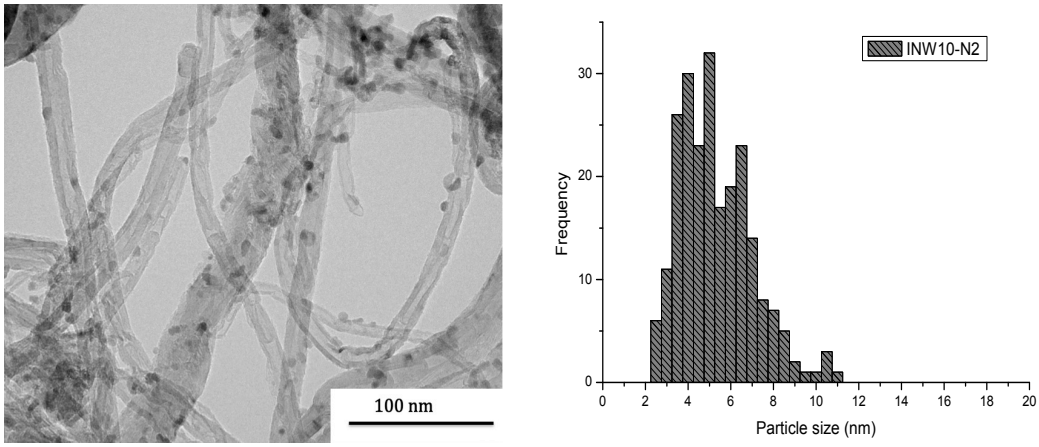

Figure 3. TEM image of catalyst INW10-N_2. *($dCo_{sw} = 5.6 \pm 1.7$ nm).*

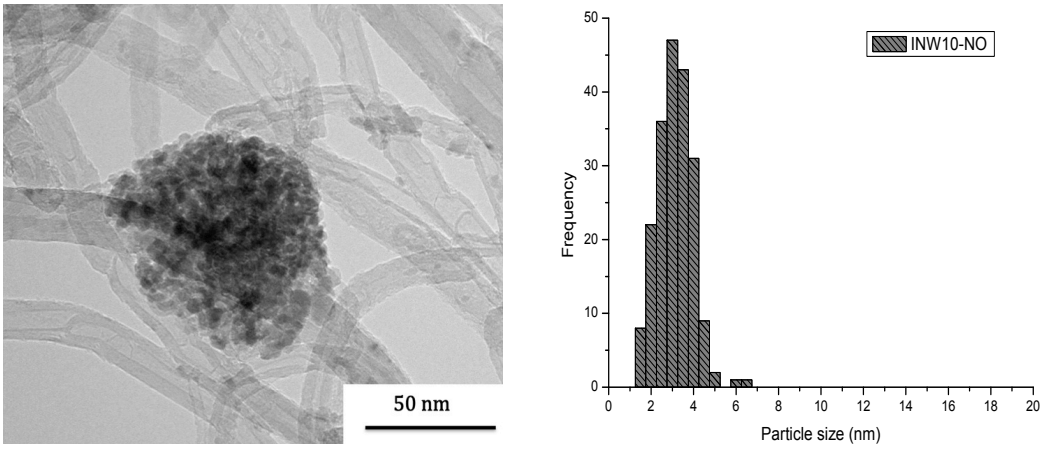

Figure 4. TEM image of catalyst INW10-NO. *($dCo_{sw} = 3.2 \pm 0.8$ nm).*

Wolters[12] reports that the prevention of redistribution can be attributed to the immobilization by means of hydrolysis. Thermal treatment of supported cobalt nitrate on a silica support in the presence of NO results in a rapid and a practically complete decomposition to cobalt hydroxynitrates, while hydrolysis in N_2 is slow and incomplete. Wolters[12] states that these cobalt hydroxynitrate species have a severe reduced mobility as compared to other cobalt species thus preventing long range redistribution. Furthermore it is postulated that the formation of highly dispersed hydroxynitrates in these cobalt on silica supported catalysts are the key to the high dispersion obtained after thermal treatment in nitric oxide. The explanation for this is the close resemblance of cobalt hydroxynitrates to cobalt hydroxides, which are generally less likely to agglomerate than metal nitrate hydrates.

When comparing the Co/CNT aqueous impregnated catalysts thermally treated in nitrogen or nitric oxide, not only a clear difference can be seen in the dispersion of the cobalt particles, but also in the distribution over the surface. As mentioned earlier, the catalysts thermally treated in nitrogen show cobalt particles well distributed over the CNT surface as ascribed to redistribution during drying, figure 3. The nitric oxide samples however show agglomeration of small cobalt particles on the CNT surface, figure 4. It should be mentioned that also individual cobalt particles in the nitric oxide treated samples can be observed. A possible explanation for the agglomeration of small cobalt particles in the aqueous NO treated catalysts, can be found by taking into account the reduced mobility of cobalt hydroxynitrates. During the thermal treatment in nitrogen or nitric oxide, cobalt clusters are broken up into smaller cobalt clusters. In nitric oxide these cobalt clusters are decomposed to hydroxynitrates which have a reduced mobility as compared to other cobalt species. In the case a large cobalt cluster is broken up in an NO atmosphere, the rapid and almost complete decomposition to cobalt hydroxynitrates[12] might be the explanation for the agglomeration of small cobalt particles. Since large clusters of cobalt can be broken into a great number of cobalt hydroxynitrate species, the reduced mobility of these clusters might cause the particles to agglomerate during the further decomposition to cobalt oxide, due to the large number of particles on a relative small area. This can be further supported by considering that in the ethanol impregnations that have been NO treated the clustering of cobalt particles is reduced significantly, figure 5. The better wetting of CNT by ethanol is accompanied by a better distribution of metal precursor and hence smaller cobalt clusters are seen in these samples as for aqueous impregnations, as was shown in figure 2 A and B. Taking into account that the cobalt clusters in the ethanol and aqueous impregnations are decomposed to similar cobalt particles sizes in a NO atmosphere, 3.6 ± 0.9 nm and 3.2 ± 0.8 nm, respectively. It can be assumed that the smaller cobalt clusters present in the ethanol impregnations will lead to a smaller number of cobalt hydroxynitrates during decomposition in NO. Even though the mobility of the cobalt hydroxynitrates is reduced, this reduced mobility possibly has less impact on agglomeration of cobalt particles during complete decomposition of cobalt hydroxynitrate to Co_3O_4 due to the smaller number of particles formed.

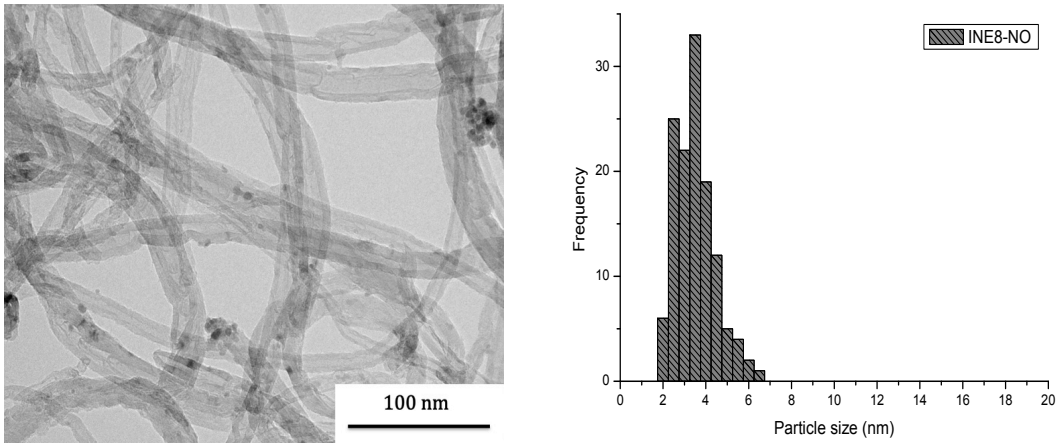

Figure 5. TEM image of catalyst INE8-NO. *($dCo_{sw} = 3.6 \pm 0.9$ nm).*

From the TEM images cobalt particle sizes ranging from 3.2 to 7.7 nm were found, table 4, with standard deviations of around 30 % of the average size.
The particle sizes as determined with the iTEM software were corrected with a correction factor as explained in the experimental part of this chapter. In appendix chapter 2 and 3 figures 4 to 18 an overview is given of all the catalysts that have been analysed with TEM and when determined accompanying particle size histograms* are presented.

The cobalt particle sizes calculated from the H_2 chemisorption measurements varied from 5.6 to 32 nm, table 1. In the H_2 chemisorption the particle sizes decreased with cobalt weight loading, with an exception of INW11, and decreased further when ethanol was used as solvent, probably due to the better wetting properties of ethanol for the hydrophobic tubes. Bezemer[13] reports the same trend for IWI oxidized carbon nanofibers (CNF). These trends were however not seen in the TEM and XRD results, table 1. Neither did the impregnated catalysts with cobalt acetate as a precursor lead to smaller particles as compared to using cobalt nitrate as precursor as was reported for IWI of oxidized CNF.[13]

The cobalt particles are shaped hemi-spherical, except for the acetate impregnations were the particles seem pyramidal, appendix chapter 2 and 3 figure 16.

* The particle size histograms show counts of particles up to of 20 nm, however for reduced INE8-N_2 a few larger particles found as well.

XRD patterns of thermally treated samples are shown in figure 6 with the diffraction lines of the main components indicated. For the CNT support two characteristic diffraction lines are observed.[14] From figure 6 – and diffraction patterns obtained from similar samples, not shown here - it can be seen that after the thermal treatment at 523 K under nitrogen or nitric oxide of a cobalt nitrate impregnated catalysts, cobalt is mainly in the Co_3O_4 state.[15,16] However, it should be mentioned that only crystalline substances are observed with XRD and amorphous phases may also be present. Surprisingly, when cobalt acetate is used as precursor and subjected to a thermal treatment under nitrogen or nitric oxide, mainly diffraction peaks are observed for CoO. This is not in accordance with literature. Xiong et al. have also prepared Co/CNT catalysts using cobalt acetate as precursor following a similar preparation method as described here, and observe Co_3O_4 peaks in the diffraction patterns.[17] Also the particle shapes reported by Xiong et al. are hemispherical where as we observe pyramidal particles. This needs to be further investigated to give an explanation.

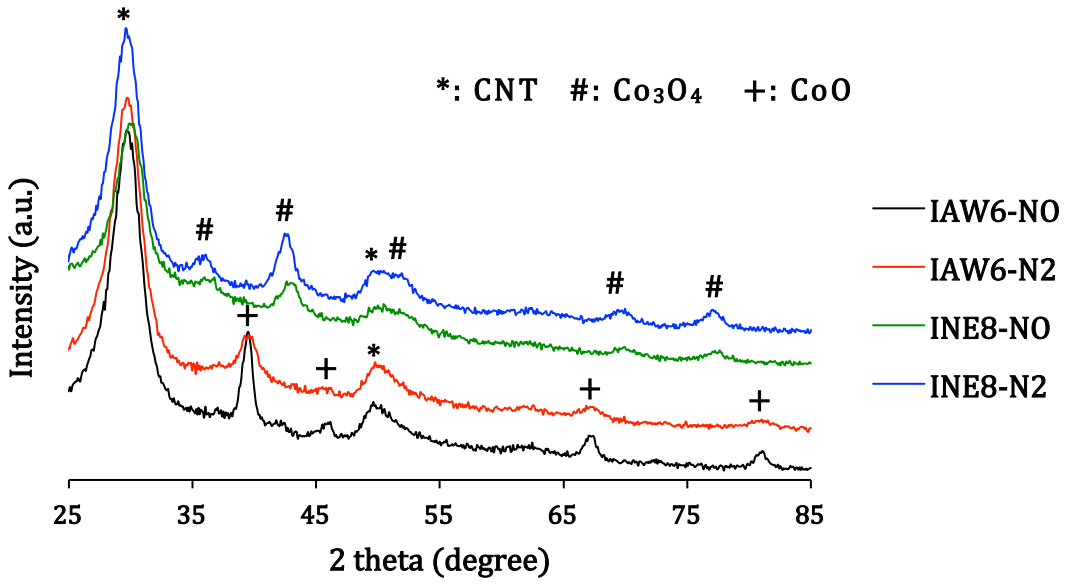

Figure 6. XRD patterns of representative thermally treated samples are shown with the strongest diffraction lines of the main components indicated.

Low pressure catalytic testing

The Co/CNT catalysts were reduced *in* situ prior to catalytic testing. The reduction temperature was selected from a temperature programmed reduction (TPR) measurement, data shown in appendix chapter 2 and 3 figure 2, where reduction onsets of cobalt(II) oxide were apparent around 563 K. Cobalt time yield (CTY) and selectivity were measured at 1 to 3 % CO conversion, with an exception of INW18-N_2 (4.8 %) and INW18-NO (3.8 %). The acetate samples are not presented here due to their low CO conversions. An overview of the catalytic testing results measured at atmospheric pressure is given in table 2. Furthermore the CTY, TOF, methane selectivity and C5+ selectivity is plotted for a selection of catalysts in figure 7 to 10 and in the figures a line is drawn to suggest possible trends. Since the product selectivity of the different catalysts depends strongly on the CO conversion[18] INW18-NO and INW18-N_2 are not plotted in the selectivity plots due to their relatively high CO conversion. The product yield for C_{19+} Fischer-Tropsch products becomes more apparent for higher CO conversions. As can be seen from equation [2] to [5] the product fraction $C_1 - C_{18}$ is considered in the selectivity calculations, X_{CO} and CTY, thus for higher CO conversions the error in these calculations becomes larger.

Table 2. Catalytic properties measured at 493, K atmospheric pressure and H_2/CO v/v 2:1.

Catalyst	TEM $d_{sw}(Co^0)$ $\pm\sigma$	XRD $d(Co^0)$ (nm)	H_2	CTY	TOF	C_1 (wt%)	C_5+ (wt%)	C_5+ (wt%)
INW18	n.d.	7.4	15	1.1	10.0	38	25	25
INW18-N2	n.d.	4.7	9.4	2.8	15.6	37	31	31
INW18-NO	3.9±1.3	4.1	8.3	2.2	11.0	44	23	23
INW11	n.d.	8.5	32	1.0	18.7	36	25	25
INW10-N2	5.6±1.7	6.1	5.6	2.4	7.9	34	39	39
INW10-NO	3.2±0.8	2.9	8.3	2.5	12.4	48	21	21
INE7	n.d.	5.3	5.9	1.5	5.4	32	32	32
INE7-N2	6.5±1.8	5.3	8.9	1.3	7.0	40	28	28
G-INE8-N_2	n.d.	4.7	n.d.	3.2	n.d.	42	28	28
INE8-NO	3.6±0.9	3.7	9.0	4.2	22.5	48	21	21
G-INE8-NO	3.5±1.0	4.1	n.d.	2.5	n.d.	42	28	28
L-INE8-NO	3.4±1.3	3.8	n.d.	1.9	n.d.	36	36	36

CTY : $10^{-5} \cdot mol_{CO} \cdot g_{Co} \cdot s^{-1}$

TOF : $10^{-3} \cdot s^{-1}$

The CTY is in good accordance with what is found in literature.[1,19,20] In figure 7 the CTY is plotted versus the cobalt particle size as determined by TEM, or XRD when TEM data is not available. For comparison the CTY measured by den Breejen[21] and Bezemer[19] are also plotted in figure 7. Going from average particle sizes of 8.5 nm (INW11) to 3.6 nm (INE8-NO), as can be seen in table 2, the CTY increases from 1.0 to 4.2 10^{-5}·mol_{CO}·g_{Co}·s^{-1}. This increase in CTY can be attributed to the increase in cobalt specific surface area when going from larger to smaller particle sizes.

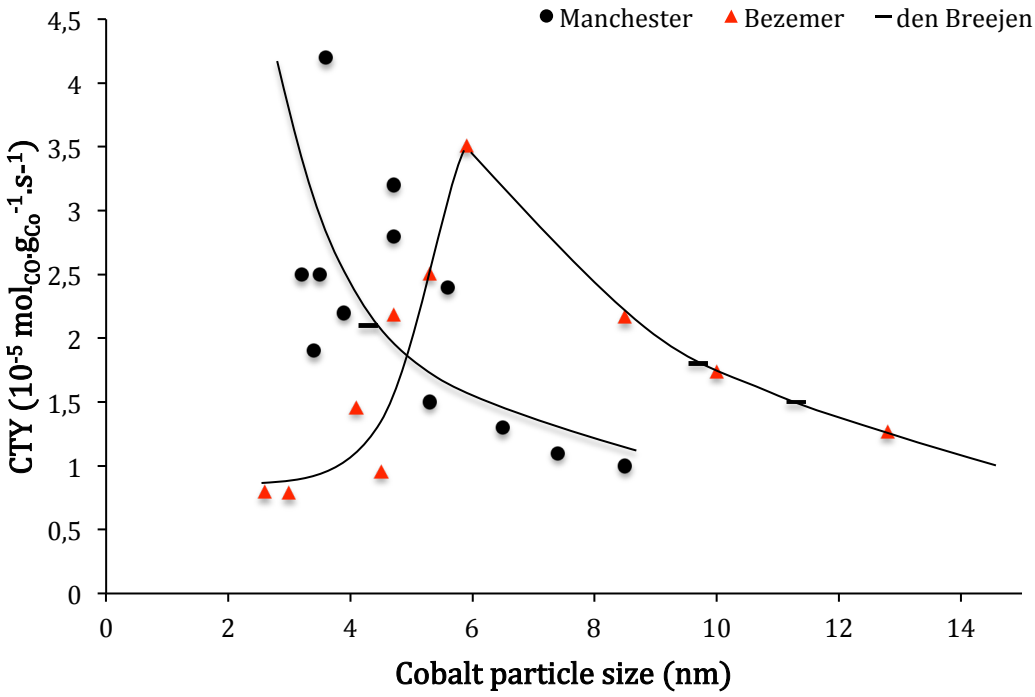

Figure 7. The influence of cobalt particle size on CTY normalized to the cobalt loading measured at 493 K, H_2/CO v/v 2:1 and 1 atm, data obtained by Bezemer[19] and den Breejen[21] are plotted for comparison.

Bezemer et al. however report a limit to the increase in CTY at 6 nm and report a strong decay in activity for particles smaller than this size. This trend cannot be seen in figure 7. The difference in trends can be explained by taking into account that the catalysts reported by Bezemer have been reduced in hydrogen for 2h at 623 K in the catalyst preparation procedure where as the catalysts discussed here have not been reduced before determining the cobalt particle size. During reduction in hydrogen cobalt particles can sinter due to high partial water pressures and an increased temperature thus leading to larger particle sizes.[17] In chapter 2 and 3 figure 11 and 17 the cobalt particle size histograms are shown for samples INE8-N_2 and reduced-INE8-N_2,

respectively. Here an increase in cobalt particle size is seen of 6.5 ± 1.8 nm to 8.8 ± 4.9 nm, respectively. Thus when taking into account the shift to larger particle sizes due to reduction induced sintering the results shown here are in good accordance to the results obtained by Bezemer even though the strong decay in CTY for catalysts with a cobalt particle smaller than 6 nm is not shown here. Possibly the cobalt particle sizes after reduction were not small enough to show this trend.

The turn over frequency (TOF), equation [6] was calculated based on the metallic cobalt surface area determined from H_2 chemisorption measurements. The TOF has been plotted against the cobalt particle sizes in figure 14. The TOF for catalyst INW11 and INE8-NO have been considered as strong outliers and for this reason left out in figure 8. The particle sizes determined with H_2 chemisorption appeared to be ~ 3 times larger than expected giving an error in the calculated cobalt surface area. The TOF in the range is 3.2 to 7.4 nm appears to be rather constant around the $10^{-2} \cdot s^{-1}$. Again considering that the results shown here are of unreduced catalysts it can be explained that a strong decay in TOF is not seen for particles sizes smaller than 6 nm, were the decay observed by Bezemer was explained for both blocking of edge/corner sites and a lower intrinsic activity at the small terraces.

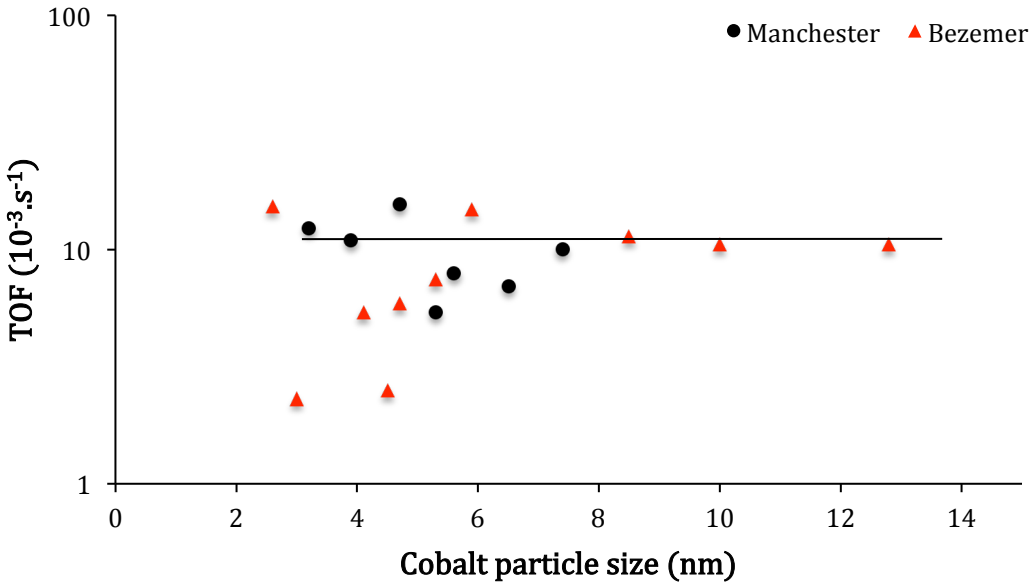

Figure 8. The influence of cobalt particle size on the TOF measured at 493 K, H_2/CO v/v 2:1, 1 atm, data plotted in red obtained from reference [19] for comparison.

The methane selectivity was found to be in the range 32 to 48 % with an average C_1 selectivity for the untreated and surface treated impregnations of 39 % and 40 %, respectively, as can be determined from table 2. In figure 9 the methane selectivity is plotted against the cobalt particle size, for comparison the data obtained by Bezemer and den Breejen are also plotted in figure 9. In this figure INW10-N_2, G-INE8-NO and INE7 are considered as outliers and are encircled with red. From the plot it can be interpreted that the methane selectivity increases for particle sizes smaller than 3.9 nm. Bezemer reports a similar trend for particle sizes smaller than 5 nm. Again considering the sintering effect during hydrogen reduction explains the discrepancy between the results. In literature there is no consensus whether in FT synthesis larger cobalt particles are more selective to higher molecular weight hydrocarbons and the smaller cobalt particles are more selective to methane and light gases.[22] Smaller particles might have a lower abundance of sites active for chain growth. This can result in more carbon species that become hydrogenated to methane, explaining the increase in methane selectivity for smaller particles.

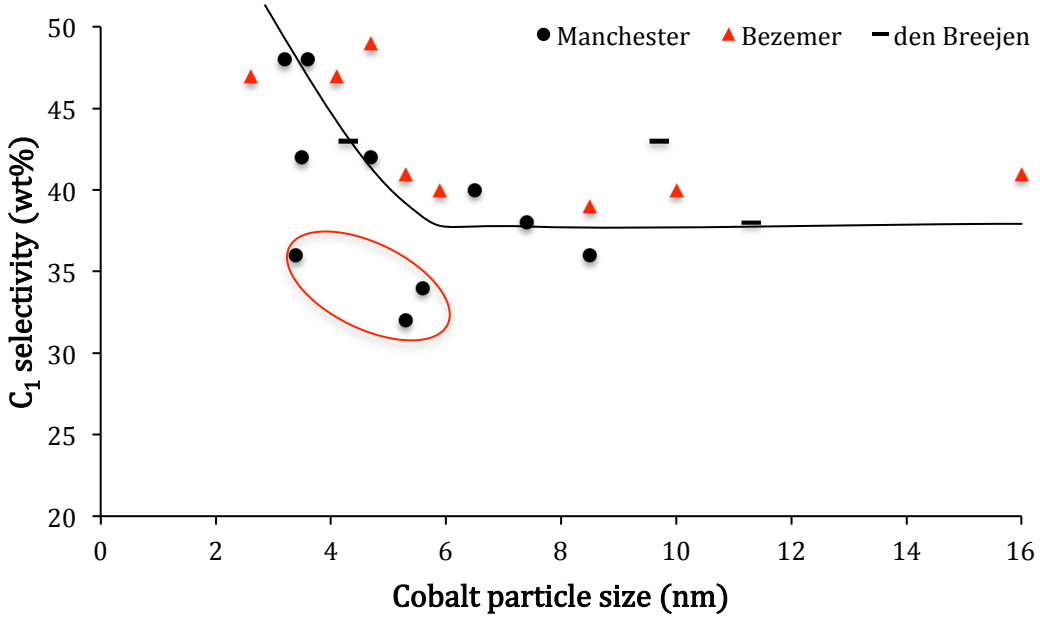

Figure 9. The influence of cobalt particle size on methane selectivity measured at 493 K, H_2/CO v/v 2:1, 1 atm, data obtained by Bezemer[19] and den Breejen[21] are plotted for comparison.

The C_{5+} selectivity was in the range 21 % to 36 %. The average C_{5+} selectivity for the untreated and surface treated impregnations were 27 % and 31 %, respectively. In figure 10 the C_{5+} selectivity is plotted against the cobalt particle size. In this figure INW10-N_2 and L-INE8-NO are considered as outliers and encircled with red. From the figure it can be seen that going from larger particle sizes to 5 nm the selectivity remains more or less constant and for smaller particles sizes the C_{5+} selectivity decreases. The same trend can be seen for the data of Bezemer. However a clear trend is difficult to obtain from this data. A possible explanation for the decrease in C_{5+} formation for smaller particles is that the ratio between edge/corner sites that have a high C_{5+} selectivity is less beneficial for smaller particles.

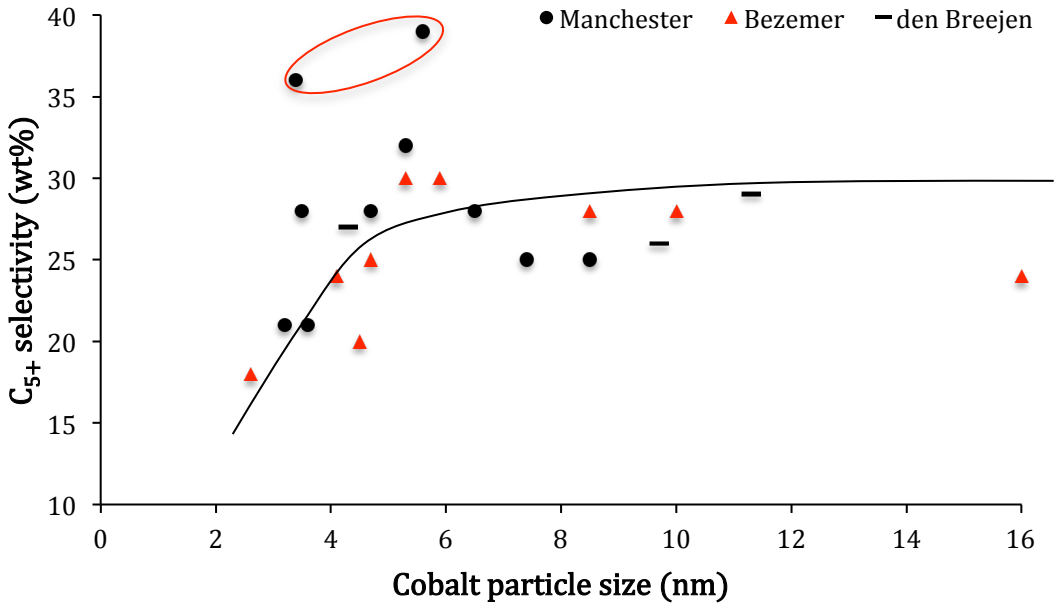

Figure 10. The influence of cobalt particle size on the C_{5+} selectivity measured at 493 K, H_2/CO v/v 2:1, 1 atm, data obtained by Bezemer[19] and den Breejen[21] are plotted for comparison.

Furthermore catalysts INE8-NO, INE8-N_2 and G-INE8-N_2 were tested at above mentioned Fischer-Tropsch conditions however with higher CO conversion and longer reaction times to possibly promote catalyst deactivation. No significant decrease in activity was seen over time. To learn more on the impact of preparation methods on catalytic properties such as activity and stability a series of catalysts was exposed to industrial Fischer-Tropsch conditions in chapter four.

Conclusions

Using cobalt nitrate and cobalt acetate as precursor, dissolved in water or ethanol, a series of cobalt on carbon nanotubes catalysts were prepared with weight loadings varying from 6 to 18 Co wt% and cobalt particle sizes in the range 3.2 to 7.7 nm. An improved distribution of cobalt clusters was seen for the ethanol impregnations as compared to the aqueous impregnations as ascribed to better wetting of the hydrophobic tubes by ethanol. Furthermore, it was demonstrated that the NO calcinations performed in our group on silica[12] can also be applied to cobalt supported on carbon nanotubes. Thermal treatment of the impregnated CNT in nitric oxide was accompanied with smaller cobalt particles and a narrower particle size distribution than after the thermal treatment in nitrogen. However, the catalysts treated in N_2 atmosphere showed an improved distribution of cobalt particles over the CNT surface where as agglomeration of small cobalt particles could be observed after the NO treatment. The agglomeration of small cobalt particles was observed significantly less for the ethanol impregnated catalysts as opposed to the aqueous impregnated catalysts after NO treatment. In the atmospheric pressure Fischer-Tropsch testing, at 493 K and H_2/CO v/v 2:1, the CTY increased going from larger particles sizes to smaller sizes, with the highest activity for catalyst INE8-NO with cobalt particle size of 3.6 ± 0.9 nm and CTY of 4.2. $10^{-5}.mol_{CO}.g_{Co}.s^{-1}$. The methane selectivity showed a strong increase for smaller cobalt particles. A clear trend is difficult to obtain for C_{5+} selectivity. The catalytic testing results were in good accordance with literature, however the trend reported by Bezemer in which a strong decay in TOF for particles smaller than 6 nm is not observed. The results presented here show that higher initial activity and more beneficial selectivity were obtained for catalysts prepared with untreated CNT supports as opposed to catalysts prepared on surface treated CNT supports. This could have serious consequences for the preparation of cobalt on carbon nanotubes catalysts.

[1] den Breejen, J.P., Sietsma, J.R.A., Friedrich, H., Bitter, J.H., de Jong, K.P., Journal of Catalysis 270 (2010) 146.

[2] Matsuzaki, T., Takeuchi, K., Hanaoka, T., Arawaka, H., Sugi, Y., Applied Catalysis A: General 105 (1993) 159.

[3] Kraum, M. Baerns, M., Applied Catalysis A: General 186 (1999) 189.

[4] Martinez, A., Lopez, C., Marquez, F., Diaz, I., Journal of Catalysis 220 (2003) 486.

[5] Bartholomew, C.H., Reuel, R.C., Journal of Catalysis 85 (1984) 63.

[6] Patterson, A.L., Physical Review 56 (1939) 978.

[7] Schanke. D., Vada, S., Blekkan, E.A., Hilmen, A.M., Hoff, A., Holmen, A., Journal of Catalysis 156 (1995) 85.

[8] Anderson, J.R., Structure of metallic catalysts; Academic Press: New York, 1975; Volume 6, Chapter 2.

[9] Sietsma, J.R.A. Friedrich, H. Broersma, A. Versluijs-Helder, M., van Dillen, A.J. de Jongh, P.E. de Jong, K.P., Journal of Catalysis 260 (2008) 227.

[10] Sietsma, J.R.A. Meeldijk, J.D., Versluijs-Helder, M. Broersma, A., van Dillen, A.J., de Jongh, P.E., de Jong, K.P., Chemistry of Materials. 20 (2008) 2921.

[11] Sietsma, J.R.A., Meeldijk, J.D., den Breejen, J.P., Versluijs-Helder, M., van Dillen, A.J., de Jongh, P.E., de Jong, K.P., Angewandte Chemie International Edition 46 (2007) 4547.

[12] Wolters, M., PhD thesis, Utrecht University (2010).

[13] Bezemer, G.L., PhD Thesis, Utrecht University (2006).

[14] Tessonnier, J.P., Rosenthal, D., Hansen, T.W., Hess, C., Schuster, M.E., Blume, R., Girgsdies, F., Carbon 47 (2009) 1779.

[15] Trépanier, M., Tavasoli, A., Dalai, A. K., Abatzoglou, N., Fuel Processing Technology 90 (2009) 367.

[16] Zhang, H., Chu, W., Zou, C., Huang, Z., Ye, Z., Zhu, L., Catalysis Letters 141 (2011) 438.

[17] Xiong, H., Motchelaho, M.A.M., Moyo, M., Jewell, L.L., Coville, N.J., Journal of Catalysis 278 (2011) 26.

[18] Yu, Z., Borg, Ø., Chen, D., Enger, B. C., Frøseth, V., Rytter, E., Wigum, H., Holmen, A. Catalysis Letters 109 (2006) 43.

[19] Bezemer, G.L., Bitter, J.H., Kuipers, H.P.C.E., Oosterbeek, H., Holewijn, J.E., Xu, X., Kapteijn, F., van Dillen, A.J., de Jong, K.P., Journal of the American Chemical Society 128 (2006) 3956.

[20] Thiessen, J., Rose, A., Meyer, J., Jess, A., Curulla-Ferré, D., Microporous and Mesoporous Materials 164 (2012) 199.

[21] den Breejen, J.P., PhD Thesis, Utrecht University (2009).

[22] Tavasol, A., Sadaghiani, K., Nakhaeipour, A., Ghalbi, M., Irannian Journal of Chemistry & Chemical Engineering 26 (2007) 9.

Chapter Four

Study on the effects of possible stabilization methods for cobalt on carbon nanotubes Fischer-Tropsch catalysts

From an industrial perspective cobalt FT catalysts are searched for with a high performance to cost ratio. Numerous research groups have undertaken various attempts to increase the cobalt FT catalyst effectiveness.[1,2,3,4,5] A rational strategy in the search for a highly active catalyst is to improve the cobalt dispersion by decreasing the cobalt particle size. One of the problems facing small cobalt particles on a support material is the tendency of cobalt crystallites to minimize their free surface energy by sintering. This process is accompanied by loss of catalysts active surface area and thus catalytic activity. Sintering is a thermodynamic driven process that is accelerated by high temperatures and the presence of water.[6,7] In industry cobalt based FT is performed at hydrothermal conditions: temperatures of 493 K - 513 K, pressure of 20 - 30 bar and high water vapour pressure[8] due to high CO conversion, favouring sintering.

Different approaches in literature report on improving the stabilization of cobalt on carbon nanotubes and thus the retardation of sintering. Tavasoli et al.[9,10] showed that deposited cobalt particles inside carbon nanotubes show lower rates of sintering than particles deposited on the outside of the tubes.
Theoretical studies reveal that deviation of the graphene layers from planarity causes the π-electron density to shift from the concave inner surface to the convex outer surface, leading to an electron-deficient interior surface and an electron-enriched exterior surface.[11,12,13] Tavasoli and co-workers postulate that due to the electron deficiency of the inner sides of the CNT, the interaction between the cobalt oxides and the support is stronger, leading to lower rates of sintering as compared with the particles located on the outer layers of the CNT. Chen et al.[14] were the first to report this confinement effect and attribute the enhanced stability to the spatial restrictions of the CNT channels for iron on CNT catalysts. The location of cobalt particles inside the tubes might be disadvantageous from a catalytic perspective, due to mass transfer limitations that might arise in the narrow tubes.

Another approach in the abatement of sintering could be by oxidative etching[15] or docking station formation.[16]Carbon in the CNT in contact with calcium carbonate nanoparticles can be selectively oxidized creating docking stations where metal particles can harbour.[15] Graham et al. conclude that the mobility of metallic nanoparticles on carbon nanotubes by using docking

stations is limited based on the excellent stability of the Fischer-Tropsch catalyst.
In a publication by Xiong et al. CNT are reported to act as reducing agent, reducing Co_3O_4 to metallic cobalt. Catalysts prepared from cobalt nitrate by incipient wetness impregnation were heated to 753 K in an inert atmosphere and were autoreduced by the support as determined by TGA, TPR, TEM and *in situ* XRD. Xiong et al. report that the autoreduced catalyst consisted of cobalt particles being embedded in cavities, they assumed that the cavities were produced by the removal of surface carbon that was in contact with the cobalt oxide species prior to reduction,[17,18] as illustrated in figure 1.
Applying this preparation route, the stability of the FT catalyst could be enhanced due to the limitation in the mobility of the metal particles on the support, thus leading to the abatement of sintering.

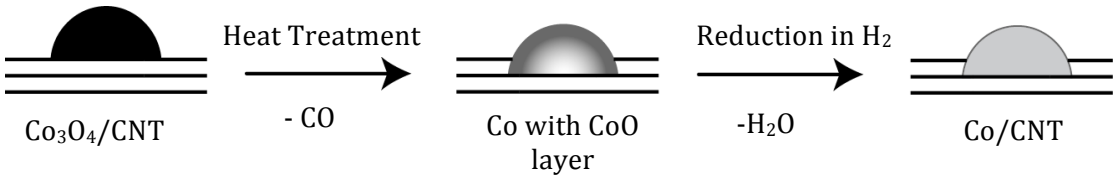

Figure 1. Illustration of the possible autoreduction pathway with Co_3O_4 on CNT.[19]

This work presents a preliminary study on the effects of surface treatment by GPO and LPO, and heat treatment, on the activity and stability of cobalt on carbon nanotubes Fischer-Tropsch catalyst. On the analogy of chapter two, cobalt particles well distributed over the CNT surface were prepared by impregnation of the support with a cobalt nitrate precursor dissolved in ethanol and thermally treated in N_2, 1 % v/v NO/N_2 or air. The heating rate in the thermal treatment step in the catalyst preparation was varied between 2 $K \cdot min^{-1}$ and 0.5 $K \cdot min^{-1}$.[20] Characterization was performed with transmission electron microscopy (TEM) and X-ray diffraction (XRD). Furthermore the autoreduction properties of CNT were studied by subjecting impregnated catalysts in an inert atmosphere to elevated temperatures and analyzing the treated catalysts with XRD, TGA and TEM. Catalytic testing was carried out in a in a Flowrence 16 reactor system by Avantium at 493 K, 503 K and 513 K with a H_2/CO v/v 2:1 at 20 bar syngas pressure.

Experimental

Surface treatment

A selection of catalyst' CNT supports was pretreated in HNO_3 by Gas Phase Oxidation or Liquid Phase Oxidation as described in the experimental part of chapter two, before IWI was conducted.

Catalyst preparation

The catalysts were prepared by IWI of the CNT with 1.0 mL of ethanol solution, at ~ 273 K containing 1.5 M cobalt nitrate (99 % Acros) as precursor. After impregnation the samples were dried overnight at room temperature in static air. Subsequently, the catalysts were subjected to three different drying methods. Batch 1 was dried at 393 K for 12 h in a fluidized bed with a ramp of 0.5 $K{\cdot}min^{-1}$ in a continuous flow of 1 $mL{\cdot}(mg^{-1}{\cdot}min^{-1})$ of N_2, air or 1% v/v NO/N_2, respectively. Batch 1 was coded with four letters indicating surface treatment (when applied), method, precursor and solvent followed by the cobalt loading with an addition of 393 K and the used flow. Batch 2 was dried at 333 K for 6 h and thermally treated for 4h at 523 K in a fluidized bed with a ramp of 0.5 $K{\cdot}min^{-1}$ in a continuous flow of 1 $mL{\cdot}(mg^{-1}{\cdot}min^{-1})$ of N_2 or air, respectively. Batch 2 was coded similar to batch 1, with the addition of 523 K and the used flow. Batch 3 was dried at 393 K for 6 h in a fluidized bed with a ramp of 0.5 $K{\cdot}min^{-1}$ and 20 h at 753 K with a ramp of 2 $K.min^{-1}$ in a continuous flow of 1 $mL{\cdot}(mg^{-1}{\cdot}min^{-1})$ N_2. Batch 3 was designated similar to batch 1, but with the subsequent addition of HT (heat treatment). An example of the different designations possible is illustrated in figure 2. An overview of all the catalysts prepared with their designations and cobalt loadings is given in table 1 in the results and discussion part. The cobalt metal loadings varied from 7.2 to 10 wt %.

X-ray diffraction and Transmission Electron Microscopy

The experimental procedures and equipment used for XRD and TEM are explained in the experimental part of chapter two and three.

Thermal Gravimetric Analysis

Thermal Gravimetric Analysis (TGA) was performed with a Perkin-Elmer Pyris 1 apparatus. Typically 10 mg of sample were heated with a ramp of 5 $K{\cdot}min^{-1}$ from 303 K to 973 K in a 10 $mL{\cdot}min^{-1}$ flow of N_2.

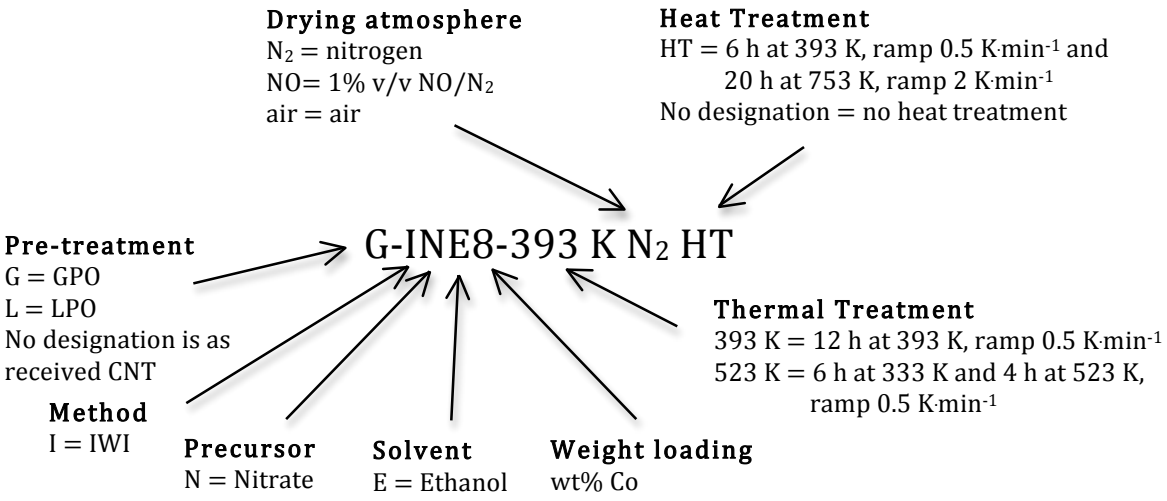

Figure 2. Illustration of the different catalyst designations.

For the preparation method and sample designation of catalysts INE8-NO, G-INE8-NO and L-INE8-NO presented in table 1, the reader is referred to chapter 2. Furthermore catalysts INW10-N2 and INE8-N2, see chapter 2 for preparation details, were subjected to a heat treatment for 4h under a continuous flow of 1 mL·(mg^{-1}·min^{-1}) N_2 at 823 K and 873 K. The reactor containing the sample was inserted into the oven when the designated temperature was reached.

High Pressure Catalytic Testing

The Fischer-Tropsch synthesis was performed at 493 K, 503 K and 513 K in a Flowrence 16 reactor system by Avantium with an H_2/CO v/v 2:1 at 20 bar. The samples were ground and sieved to 75 – 150 μm. Typically 35 mg of sample were diluted with ~ 90 mg of SiC (0.2 mm) and loaded gently into the reactors to prevent demixing of SiC and the catalyst. The samples were dried in a flow of He at 373 K for 2 h. Subsequently, the samples were heated with 1 K·min^{-1} to 623 K and held at this temperature for 8h in a continuous flow of H_2/He v/v 1:3. After this the samples were cooled down to 453 K and pressurized to 20 bar under a flow of H_2. After this the mass flow controller was switched to syngas H_2/CO v/v 2:1, GHSV 1600 h^{-1}, and heated at 493 K, 503 K and 513 K for different durations with a heating ramp of 1 K·min^{-1} between the designated temperatures. After catalytic testing remaining carbonaceous material was removed by hydrogen stripping in a continuous flow of H_2 at 473 K. Under a flow of He the samples were cooled down to

323 K. Online gas chromatography was performed with an Agilent 7890 A GC System, permanent gases are separated in a packed ISC 89019043 column. The hydrocarbons products (C_1-C_9) are separated on a J&W PB-Q column and quantified with a FID. The CO conversion, cobalt time yield and selectivity's were calculated according to equation [1] to [4].

$$X_{CO} = \left(\frac{CO_{flow,in} - CO_{flow,out}}{CO_{flow,in}}\right) \cdot \ 100\ \% \qquad [1]$$

$$CTY = \frac{CO_{flow,in} \cdot X_{CO}}{mCo\ (g) \cdot s} \qquad [2]$$

$$S_{C_1} = \frac{C_{1carbon\ flow}(mL \cdot min^{-1})}{CO_{converted}(mL \cdot min^{-1})} \cdot 100\ \% \qquad [3]$$

$$S_{C_{5+}} = \frac{CO_{converted}(mL \cdot min^{-1}) - \sum_1^4 C_{n\,carbon\ flow}(mL \cdot min^{-1})}{CO_{converted}(mL \cdot min^{-1})} \cdot 100\ \% \qquad [4]$$

In table 2 the reported CTY and selectivity have been determined by discarding the measurements in the first ~ 19 h within a certain temperature regime and the average has been calculated of the remaining measurements, outliers have been excluded.

Results and discussion

Catalyst preparation

An overview of the IWI prepared catalysts and their properties is listed in table 1. In table 1 ST stands for surface treatment and HT for heat treatment.

Table 1. Catalyst codes, preparation procedures, cobalt loadings and metallic sizes as determined by TEM, and XRD.

Catalyst	ST	Solvent	Precursor	HT	Co (wt %)	TEM $d_{sw}(Co^0)$ $\pm\sigma$ (nm)	XRD $d(Co^0)$ (nm)
INE8-393 K N_2	-	Ethanol	Nitrate	C	7.7	3.6±1.4	3.8
INE8-393 K air	-	Ethanol	Nitrate	C	7.7	n.d.	3.8
INE8-393 K NO	-	Ethanol	Nitrate	C	8.5	2.0±0.9[a]	n.d.
G-INE8-393 K N_2	G	Ethanol	Nitrate	C	7.7	2.7±1.1[b]	3.2
L-INE8-393K N_2	L	Ethanol	Nitrate	C	8.4	n.d.	4.4[d]
INE8-393 K N_2 HT	-	Ethanol	Nitrate	D	8.5	6.9±3.8	7.5
G-INE8-393 K N_2 HT	G	Ethanol	Nitrate	D	7.7	4.8±3.8	4.5[e]
L-INE8-393 K N_2 HT	L	Ethanol	Nitrate	D	8.4	6.5±2.2	6.4
INE8-523 K N_2	-	Ethanol	Nitrate	E	7.7	4.9±1.9	4.8
INE8-523 K air	-	Ethanol	Nitrate	E	7.7	n.d.	4.6
INE8-NO	-	Ethanol	Nitrate	B	7.9	3.6±0.9[c]	3.7
G-INE8-NO	G	Ethanol	Nitrate	B	7.5	3.5±1.0	4.1
L-INE8-NO	L	Ethanol	Nitrate	B	8.4	3.4±1.3	3.8
INE7	-	Ethanol	Nitrate	A	7.2	n.d.	7.0
INE7-N_2	-	Ethanol	Nitrate	B	7.2	6.5±1.8[e]	7.1
INE7-N_2 4h 873 K N_2	-	Ethanol	Nitrate	F	7.2	n.d.	n.d.
INW10-N_2	-	Water	Nitrate	B	10	5.6±1.7	8.2
INW10-N_2 4h 823 K N_2	-	Water	Nitrate	F	10	n.d.	n.d.

A Overnight 393 K in static air.

B Overnight 333 K in static air, subsequent thermal treatment 4 h 523 K ramp 2 $K{\cdot}min^{-1}$ in a flow of N_2 or NO.

C Overnight 293 K in static air, thermal treatment 12 h 393 K ramp 0.5 $K{\cdot}min^{-1}$ in a flow of N_2, air or NO.

D Overnight 293 K in static air, heat treatment 6 h 393 K ramp 0.5 $K{\cdot}min^{-1}$ and 20 h 753 K ramp 2 $K{\cdot}min^{-1}$ in a flow of N_2.

E Overnight 293 K in static air, thermal treatment 12 h 333 K ramp 0.5 $K{\cdot}min^{-1}$ and 4 h 523 K ramp 0.5 $K{\cdot}min^{-1}$ in a flow of N_2 or NO.

F Heat treatment, 4 h 823 K and 873 K in a flow of N_2.

G Gas Phase Oxidation 2.5 h.

L Liquid Phase Oxidation 2 h.

a About 100 particles.

b About 60 particles.

c About 140 particles

d Used Co_3O_4 peak 2Θ: 74^0-79^0 to determine crystallite size.

e Used Co_3O_4 peak 2Θ: 40^0-45^0 to determine crystallite size.

The cobalt metal loadings varied from 7.2 to 10 wt %. The cobalt particles sizes were determined with TEM and XRD. From the TEM images cobalt particle sizes ranging from 3.4 to 6.9 nm were determined for the fresh catalysts and 6.2 to 11 nm for the spent catalysts, table 1 and 3. The particle sizes as determined with the iTEM software were corrected with a correction factor as explained in the experimental part of chapter 3, with the assumption that the particles for the spent catalysts and the heat treated catalysts were in the CoO phase. The catalysts that have been analysed with TEM are presented in appendix chapter 4 figures 1 to 20 and when determined accompanying particle size histograms are given.*

TEM images reveal that the catalyst dried at 393 K in N_2 and 1% NO/N_2 with a ramp of 0.5 $K{\cdot}min^{-1}$ have an improved distribution of cobalt clusters over the surface as opposed to the catalyst dried at 393 K in static air, figure 3. From the XRD patterns of the samples INE8-393 K N_2, INE8-393 K air,
INE8-393 K NO and INE8 the difference in decomposition path can be seen for the different drying atmospheres, figure 4. For the nitrogen and air dried samples at 393 K the crystalline Co_3O_4 phase is observed.[21] For the catalyst dried in nitric oxide at 393 K however, a cobalt hydroxide phase was observed, α-$Co_2(OH)_3NO_3$, which is in good accordance with literature.[22] From diffraction line broadening using the Scherrer equation the average crystallite sizes were calculated, and are listed in table 1. Please note that only crystalline substances are observed with XRD and amorphous phases may also be present. The crystallite sizes for the samples dried with a ramp of 0.5 $K{\cdot}min^{-1}$, INE8-393 K N2 and INE8-393 K air, were significant smaller than for the sample dried instantly, INE8, 3.8 nm and 5.3 nm, respectively. For sample INE8-393 K NO the crystallite sizes were probably too small to detect with XRD as line broadening was unsuccessful for this sample.

For the catalysts dried at 523 K in nitrogen and air with a ramp of 0.5 $K{\cdot}min^{-1}$ and 2 $K{\cdot}min^{-1}$, a similar trend was seen as for the samples dried at 393 K. Smaller particles were determined by XRD, table 1, for the samples dried with a slow ramp. XRD patterns are presented in appendix chapter 4 figure 30.

* The particle size histograms show counts of particles up to of 20 nm, however for catalysts INE8-393 K N_2 HT, spent IN8-393 K N_2 HT, L-INE8-393 K N_2 HT, spent L-INE8-393 K N_2 HT, spent G-INE8-NO and spent INE8-NO larger particles were found as well.

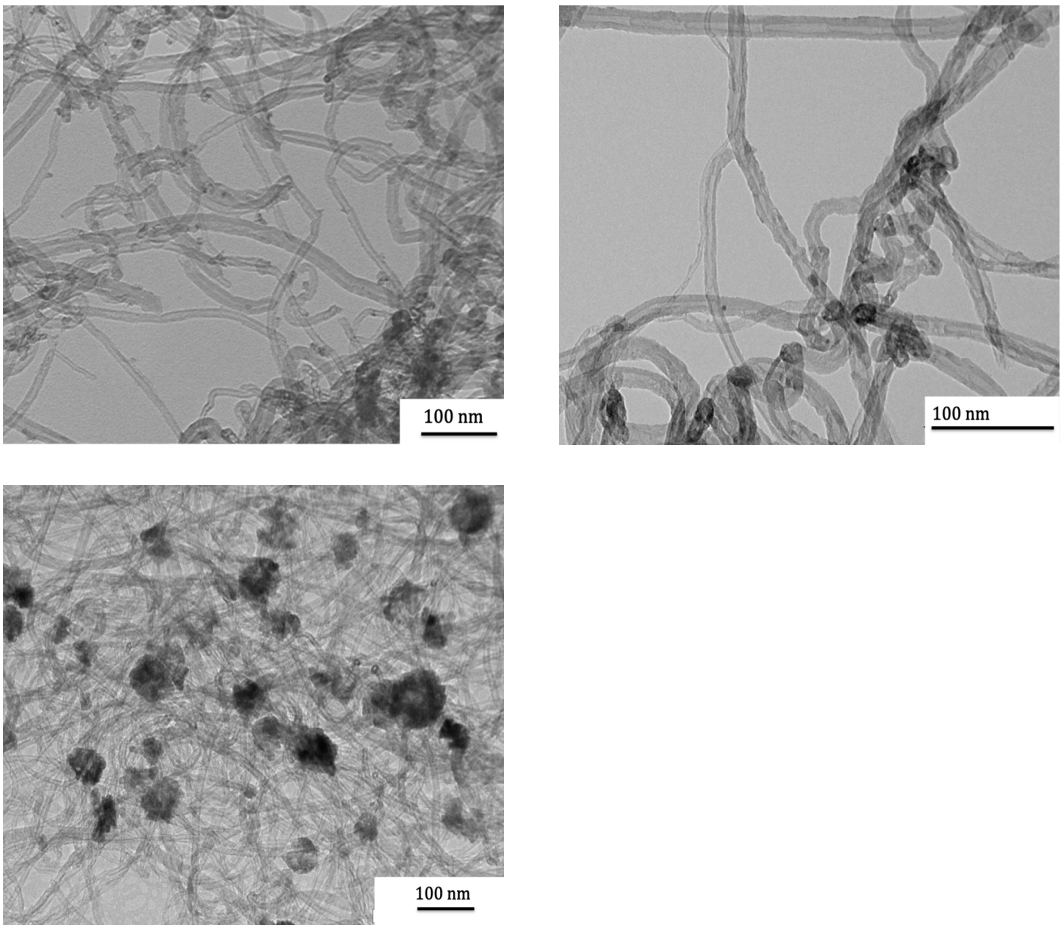

Figure 3. A: INE8-393 K N_2 (ramp of 0.5 K·min^{-1}).
B: INE8-393 K NO (ramp of 0.5 K·min^{-1}). C: INE8 (static air).

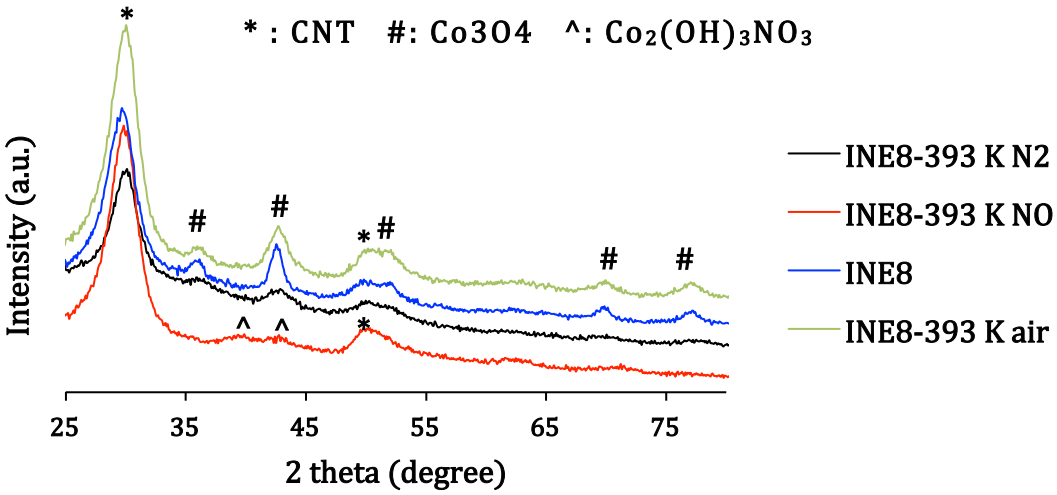

Figure 4. XRD patterns of samples INE8-393 K N_2, INE8-393 K NO, INE8-393 K air and INE8.

We investigate here the possible autoreduction of cobalt supported on CNT by heating a selection of impregnated catalysts to elevated temperatures in an inert atmosphere. Catalysts INE7-N_2 and INW10-N_2 were subjected to heat treatments at 823 K and 873 K under a flow of nitrogen. TEM images of the heat treated catalysts reveal that after heat treatment a light grey passivation layer can be observed around the particles, which can be interpreted as a CoO layer.[23] Before heat treatment the cobalt particles were well distributed over the surface and more or less in a similar size range, table 1, whereas after heat treatment to a great extent empty tubes with large cobalt particles in the middle can be observed. This migration of cobalt particles can be interpreted as sintering. In appendix chapter 4 figures 18 and 19 an overview of the heat treated samples is presented.

Figure 5 illustrates TEM images of sample INW10-N_2, heat treated for 4 h at 873 K in an inert atmosphere. From the EDX lineprofile of the particle shown in figure 6 B, appendix chapter 4 figure 21, it can be seen that the cobalt to oxygen ratio increases significantly when scanning from the outside of the particle to the centre, indicating a metallic core of cobalt. EDX line scans performed on other particles of the heat treated samples INE8-N_2 and INW10-N_2 showed a similar profile.

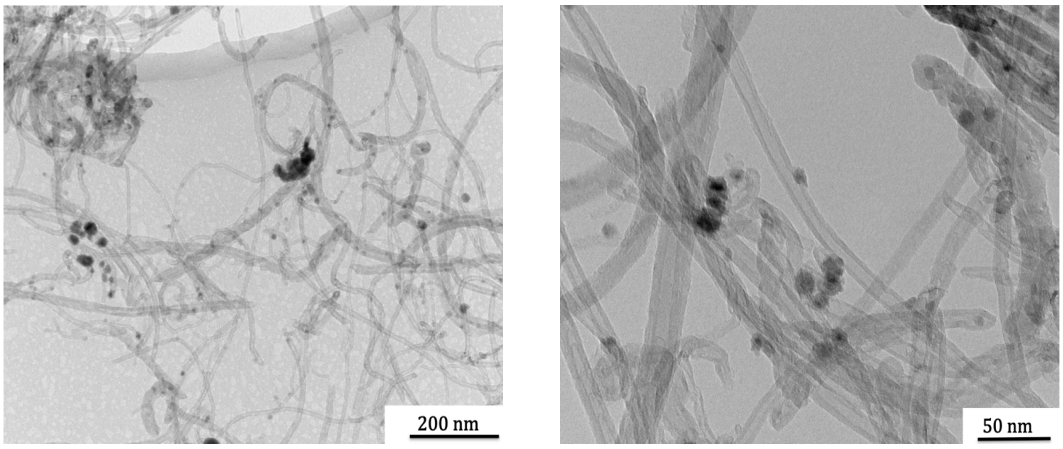

Figure 5. TEM images INW10-N_2 4h 823 K N_2.

From the XRD patterns of sample INE7-N_2 the impact of the heat treatment on the cobalt particles can be seen, figure 6.
For sample INE7-N_2 no peaks are seen for cobalt indicating the cobalt is not crystalline. After heat treatment mainly metallic cobalt peaks are seen,

INE7-N_2 4h 873 K N_2. For sample INE7-N2 it can be seen that the crystalline cobalt is predominantly in Co_3O_4 phase.[21] After heat treatment mainly metallic cobalt peaks are observed.

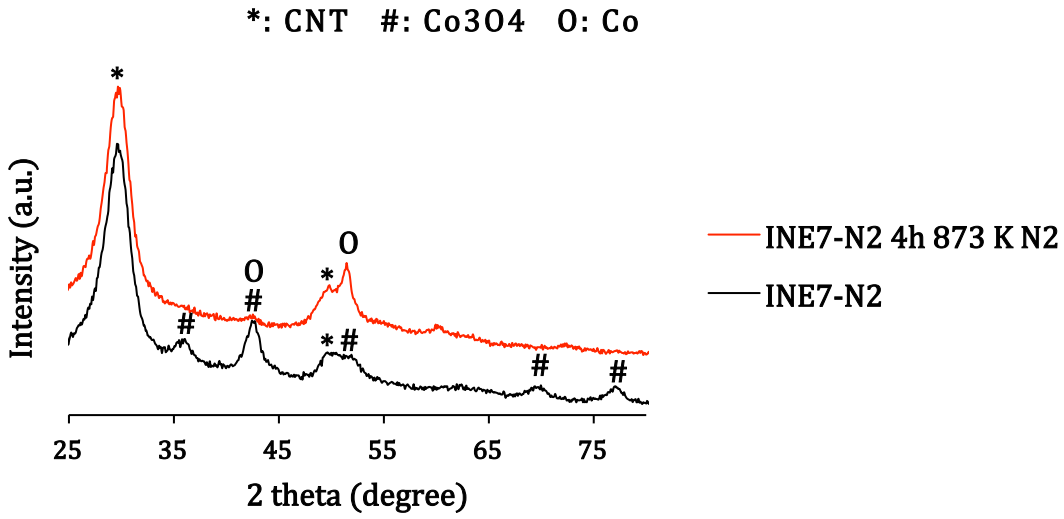

Figure 6. XRD patterns of samples INE7-N_2, INE7-N_2 4h 873 K N_2, IAW6 and IAW6 4h 973 K N_2.

From HSC chemistry calculations, appendix chapter 4 figure 21 and literature[24], it is expected that Co_3O_4 is reduced to metallic cobalt in two steps, shown in equation [5] and [6]. According to HSC chemistry calculations CoO is expected to be stable in the temperature regime 323 K – 723 K and above 723 K Co is more stable.

$$Co_3O_4 + 3\,C \longrightarrow 3\,CoO + 3\,CO \qquad [5]$$

$$CoO + C \longrightarrow Co + CO \qquad [6]$$

TGA measurements were performed to determine the possible weight loss expected due to the oxidation of carbon according to equation [5] and [6]. CNT as received and catalyst INE8-N_2 – having Co_3O_4 supported on the CNT – were subjected to a heat treatment in an inert atmosphere, TGA measurements are presented in figure 7. The slight increase in weight for the CNT curve between 300 K to 750 K can possibly be attributed to buoyancy, since the measurements are not buoyancy corrected. The slight weight loss for the CNT sample above 770 K can be attributed to the loss of non-graphitic carbon.[25] From the INE8-N_2 curve it can be seen that the onset temperature of

the weight loss is ~ 550 K and a strong decrease in weight is seen ~ 850 K. Between 550 K – 670 K a weight loss is expected due to the decomposition of cobalt nitrate that is not in the Co_3O_4 phase.[25] This is not in complete accordance with HSC Chemistry calculations. The deviations can be explained by taking into account that HSC Chemistry calculations are based on thermodynamics whereas kinetics should be taken into account as well, also measurements errors might have an influence on the determined TGA data.

From the stoichiometric calculations the theoretical weight loss for sample INE8-N_2 should be 1.3 % and 3.8 % according to equation [5] and [6], respectively. Xiong et al. report the onset temperature for the autoreduction of Co on CNT at 753 K.[18] From figure 7 it can be seen that the normalized weight loss between 753 K – 859 K is 1.3 % and between 859 K – 973 K this is 4.5 %. This is in good accordance with the stoichiometric calculations. The deviations from the stoichiometric calculations can be explained by taking into account the weight losses due to possible decomposition of cobalt nitrate and the loss of non-graphitic carbon during heat treatment. From the TEM, XRD and TGA observations it can be concluded that the CNT have autoreducing properties. The autoreduction mechanism however still remains unclear. Xiong et al. report that they observe cobalt particles trapped in the tubes from the TEM images suggesting that the carbon at the interface of the cobalt particle is consumed during autoreduction. To further support their observations of cobalt being embedded in the tubes they report that the XRD peak intensity of the CNT between 2θ 20^o – 30^o became weak and the peak became narrower after the heat treatment, suggesting the CNT support was disturbed. Theoretical calculations on the reduction of 1 cobalt particle supported on a CNT suggest that assuming the carbon at the interface is consumed during reduction, the cobalt particles should be easily embedded in the tubes or even dig themselves through all the layers of the tubes, appendix chapter 4 figure 22. Extensive TEM studies however on the catalysts reported here have unfortunately not revealed this.

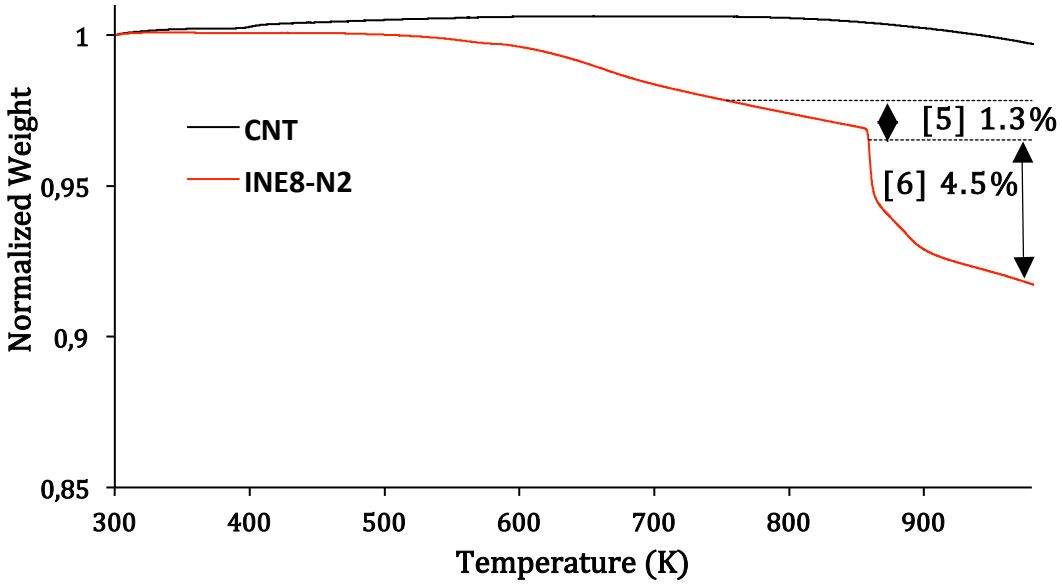

Figure 7. TGA of as received CNT and INE8-N_2.

On the analogy of Xiong et al. the impact of the milder thermal treatment - performed for 20 h at 753 K in a flow of nitrogen - on surface treated and untreated catalysts was studied with XRD and TEM.

From the XRD patterns, presented in appendix chapter 4 figure 30, it can be seen that for sample INE8-393 K N_2 mainly Co_3O_4 diffraction peaks[21] can be observed. After heat treatment, the diffraction pattern of sample INE8-393 K N_2 HT also shows metallic cobalt peaks.[18] Indicating that also under the milder conditions autoreduction can take place. However the weaker intensity and narrowing of the CNT peak at 2θ 20° – 30° was not observed.

The TEM images of the milder heat treated samples reveal that also for these conditions sintering has probably taken place, however this is significant reduced for the surface treated samples. Before the heat treatment the cobalt particles appear to be well distributed over the CNT surface whereas after the heat treatment empty areas without cobalt particles can be observed. Also cobalt particles can be observed that appear to be partly coalesced for catalyst INE8-393 K N_2 HT, encircled in red number 1, figure 8. From figure 9 it can be seen that the distribution of particles over the surface for the surface treated sample, G-INE8-393 K N_2 HT figure 9 B, appears to be better than for the untreated sample after a heat treatment, INE8-393 K N_2 HT, where some agglomeration of particles can be seen, encircled with red 2, figure 8 B. From

the particle size histograms for catalysts INE8-393 N_2 and INE8-393 K N_2 HT, appendix chapter 4 figure 1 and 8, a strong increase in particle sizes is observed, from *3.6 ± 1.4 nm* to *6.9 ± 3.8 nm*. For the surface treated samples the increase in average cobalt particle sizes was significantly less as determined by XRD and TEM. For sample G-INE8-393 K N_2 and G-INE8-393 K N_2 HT this was from *3.2 nm (XRD) to 4.8 ± 3.8 nm* and for sample L-INE8-393 K N_2 and L-INE8-393 K N_2 HT this was from *4.4 nm (XRD) to 6.5 ± 2.2 nm*.

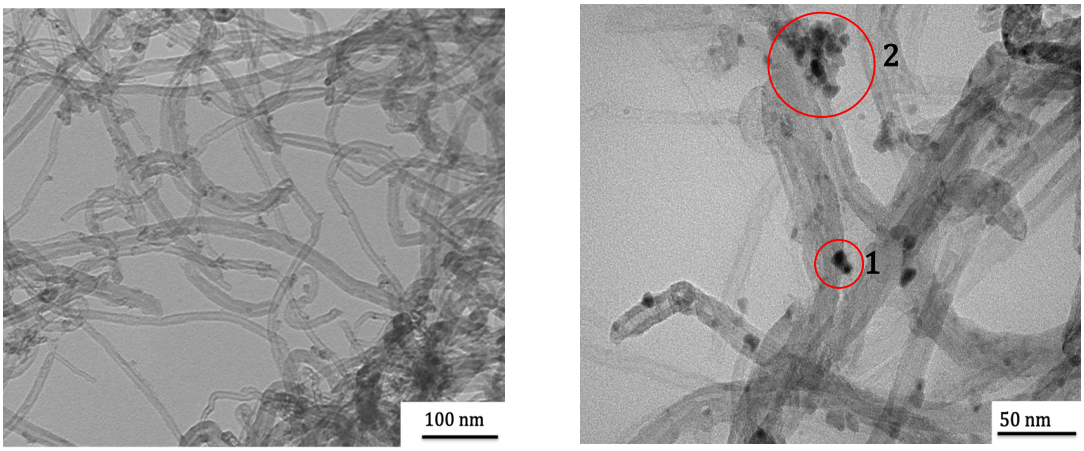

Figure 8. A: INE8 – 393 K N_2 *($dCo_{sw} = 3.6 \pm 1.4$ nm).* B: INE8 – 393 K N_2 HT *($dCo_{sw} = 6.9 \pm 3.8$ nm).*

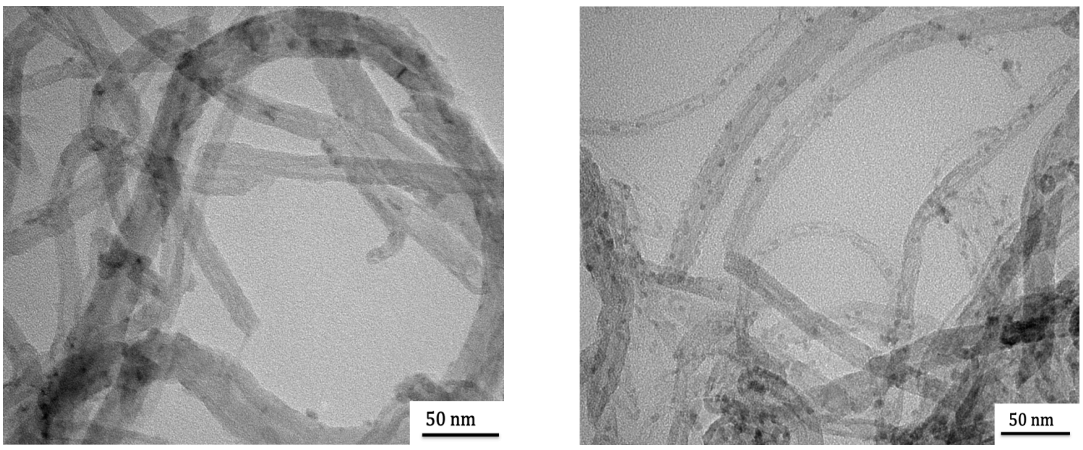

Figure 9. A: G-INE8-393 K N_2 *dCo =3.2 nm.* B: G-INE8-393 K N_2 HT (*$dCo_{sw} = 4.8 \pm 3.8$ nm)*

From the increase in average particle sizes for the surface and untreated catalysts after heat treatment, and the observation of coalesced particles in the TEM images, it can be determined that sintering has taken place during heat treatment. Furthermore it can be observed from the differences in increase in

particle sizes for the different catalysts, that the surface treatment appears to have a stabilizing effect on the cobalt particles, since the average increase in cobalt particles sizes is significantly less for the surface treated catalysts as opposed to the untreated catalyst.

From the particle size histogram of G-INE8-393 K N_2 HT, appendix chapter 4 figure 9, it can be determined that the particles sizes have shifted to smaller and larger particle sizes. This is possibly an indication for the Ostwald ripening sintering mechanism during heat treatment.[6] From the particle size histograms for INE8-393 K N_2 HT and L-INE8-393 K N_2 HT, appendix chapter 4 figures 8 and 10, it can be seen that the particles sizes have shifted to larger particle sizes. This is possibly an indication for the coalescence sintering mechanism during heat treatment.[6] For catalyst INE8-393 K N_2 HT coalescence of cobalt particles is possibly observed in figure 8 B.

Various heat treated samples have been studied with TEM, however, embedded particles have not been identified, even when the sample holder was tilted.

High Pressure Catalytic Testing

High pressure catalytic testing was performed to study the impact of different preparation methods on activity, stability and selectivity under industrial Fischer-Tropsch conditions. In table 2 the CTY and selectivity measured at 20 bar syngas pressure and 493 K, 503 K and 513 K are listed. The reported CTY and selectivity were determined at CO conversion between 4 to 58 %. The CTY at 493 K varied from 3 to 17.10^{-5}·mol_{CO}·g_{Co}.s^{-1}, at 503 K from 4 to $25{\cdot}10^{-5}$·mol_{CO}·g_{Co}·s^{-1} and at 513 K from 5 to 31.10^{-5}.mol_{CO}.g_{Co}.s^{-1}. Unfortunately no selectivity measurements are available at 513 K and neither has CTY been measured in the elapsed runtime 115 h to 168 h, due to problems with the gas chromatograph. To give an overview of the catalytic performances of the different samples the CO conversions are plotted versus the reaction runtime in figure 10, the corresponding CTY graph is plotted in appendix chapter 4 figure 23.

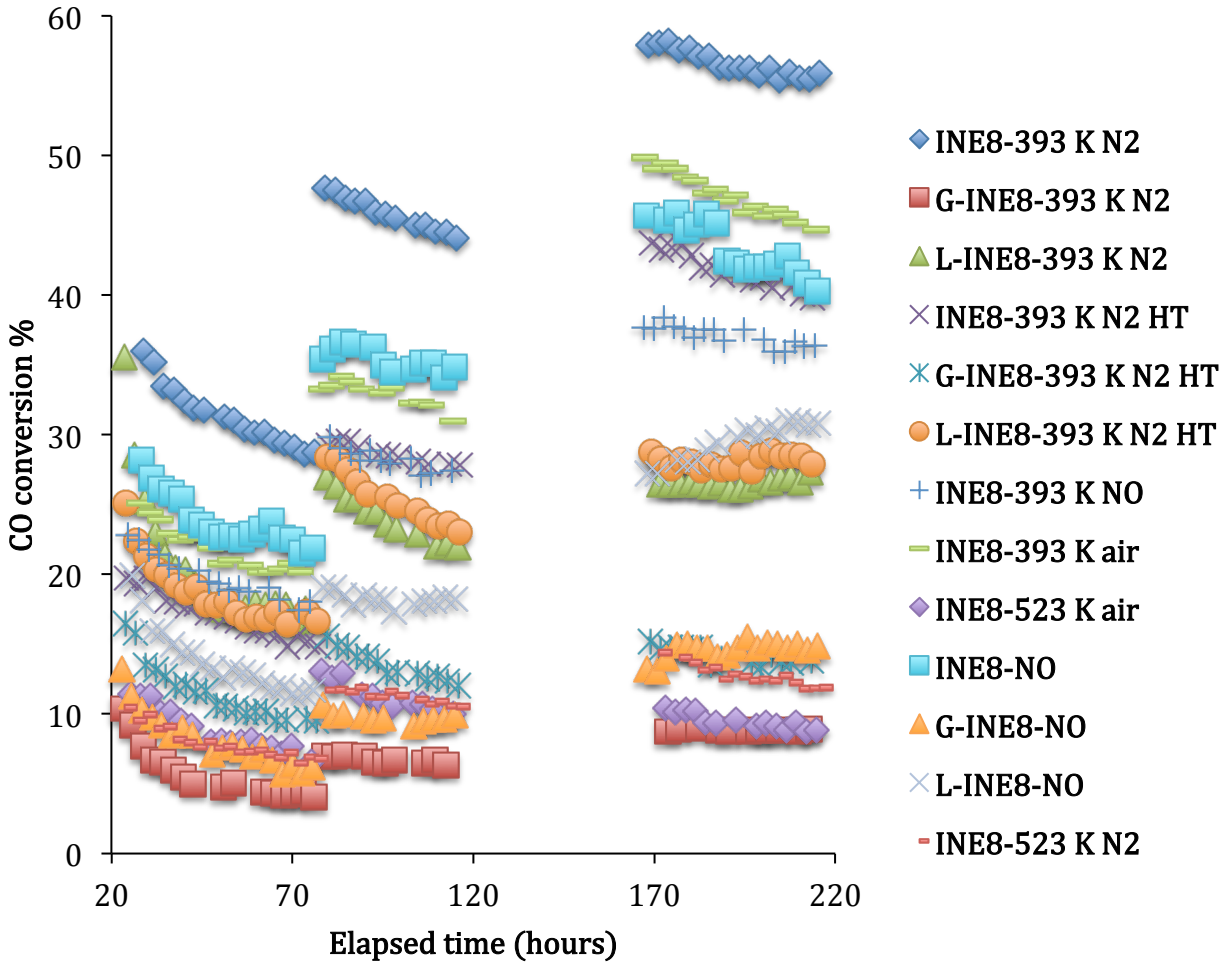

Figure 10. Overview CO conversions measured at 493 K (22 h – 78 h), 503 K (79 h – 167 H) and 513 K (168 h – 216 h), H_2/CO v/v 2:1 at 20 bar syngas pressure.

The apparent activation energy was determined from the slope of the Arrhenius plot assuming first-order kinetics, appendix chapter 4 figure 31. The determined apparent activation energy, listed in table 2 is in good accordance with literature[26] were E_a is expected to be in the range 90 - 110 kJ·mol^{-1}. However, a strong deviation of the expected activation energy is seen for catalysts L-INE8-393 K N_2, G-INE8-393 K N_2 HT and INE8-523 K air which can be interpreted as mass transfer limitations being present or deactivation. From table 2 it can be seen that the methane selectivity increases slightly when the temperature is increased from 493 K to 503 K as is expected since chain termination reactions are favoured at higher temperatures. No clear trend is seen for the C_{5+} selectivity when the temperature is increased. Since the product selectivity of the different catalysts depends strongly on the CO conversion, the selectivity should be compared at the same level of conversion to have a fair comparison.[27] In this study however the range in CO conversion is broad and for this reason trends in selectivity for all catalysts should be discussed carefully. The CO conversions in the text reported for the different are measured at 493 K.

Table 2. Catalytic properties measured at 493 K, 503 K and 513 K, H_2/CO v/v 2:1 at 20 bar syngas pressure.

Catalyst	CTY 493 K	CTY 503 K	CTY 513 K	C_1 493 K	C_1 503 K	C_{5+} 493 K	C_{5+} 503 K	E_a kJ·mol^{-1}
INE8-393 K N_2	17	25	31	12	13	76	77	92
INE8-393 K air	12	19	27	10	11	79	80	101
INE8-393 K NO	10	15	19	12	13	77	77	86
G-INE8-393 K N_2	2,8	4,3	5,5	28	14	51	78	81
L-INE8-393 K N_2	5,2	6,6	7,7	22	25	64	60	55
INE8-393 K N_2 HT	10	17	22	12	12	73	75	119
G-INE8-393 K N_2 HT	5,8	7,1	6,7	22	26	61	57	41
L-INE8-393 K N_2 HT	8,1	11	12	17	19	69	67	61
INE8-523 K N_2	7,3	11	12	18	19	65	66	64
INE8-523 K air	4,5	6,0	5,2	23	25	56	55	26
INE8-NO	12	19	22	10	11	80	79	79
G-INE8-NO	3,3	4,5	6,9	26	31	56	53	98
L-INE8-NO	4,4	6,2	11	28	32	55	52	116

CTY : 10^{-5} .$mol_{CO}.g_{Co}.s^{-1}$

Furthermore, to gain a deeper insight in the loss of activity of the different catalysts over time, the normalized CTY has been plotted versus the elapsed time in figure 11 to 15. The graphs have been normalized by using the first measuring point as normalization constant over the complete temperature range and in the case this point was an outlier, the next available measuring point was used. The accompanying CTY measurements of the normalized samples have been plotted in appendix chapter 4 figures 24 to 28. In origin 8 the normalized graphs were fitted according to a Pow2P2 function using the fitting function. The determined fitting constants are listed in appendix chapter 4 table 1, and an example of a fitted curve is given in appendix chapter 4 figure 31.

Drying atmopsheres

When comparing the INE8-393 K catalysts dried in different gas atmospheres it can be seen in table 1 that the highest CTY - with CO conversion in the range 18 – 28 % - is achieved for the INE8-393 K catalyst dried in N_2, followed by air and then 1% NO/N_2. The normalized CTY is plotted in figure 11. The methane, 10 - 12 %, and C_{5+} selectivity, 76 - 79 %, are in a similar range. The apparent activation energy of these systems are in a similar range 86 – 101 kJ.mol^{-1}, with nitric oxide sample on the low side.

Even though catalysts INE8-393 K NO presumably has the largest cobalt specific surface area of this series, due to the small average particle size for this catalyst, the CTY is lower than for the nitrogen and air dried catalyst. When taking into account the strong decay in TOF as reported by Bezemer[28] for cobalt particles smaller than 6 to 8 nm it might be explained that catalyst INE8-393 K NO shows a lower activity assuming the average particle size is smaller than 8 nm after reduction. Analysing the particle sizes of the spent INE8-393 K N_2 and INE8-393 K air, table 3, from which it can be calculated that the surface area of the nitrogen dried sample is 5 % larger than the air dried sample, does not fully explain the difference in CTY for these samples.

From figure 11 it can be seen that the rate of loss in activity for the nitrogen and nitric oxide sample is more or less similar between 493 K and 513 K. Even though at 493 K the loss in activity for nitric oxide is stronger and at 513 K the loss in activity for nitrogen is stronger, as can be seen from the curve fitting, appendix chapter 4 table 1. For the air dried sample the loss in activity is

similar to nitrogen and nitric oxide at 493 K however at 503 K the loss in activity is slightly steeper for this sample and at 513 K the loss in activity becomes significant stronger. Possibly the INE8-393 K air sample is more sensitive to the increase in temperature.

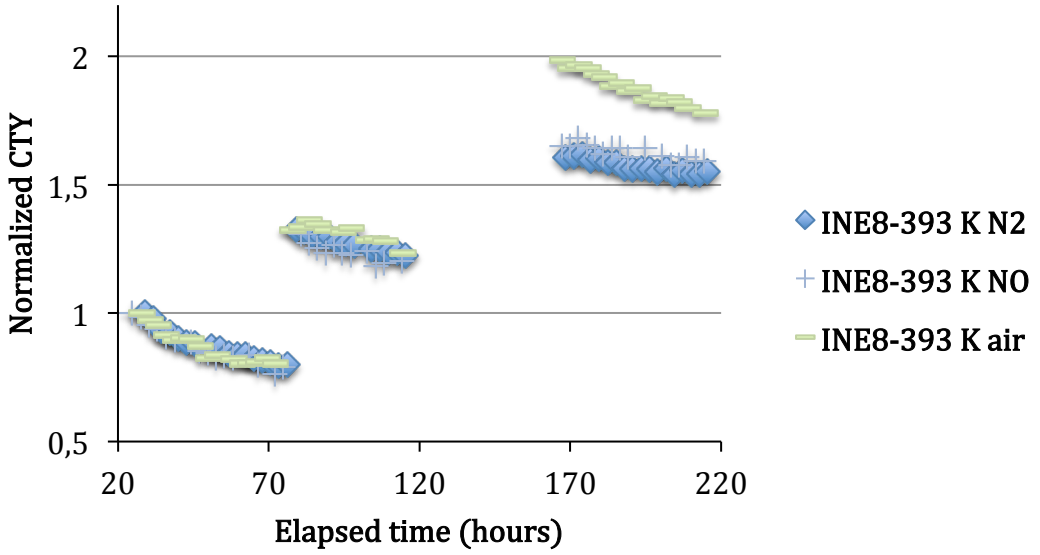

Figure 11. Normalized CTY for catalysts INE8-393 K N_2, INE8-393 K NO and INE8-393 K air measured at 493 K (22 h – 78 h), 503 K (79 h – 167 H) and 513 K (168 h – 216 h), H_2/CO v/v 2:1 at 20 bar syngas pressure.

A comparison of the catalysts INE8-393 K and INE8-523 K, table 2, shows that the highest CTY - with CO conversions in the range 7 – 28 % - is achieved for the catalysts dried at 393 K. For both the air and nitrogen dried samples, drying at elevated temperatures shows a decrease in initial activity. Also the apparent activation energy for the samples dried at 523 K, 26 - 64 $kJ \cdot mol^{-1}$, were significant lower than for the samples dried at 393 K 92 – 101 $kJ \cdot mol^{-1}$. Surprisingly catalyst INE8-523 N_2 has similar activity and selectivity as INE8-393 K N_2 when tested at atmospheric pressure, data not shown here.

In figure 12 the normalized CTY is plotted versus the elapsed time. Overall, the catalysts dried at 523 K show the strongest rate in loss in activity between 493 K and 513 K, with an exception of sample INE8-393 K air at 523 K. Remarkably increasing the temperature hardly has an effect on the CTY of INE8-523 K air. From the normalized curve and the low apparent activation energy it can be observed that strong deactivation has taken place for catalyst INE8-523 K air. Since increasing the temperature has no effect on the activity

of catalyst INE8-523 K air, possibly disaggregation of the support material has taken place in the initial stage of the catalytic testing as brown waxes were collected after the FT run, as can be seen in figure 16.

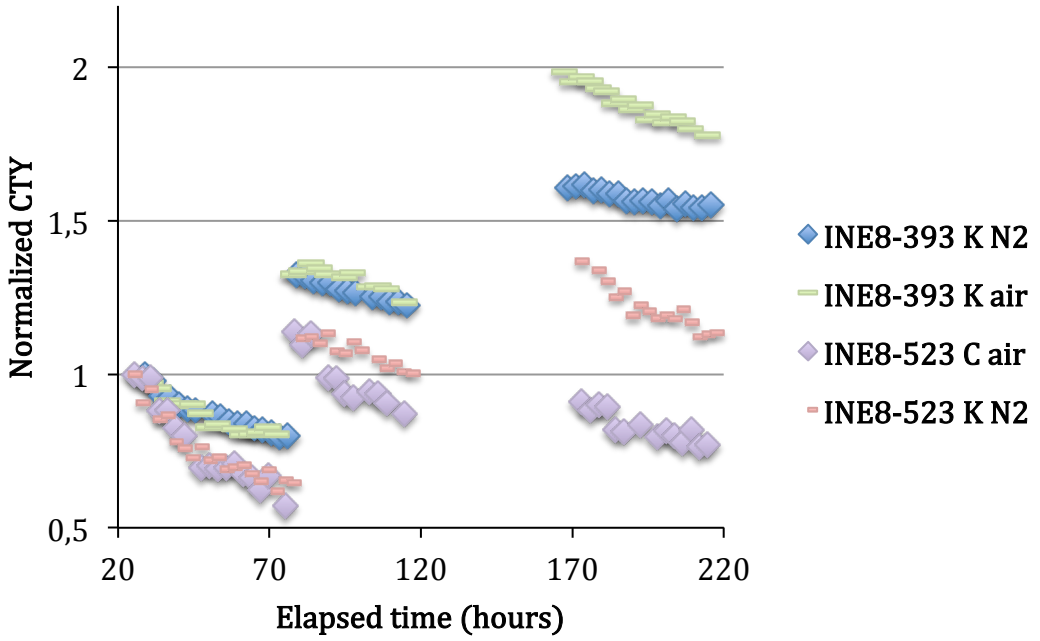

Figure 12. Normalized CTY for catalysts INE8-120 C N_2, INE8-120 C air, INE8-250 C N_2 and INE8-250 C air and measured at 493 K (22 h – 78 h), 503 K (79 h – 167 H) and 513 K (168 h – 216 h), H_2/CO v/v 2:1 at 20 bar syngas pressure.

Surface treatment

The impact of a surface treatment on the catalytic properties for a INE8-NO catalyst was studied. When comparing the surface treated and untreated INE8-NO catalysts it can be seen from table 2 that the highest CTY - with CO conversions in the range 6 – 22 % - is found for an untreated CNT catalyst. The same trend is seen for the atmospheric pressure data, chapter 3. The apparent activation energy for these samples is in a similar range, 79 – 116 kJ.mol^{-1}, with the activation energy for INE8-NO on the low side. The methane selectivity for L-INE8-NO (CO conversion 12 %) is nearly three times as high as for INE8-NO (CO conversion 22 %), and the C_{5+} selectivity is significant lower than for the untreated samples. For the atmospheric pressure testing data, chapter 2, the trend is the opposite. Higher methane selectivity is measured for INE8-NO than L-INE8-NO and higher C5+ selectivity for L-INE8-NO.

From the normalized CTY plot, figure 13, it can be seen that the surface treated samples show a stronger loss in activity at 493 K. Please note that the pressure of the reactor containing sample INE8-NO was unstable during experiment, which might explain the irregular shape of the curve. The LPO treated sample decreases the strongest in the initial part, as was determined by fitting the initial part of the curve, after the strong loss in activity the activity appears to stabilize for this sample. The GPO treated sample however shows the strongest deactivation at 493 K. At 503 K the catalysts appear to stabilize. However at 513 K the surface treated catalysts increase in activity the first ~ 30 hours and stabilises for the remainder of the run, whereas the untreated catalysts loses activity over time.

From the shape of the particle size histograms, appendix chapter 4 figure 13 to 15, and the shift to larger particle sizes it can be hinted that coalescence sintering has prevailed. From table 3 it can be seen that the increase in particle sizes is significant larger for the untreated catalyst. This could be an indication that the surface treatment reduces loss in the activity caused by sintering. Interestingly the loss in activity for the surface treated catalysts is stronger even though the average particle sizes for the untreated catalysts have increased the strongest. This indicates that not all loss in activity can be ascribed to sintering.

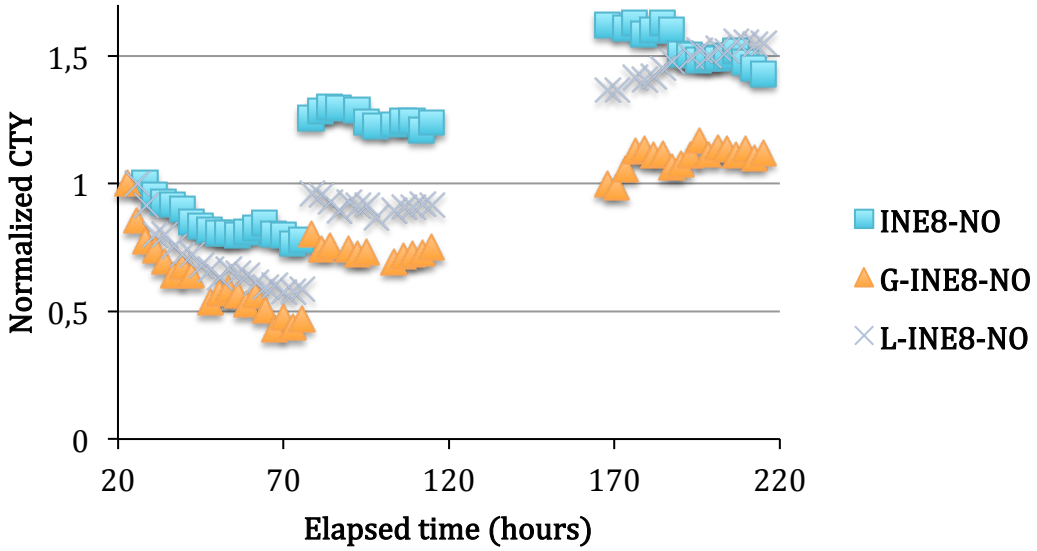

Figure 13. Normalized CTY for catalysts INE8-NO, G-INE8-NO and L-INE8-NO and measured at 493 K (22 h – 78 h), 503 K (79 h – 167 H) and 513 K (168 h – 216 h), H_2/CO v/v 2:1 at 20 bar syngas pressure.

When comparing the surface treated and untreated INE8-393 K N_2 catalysts the same trend can be observed for CTY and selectivity as for the INE8-NO catalysts. From table 2 it can be seen that the highest CTY - with CO conversions in the range 4 – 28 % - is found for the untreated catalyst. The apparent activation energy for catalyst INE8-393 K N_2 and G-INE8-393 K N_2 is in the same range 81 – 92 kJ·mol^{-1}, whereas the activation energy for L-INE8-393 K N_2 is considerably lower, 55 kJ·mol^{-1}.

From the normalized CTY graph, figure 14, a similar trend is seen as for the INE8-NO samples. At 493 K a stronger decrease in activity is seen for the surface treated samples as opposed to the untreated sample. At 503 K the loss in activity for L-INE8-393 K N_2 and INE8-393 K N_2 is similar and loss in activity for G-INE8-393 K N_2 is the smallest, as can be seen from appendix chapter 4 table 1. At 513 K the surface treated samples appear to stabilize whereas the untreated sample, INE8-393 K N_2, loses activity.

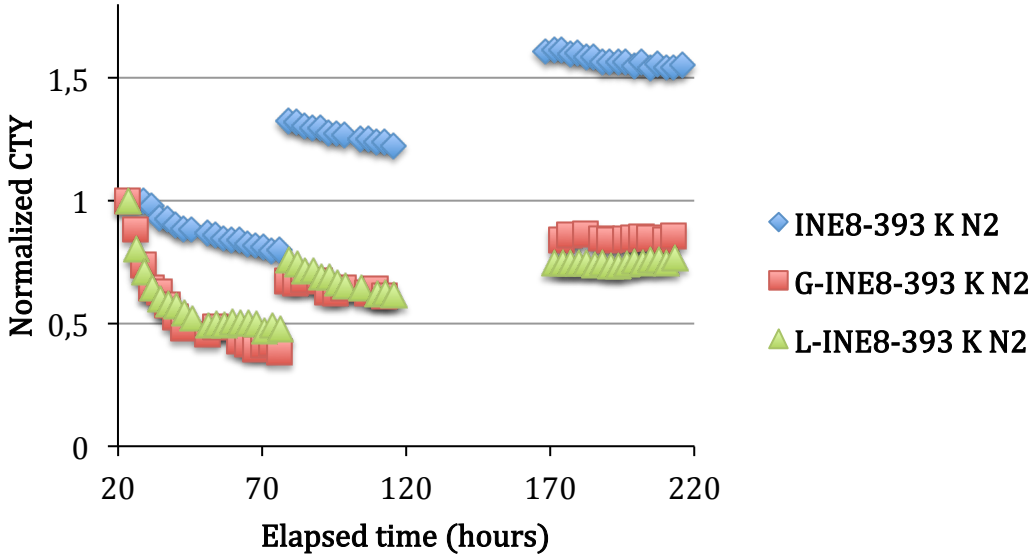

Figure 14. Normalized CTY for catalysts INE8-120 C N_2, G-INE8-120 C N_2 and L-INE8-120 C N_2 and measured at 493 K (22 h – 78 h), 503 K (79 h – 167 H) and 513 K (168 h – 216 h), H_2/CO v/v 2:1 at 20 bar syngas pressure.

Table 3. Cobalt particle sizes of the fresh and spent catalyst.

Catalyst	Fresh TEM $d_{sw}(Co^0)\pm\sigma$	XRD $d(Co^0)$	Spent TEM $d_{sw}(Co^0)\pm\sigma$
INE8-393 K N_2	3.6±1.4	3.8	8.4±2.3
INE8-393 K air	n.d.	3.8	8.8±2.5
INE8-393 K N_2 HT	6.9±3.8	7.5	11±4.7
L-INE8-393 K N_2 HT	6.5±2.2	6.4	8.2±4.0
INE8-NO	3.6±0.9	3.7	8.6±5.6
G-INE8-NO	3.5±1.0	4.1	7.0±2.4
L-INE8-NO	3.4±1.3	3.8	6.2±1.8

Heat treatment

When comparing the catalysts INE8-393 K N_2 and INE8-393 K N_2 HT it can be seen from table 2 that the highest CTY - with CO conversions in the range 15 – 28 % - is achieved for the catalysts that has not been heat treated. Assuming spherical particles and a linear relation between CTY and cobalt surface area, and taking into account that the surface area of the spent INE8-393 K N_2 catalysts is ~ 31 % larger than INE8-393 K N_2 HT, calculated from table 3, then the CTY of the heat treated catalyst approaches the non heat treated catalysts, respectively 31 and $29.10^{-5}\cdot mol_{CO}\cdot g_{Co}\cdot s^{-1}$ at 513 K. The activation energy for these catalysts is in the same range 92 – 119 $kJ\cdot mol^{-1}$.The methane selectivity for INE8-393 K N_2 and INE8-393 K N_2 HT is similar and the C_{5+} selectivity is slightly lower for the heat treated sample, INE8-393 K N_2 shows an increase in C_1 selectivity when the temperature is increased.

From table 2 it can be seen that for the catalysts G-INE8-393 K N_2 and L-INE8-393 K N_2 the CTY increases - with CO conversions in the range 4 – 17 % - after heat treatment. This is the opposite for what is seen for the sample INE8-393 K N_2 catalyst after heat treatment. These observations can be explained by analysing the particle sizes before and after heat treatment. After heat treatment of L-INE8-393 K N2 the cobalt particle sizes increases from ~ 4.4 nm (XRD) to 6.5 ± 2.2 nm, table 2, as explained by Bezemer the TOF decays strongly at for particles sizes smaller than 6 to 8 nm. Possibly the sintering due to the heat treatment has a positive effect on the CTY due to the average increase in particle size to particle sizes with a higher TOF. The activity increases after heat treatment for the surface treated samples. The methane selectivity for heat treated samples is lower than for the non heat

treated samples and the C5+ selectivity is higher for the heat treated samples than for the non heat treated samples.

In figure 15 the normalized CTY is plotted for the heat treated samples and the non heat treated sample. For the INE8-393 K N_2 sample the loss in activity is similar at 493 K and 503 K and at 513 K the sample INE8-393 K N_2 HT shows a stronger loss in activity than for INE8-393 K N_2. For sample G-INE8-393 K N_2 and L-INE8-393 K N_2 the loss in activity at 493 K has decreased after heat treatment. At 503 K the rate in loss in activity is stronger for the heat treated samples than for the non heat treated samples. At 513 K the activity decrease for sample G-INE8-393 K N_2 HT is stronger than for sample for G-INE8-393 K N_2, where stabilization was seen at this temperature. At 513 K the activity appears to stabilize for sample L-INE8-393 K N_2 and L-INE8-393 K N_2 HT.

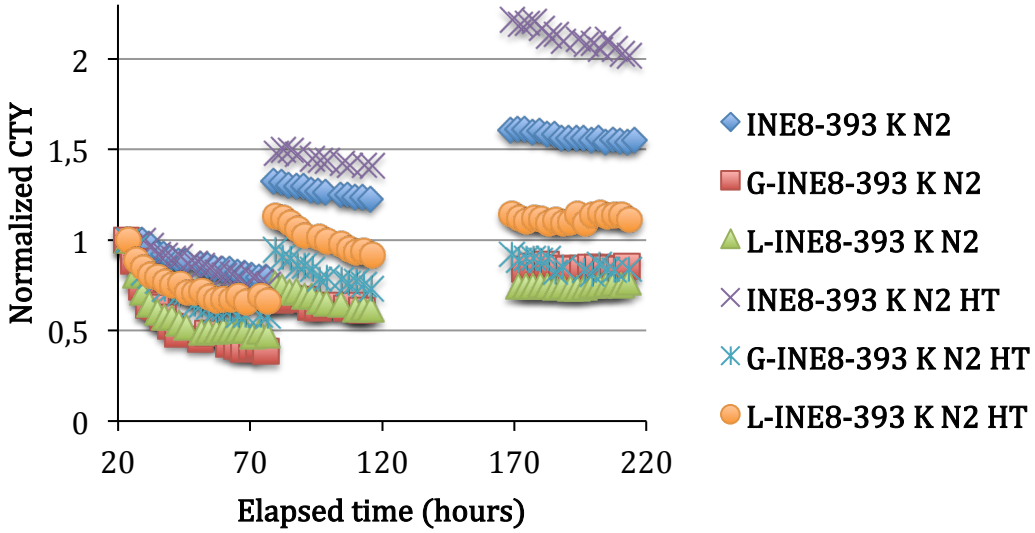

Figure 15. CTY for the catalysts INE8-120 C N_2, G-INE8-120 C N_2, L-INE8-120 C N_2, INE8-120 C N_2 HT, G-INE8-120 C N_2 HT and L-INE8-120 C N_2 HT measured at 493 K (22 h – 78 h), 503 K (79 h – 167 H) and 513 K (168 h – 216 h), H_2/CO v/v 2:1 at 20 bar syngas pressure.

General Discussion

The determined CTY at 493 K, H_2/CO v/v 2:1 at 20 bar syngas pressure – measured at 4 to 29 % CO conversion - is within the range 3 to $17 \cdot 10^{-5} \cdot mol_{CO} \cdot g_{Co} \cdot s^{-1}$ with C_1 selectivity 10 - 28 % and C_{5+} selectivity of 55 – 79 %. The CTY reported here is significant higher than what is reported in literature for cobalt on carbon nanotubes. For surface treated and untreated cobalt on carbon nanotubes catalysts prepared by IWI with 10 – 30 wt% Co dried at 363 - 393 K and thermally treated for 3 - 5 h at 493 – 723 K with a ramp of 1 - 10 $K \cdot min^{-1}$ in a flow of air, Ar or N_2, CTY is reported $2.1 – 7.9 \cdot 10^{-5} \cdot mol_{CO} \cdot g_{Co} \cdot s^{-1}$ – measured at CO conversion 20 – 86 % - with C_1 selectivity 16 - 25 % and C_{5+} selectivity of 68 – 87%.[21,29,30,31,32,33] Interestingly in all the reported literature the highest CTY was measured for the surface treated CNT. The higher CTY was in most cases attributed to cobalt particles having a higher dispersion on the surface treated samples. Also the product distribution was reported to shift to lighter hydrocarbons after LPO treatment. The same is seen here after GPO and LPO treatment here. However, here we report the best catalytic performance for the untreated catalysts dried 12 h at 393 K in a fluidized bed with a ramp of 0.5 $K \cdot min^{-1}$ in a continuous flow of 1 $mL \cdot mg^{-1}$ of N_2, air or 1% v/v NO/N_2, respectively, with measured CTY of $10 – 17 \cdot 10^{-5} \cdot mol_{CO} \cdot g_{Co} \cdot s^{-1}$ - at CO conversion in the range 18 – 28 % - and C_1 selectivity 10 - 12 % and C_{5+} selectivity of 76 – 79 %.

The results presented here stress the importance of various parameters in the preparation of active Co on CNT Fischer-Tropsch catalysts. We conclude here that for the preparation of cobalt on carbon nanotubes catalysts with a high dispersion and good distribution of cobalt particles, and presumably a high activity, surface treatment is not necessarily needed, this can also be achieved by tuning the drying ramp. Furthermore it should be noted that catalyst INE8-NO, which showed an excellent Fischer-Tropsch performance at atmospheric pressure testing, also performed well at 20 bar pressure. CTY at 493 K was measured at $12 \cdot 10^{-5} \cdot mol_{CO} \cdot g_{Co} \cdot s^{-1}$ - with CO conversion 22 % - and C_1 selectivity 10 % and C_{5+} selectivity of 80 %.

To place the above mentioned results in perspective, at 493 K and 20 bar pressure and operating at high CO conversions the FT synthesis rate of commercial alumina, silica and titania supported catalysts is

0.25 - 0.32 $g_{CH}{\cdot}g_{cat}^{-1}{\cdot}h^{-1}$ with C_1 and C_{5+} selectivity of 4 to 6 % and 86 to 93%, respectively.[34 35 36] The best performing catalysts reported here was INE8-393 K N_2 with a FT synthesis rate of 0.64 $g_{CH}{\cdot}g_{cat}^{-1}{\cdot}h^{-1}$ at a CO conversion of ~ 29 % and C_1 and C_{5+} selectivity of 13 % and 77 %, respectively. This shows the potential for cobalt on carbon nanotubes catalysts in terms of activity.

The impact of the stabilizing measures, surface and heat treatment, overall was negative on the initial activity. An exception were the surface treated samples followed by a heat treatment. The increase here is explained by particles sintering to more beneficial particle sizes for the Fischer-Tropsch catalysis. Overall the surface treated and the surface and heat treated samples stabilize at 513 K, an exception here is INE8-393 K N_2 HT, the catalyst loses activity in the temperature regime 493 – 513 K. The question remains if this stability at 513 K can be ascribed to the stability measures taken by means of surface and heat treatment, or to the significant loss in activity these catalysts experience during the initial part of the testing. Especially the surface treated catalysts who lose half of their initial activity after ~50 h at 493 K are critical.
Interestingly Xiong et al. report that the impregnated catalysts thermally treated at 753 K Fischer-Tropsch tested at 498 K H_2/CO v/v 2:1 at 8 bar pressure show good stability. From the reported CO conversion versus time on stream plot no significant loss of activity is seen over 260 hours. Also the highest reported CTY for a 15 wt% Co impregnated CNT is $639{\cdot}10^{-5}{\cdot}mol_{CO}{\cdot}g_{Co}{\cdot}s^{-1}$, this is a factor 100 higher than above reported values, which is quite surprising.

From the normalized CTY curves it can be seen that the first part of the deactivation curves is steeply sloped and the results obtained by curve fitting in the temperature regime of 493 K can be fitted by a power function.
In the case the fit was linear this would suggest that the order in deactivation to CO conversion is zero and the FT deactivation rate is solely caused by exterior factors.[35,37] Nevertheless, the initial part of activity loss can probably be ascribed to pore filling. Even though the total pore volume of the surface treated samples, ~ 1.4 $mL{\cdot}g^{-1}$, is larger than the untreated samples, ~ 1.2 $mL.g^{-1}$, this is not a complete explanation for the difference in initial deactivation for the samples. Disaggregation of the CNT support material could also be an explanation for the significant loss in activity over time. In figure 16 an image is shown with the waxes collected after a FT run for a cobalt

on carbon nanotube catalyst and a cobalt on silica catalyst. In the image it can be seen that the waxes in the right image, Co/CNT, are coloured darker than the waxes in the left image, Co/SiO_2. This is an indication that the CNT and supported cobalt have ended up in the final Fischer-Tropsch products. This possibly plays an important factor in the loss in activity for the different catalysts. The catalysts were grinded prior to catalytic testing, possibly smaller fractions were also present and were transported through the catalyst bed during catalytic testing. Also the surface treatments by oxidation might have also played a role. Especially the LPO treatment is a harsh treatment on the tubes, as is discussed in chapter 2.

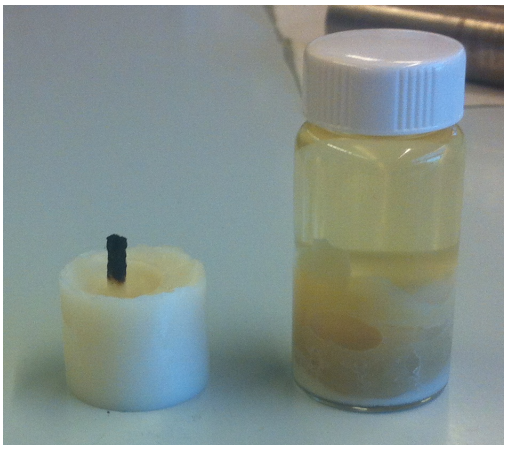

Figure 16. Image of waxes collected after FT synthesis for Co/SiO_2 (left) and Co/CNT (right) catalysts.

Conclusions

Using IWI a series of cobalt on carbon nanotubes catalysts with weight loadings of 7.2 - 10 wt % and average cobalt particle sizes ranging from 3.4 to 6.9 nm were prepared. Drying the impregnated catalysts with a ramp of 0.5 $K \cdot min^{-1}$ improved the dispersion of cobalt particles and the distribution of cobalt particles over the CNT surface as compared to drying with a ramp of 2 $K \cdot min^{-1}$ or instantaneous.

The autoreduction properties of CNT for cobalt catalysts supported on CNT and thermally treated in an inert atmosphere at 753 K – 973 K have been confirmed by TEM, TGA and XRD. The embedding of cobalt particles, due to the possible oxidation of carbon at the interface of cobalt particles, has not been observed.

Furthermore the impact of stabilization measures by means of surface and heat treatment on catalysts properties and performance were studied. The heat treatment was accompanied by sintering of cobalt particles. However the surface treated catalysts were accompanied by a significantly smaller increase in cobalt particle size after heat treatment.

Overall the surface treated systems were accompanied with a stronger initial loss in CTY as opposed to the non surface treated systems. At elevated temperatures the surface treated catalysts stabilized in activity whereas the untreated systems deactivated over time. The heat treated catalysts did not show an improved stability during catalytic testing.

The best catalytic performance was achieved for the untreated catalysts dried 12 h at 393 K in a fluidized bed with a ramp of 0.5 $K \cdot min^{-1}$ in a continuous flow of 1 $mL \cdot (mg^{-1} \cdot min^{-1})$ of N_2, air or 1% v/v NO/N_2, respectively, with measured CTY of 10 – $17 \cdot 10^{-5} \cdot mol_{CO} . g_{Co} . s^{-1}$ - at CO conversion in the range 18 – 28 % - and C_1 selectivity 10 - 12 % and C_{5+} selectivity of 76 – 79 %.

[1] den Breejen, J.P., Frey, A.M., Yang, J., Holmen, A., Schooneveld, M.M., Groot, F.M.F., Stephan, O., Bitter, J.H., de Jong, K.P., Topics in Catalysis 54 (2011) 768.

[2] Chen, J., Zhang, Y., Tan, L., Zhang, Y., American Chemical Society 50 (2011) 4212.

[3] Zhao, Y., Zhang, Y., Chen, J., Li, J., Liew, K., Ridzuan, M., Nordin, B., ChemCatChem 4 265.

[4] Girardon, J., Lermontov, A., Gengembre, L., Chernavskii, P., Gribovalconstant, A., Khodakov, A.Y., Journal of Catalysis, 230 (2005) 339.

[5] Chen, L., Shen, J., Chinese Journal of Catalysis 33 (2012) 621.

[6] Bartholomew, C.H., Applied Catalysis A: General 212 (2001) 17.

[7] Bezemer, G.L., Remans, T.J., van Bavel, A.P., Dugulan, A.I., Journal of the American Chemical Society 132 (2010) 8540.

[8] Khodakov, A.Y., Chu, W., Fongarland, P., Chemical reviews 107 (2007) 1692.

[9] Dalai, A. K., Tavasoli, A., Sanaz, A., Trepanier, M., Iranian Journal of Chemistry and Chemical Engineering 30 (2011) 37.

[10] Tavasoli, A., Tre, M., Dalai, A. K., Abatzoglou, N., Journal of Chemical & Engineering Data 55 (2010) 2757–2763.

[11] Haddon, R.C., Science 261 (1993) 1545.

[12] Ugarte, D., Chatelain, A., Deheer, W.A., Science 274 (1996) 1897.

[13] Shan, B., Cho, K., Physical Review B 73 (2006) 081401.

[14] Chen, W., Fan, Z., Pan, X., Bao, X., Journal of the American Chemical Society 130 (2008) 9414.

[15] Landau, M.V., Savilov, S.V., Ivanov, A.S., Lunin, V.V., Titelman, L., Koltypin, Y., Gedanken, A., Journal of Materials Science 46 (2010) 2162.

[16] Graham, U.M., Dozier, A., Khatri, R.A., Bahome, M.C., Jewell, L.L., Mhlanga, S.D., Coville, N.J., Dabis, B.H., Catalysis Letters 129 (2009) 39.

[17] Xiong, H., Moyo, M., Rayner, M.K., Jewell, L.L., Billing, D.G., Coville, N.J., ChemCatChem 2 (2010) 514.

[18] Xiong, H., Motchelaho, M.A.M., Moyo, M., Jewell, L.L., Coville, N.J., Journal of Catalysis 278 (2011) 26.

[19] Eschemann, T.O., Project proposal: preparation of Carbon-stabilized Co-catalysts for the Fischer-Tropsch reaction, Utrecht University (2011).

[20] van de Loosdrecht, J., Barradas, S., Caricato, E.A., Ngwenya, N.G., Nkwanyana, P.S., Rawat, M.A.S., Sigwegbela, B.H., van Berge, P.J., Visagie, J.L., Topics in Catalysis 26 (2003) 121.

[21] Zhang, H., Chu, W., Zou, C., Huang, Z., Ye, Z., Zhu, L., Catalysis Letters 141 (2011) 438.

[22] Wolters, M., PhD thesis, Utrecht University (2010).

[23] Bezemer, G.L., PhD Thesis, Utrecht University (2006).

[24] Lü, J., Huang, C., Bai, S., Jiang, Y., Li, Z., Journal of Natural Gas Chemistry 21 (2012) 37.

[25] Xiong, H., Motchelaho, M.A.M., Moyo, M., Jewell, L.L., Coville, N.J., Journal of Catalysis 278 (2011) 26.

[26] Thiessen, J., Rose, A., Meyer, J., Jess, A., Curulla-ferré, D., Microporous and Mesoporous Materials 164 (2012) 199.

[27] Yu, Z., Borg, Ø., Chen, D., Enger, B. C., Frøseth, V., Rytter, E., Wigum, H., Holmen, A., Catalysis Letters 109 (2006) 43.

[28] Bezemer, G.L., Bitter, J.H., Kuipers, H.P.C.E., Oosterbeek, H., Holewijn, J.E., Xu, X., Kapteijn, F., van Dillen, A.J., de Jong, K.P., Journal of the American Chemical Society 128 (2006) 3956.

[29] Trépanier, M., Tavasoli, A., Dalai, A. K., Abatzoglou, N., Applied Catalysis A: General 353 (2009) 193.

[30] Trépanier, M., Tavasoli, A., Dalai, A. K., Abatzoglou, N., Fuel Processing Technology 90 (2009) 367.

[31] Trépanier, M., Dalai, A.K., Abatzoglou, N., Applied Catalysis A: General 374 (2010) 79.

[32] Lv, J., Ma, X., Bai, S., Huang, C., Li, Z., Gong, J., International Journal of Hydrogen Energy 36 (2011) 8365.

[33] Zhang, H., Lancelot, C., Chu, W., Hong, J., Khodakov, A.Y., Chernavskii, P. A., Zheng, J., Tong, D., Journal of Materials Chemistry 19 (2009) 9241.

[34] Jacobs, G., Patterson, P.M., Das, T.K., Luo, M., Davis, B.H., Applied Catalysis A: General 270 (2004) 65.

[35] Tavasoli, A., Irani, M., Malek Abbaslou, R.M., Trepanier, M., Dalai, A.K., Canadian Journal of Chemical Engineering 86 (2008) 1070.

[36] Tavasoli, A., Sadagiani, K., Khorashe, F., Seifkordi, A.A., Rohani, A.A., Nakhaeipour, A., Fuel Processing Technology 89 (2008) 491.

[37] Tavasoli, A., Nakeaipour, A., Sadaghiani, K., Fuel Processing Technology 88 (2007) 461.

Chapter Five
Summary, concluding remarks and outlook

Summary and Concluding remarks

In the Fischer-Tropsch synthesis – the heterogeneously catalyzed conversion of syngas into hydrocarbon chains - transportation fuels can be produced from alternative sources to crude oil. In cobalt based Fischer-Tropsch catalysis the support material is generally oxidic in nature. A drawback of using oxidic supports is that they can form mixed compounds with cobalt that are not active in the FT catalysis and are only reducible at high temperatures. One way to overcome this problem is by the use of an inert support, e.g. carbon nanotubes (CNT). CNT exhibit a variety of interesting properties for support materials, including high mechanical strength, high thermal conductivity, and good chemical inertness in aggressive media. However, the well defined structures of the tubes would facilitate the study of the stability measures taken by means of surface roughening and heat treatment.

The aim of this project was to prepare highly active cobalt on carbon nanotubes Fischer-Tropsch (FT) catalyst with low methane selectivity and a high C_{5+} selectivity, and to study the effects of surface roughening and heat treatment on the activity and stability of Co/CNT FT catalysts. In chapter two the structure and texture of surface treated and untreated CNT as received by Bayer Material Science (Baytubes® C150 HP) were studied with TEM, N_2 physisorption and titration. Gas phase oxidation (GPO) and liquid phase oxidation (LPO) in HNO_3 were used to modify the surface and introduce functional groups into the CNT. The graphite-like structure of the CNT remained intact after surface treatment, however structural damage could be observed after the LPO treatment. Results demonstrate that after the oxidation treatment by GPO and LPO in HNO_3, the graphite-like structure remained intact, however structural damage could be observed after the LPO treatment. With the harshness of the surface treatment during oxidation, specific surface area increased, micropore area decreased and the number of acidic oxygen containing surface groups introduced increased. The GPO method is accompanied with less carbon loss due to the prevention of the filtration step and has shown to be a milder method in introducing functional groups into the CNT surface than the LPO method. In chapter three the preparation of Co catalysts supported on surface treated and untreated CNT was studied. A series of catalysts was prepared by incipient wetness impregnation (IWI) using cobalt nitrate or cobalt acetate as precursors dissolved in water or ethanol, thermally treated in N_2, 1 % v/v NO/N_2 or dried

in static air. Catalysts were prepared with weight loadings varying from 6 to 18 wt% Co and cobalt particle sizes in the range of 3.2 to 7.7 nm. Enhanced distribution of cobalt clusters was seen for the ethanol impregnations as compared to the aqueous impregnations as ascribed to better wetting of the untreated hydrophobic tubes by ethanol. Smaller cobalt particles and a narrower particle size distribution were achieved with a thermal treatment in 1 % v/v NO/N_2 as compared to a thermal treatment in N_2. However, the NO treatment was accompanied with agglomeration of small cobalt particles whereas cobalt particles were well distributed over the CNT surface after treatment in nitrogen atmosphere. The effects of different preparation procedures on catalytic performance were tested at atmospheric pressure Fischer-Tropsch testing, 493 K and H_2/CO v/v 2:1. Going from larger particles sizes to smaller sizes the CTY increased as attributed to the increase in cobalt specific surface area for smaller particles. The highest activity was found for CNT impregnated with a cobalt nitrate precursor dissolved in ethanol and thermally treated in NO, INE8-NO, with average cobalt particle size of 3.6 ± 0.9 nm and corresponding CTY of $4.2 \cdot 10^{-5} \cdot mol_{CO} \cdot g_{Co} \cdot s^{-1}$. The methane selectivity showed a strong increase for smaller cobalt particles however a clear trend for the C_{5+} selectivity was not observed. The catalytic testing results were in good accordance with literature, however the trend reported by Bezemer in which a strong decay in TOF for particles smaller than 6 nm is not observed. The best performing catalyst was highly active. The results presented here showed higher initial activity and more beneficial selectivity for catalysts prepared with untreated CNT supports as opposed to catalysts prepared on surface treated CNT supports. These findings could have serious consequences for the preparation of Co/CNT catalysts. In chapter four the preparation of cobalt on carbon nanotubes Fischer-Tropsch catalysts by IWI is further optimized building on the observations done in chapter three. Co/CNT are synthesised by impregnation of the support with a cobalt nitrate precursor dissolved in ethanol and thermally treated in N_2, 1 % v/v NO/N_2 or air, varying the heating rate between 2 $K \cdot min^{-1}$, 0.5 $K \cdot min^{-1}$ or instantaneous drying. Drying the impregnated catalysts with a ramp of 0.5 $K \cdot min^{-1}$ improved the dispersion of cobalt particles and the distribution of cobalt particles over the CNT surface as compared to drying with a ramp of 2 $K.min^{-1}$ or instantaneous. A preliminary study is presented on the effects of surface treatment by oxidation and heat treatment on the activity and stability of Co/CNT FT catalyst. Heat treatment of Co/CNT in an inert atmosphere

resulted in the reduction of Co_3O_4 to metallic cobalt as determined by TGA, XRD and TEM. The heat treatment was accompanied by sintering of cobalt particles. Nevertheless, sintering seemed to be reduced on the surface treated catalysts, as these catalysts were accompanied by a significantly smaller increase in cobalt particle size after heat treatment as compared to the untreated catalysts. To study the impact of stabilisation measures on catalytic properties the catalysts were subjected to high pressure Fischer-Tropsch testing at temperatures 493 K – 513 K, H_2/CO v/v 2:1 and 20 bar pressure. The surface treated systems were accompanied with a stronger initial loss in CTY as opposed to the non surface treated systems. No stabilization was observed for the heat treated catalysts during catalytic testing. The surface treated catalysts showed enhanced stabilization during catalytic testing however these catalyst were accompanied by significant loss in activity during the first hours of testing. The highest catalytic performance was achieved for the untreated catalysts dried 12 h at 393 K in a fluidized bed with a ramp of 0.5 $K{\cdot}min^{-1}$ in a continuous flow of 1 $mL(mg^{-1}{\cdot}min^{-1})$ of respectively N_2, air or 1% v/v NO/N_2, with measured CTY of 10 – 17. $10^{-5}{\cdot}mol_{CO}{\cdot}g_{Co}{\cdot}s^{-1}$ - at CO conversion in the range 18 – 28 % - and C_1 selectivity 10 - 12 % and C_{5+} selectivity of 76 – 79 %. Presented results demonstrate the importance of different preparation procedures in obtaining highly active cobalt on carbon nanotubes Fischer-Tropsch catalysts.

Research presented in this thesis has shown the potential cobalt supported on CNT have in Fischer-Tropsch catalysis. With a relatively simple preparation route, highly active Fischer-Tropsch catalysts were prepared.

Outlook

To stay in line with the aim of this thesis it would be interesting to further investigate the effects of varying the heating rate in the fluidized bed thermal treatment. Since drying at 393 K with a ramp of 0.5 $K{\cdot}min^{-1}$ resulted in cobalt particles well distributed over the surface and high CTY. Possibly varying the air space velocity during drying or thermal treatment, could also benefit the distribution of cobalt particles and could further contribute to the activity of Co/CNT FT catalysts.

On the aspects of surface roughening, oxidative etching[1], also mentioned in the introduction of chapter four, might be a feasible option in the stabilization

of cobalt. The selective catalytic combustion of carbon in CNT creating cavities where metallic particles can harbour might limit the mobility of cobalt crystallites over the surface and thus limit sintering. In line with the embedding of metal particles, Larrude et al. report on the embedding cobalt particles in CNT prepared from a cobalt nitrate precursor dissolved in acetone. The CNT were dispersed in a cobalt nitrate acetone solution under ultrasonic treatment and magnetic stirring, the solution was dehydrated at 573 K and dried at 573 K for 3h in air. The dissociation of $Co(NO_3)_2$ in acetone could oxidize the external walls of the CNT, creating an oxide layer on the tubes which could be responsible for the sufficient particle anchoring.[2] The authors observe a homogeneous distribution of particles over the surface, however the particle sizes ~ 60 nm are less beneficial for Fischer-Tropsch catalysis. Perhaps the particle sizes can be tuned to more beneficial sizes by using a different thermal treatment. A drawback of IWI with a cobalt nitrate precursor dissolved in acetone however is the limited solubility of cobalt nitrate in acetone meaning several IWI are necessary to achieve high cobalt loadings.

Another possible modification enhancing the stability of cobalt on carbon nanotubes could lie in the coating of CNT with a metal oxide. Creating an ultrathin titania[3] coat of ~ 3 nm or alumina coat[4] might be an interesting option to overcome the weak interactions of ~ 5 $kJ \cdot mol^{-1}$ between cobalt and carbon.[5] The strong metal-support interactions forming inactive cobalt species might be reduced when a thin layer of metal is applied on the tubes. Possibly the catalytic advantages of titania - high C_{5+} selectivity - and CNT - high surface area, pore volume and mechanical strength – could be combined. The relatively strong interactions between cobalt and titania could possibly offer a new way in stabilizing cobalt on CNT and thus inhibit sintering.

Furthermore it would be interesting to study the evolution of a cobalt on CNT catalysts prepared by aqueous IWI with an cobalt acetate precursor thermally treated at 523 K with a ramp of 2 $K \cdot min^{-1}$. The CoO phase and the pyramidal particles observed for these catalysts were unexpected as shown in chapter three.

Also a fundamental study on the mechanism of the autoreduction of CNT would make an interesting study. Heating cobalt oxide particles on Highly Ordered Pyrolytic Graphite in an inert atmosphere and analysis of the samples with Atomic Force Microscopy or electron tomography might provide further insight in how carbon is consumed during autoreduction, whether this it is carbon that is deposited on the CNT surface, carbon out of 1 layer or multiple layers.

[1] Landau, M.V., Savilov, S.V., Ivanov, A.S., Lunin, V.V., Titelman, L., Koltypin, Y., Gedanken, A., Journal of Materials Science 46 (2010) 2162.

[2] Larrude, D.G., Ayala, P., Maia da Costa, M.E.H., Freire, F. L.. Multiwalled Carbon Nanotubes Decorated with Cobalt Oxide Nanoparticles. Journal of Nanomaterials (2012) 1.

[3] Akalework, N.G., Pan, C.-J., Su, W.-N., Rick, J., Tsai, M.-C., Lee, J.F., Lin, J.M., Tsai, L.-D., Hwang, B.J., Journal of Materials Chemistry 22 (2012) 20977.

[4] Gupta, V.K., Agarwal, S., Saleh. T.A., Journal of Hazardous Materials 185 (2011) 17.

[5] Bartholomew, C.H., Applied Catalysis A: General 212 (2001) 17.

Appendix

Chapter Two and Three

Appendix

Table 1. Overview illustrating the impact of pre-drying temperatures on the measured specific surface areas. The surface areas were determined by N_2 physisorption. The micropore areas were determined with the t-plot method.

Support name	B.E.T. area ($m^2 \cdot g^{-1}$)	Micropore area ($m^2 \cdot g^{-1}$)	Total pore volume ($mL \cdot g^{-1}$)
CNT[a]	200	24	0.7
L-CNT 0.5h[a]	240	16	0.6
L-CNT 2h[a]	270	14	0.6
CNT[b]	190	15	1.2
G-CNT 2.5 h[b]	250	18	1.4
L-CNT 0.5h[b]	230	15	1.4
L-CNT 2.5h[b]	260	9	1.1

a: vacuum dried at 498 K

b: vacuum dried at 393 K

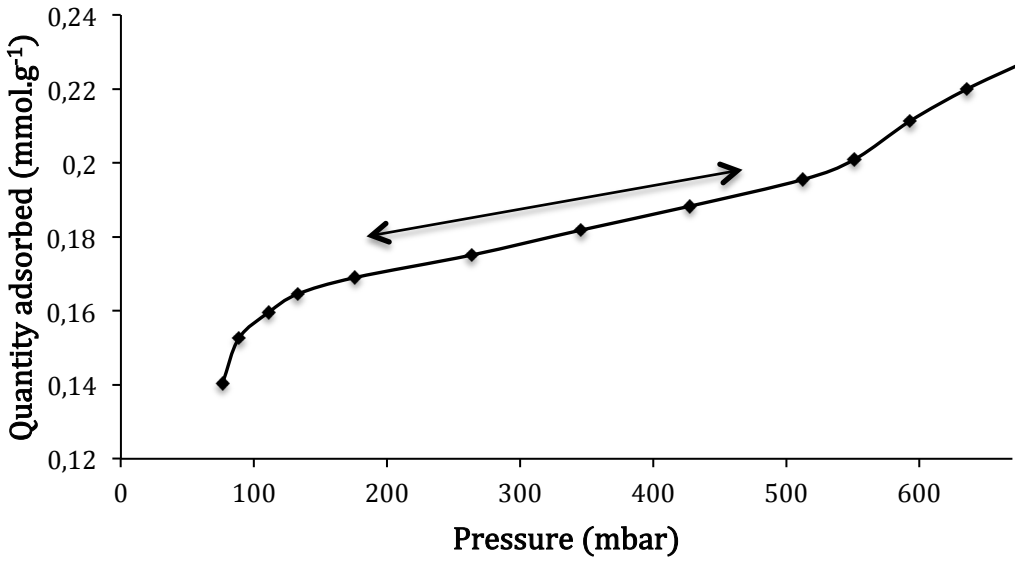

Figure 1. H_2 chemisorption isotherm of catalyst INW10-N_2. The plateau indicated with the double arrow is used for extrapolation of the isotherm.

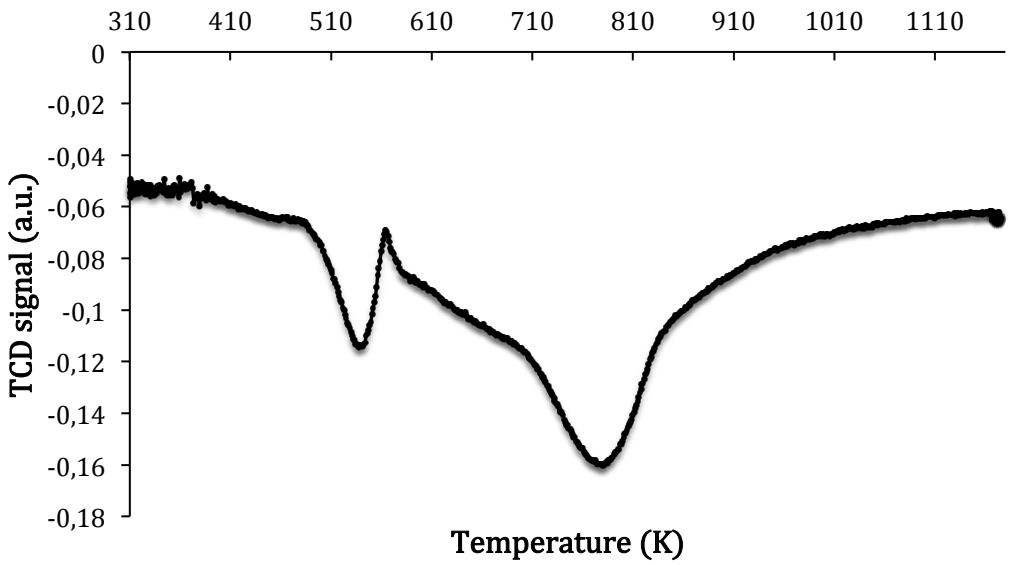

Figure 2. Temperature Programmed Reduction experiment on catalyst INW10-N_2. Ramp 10 K^{-1}, from room temperature to 1173K, performed with a Micromeritics ASAP 2920 apparatus.

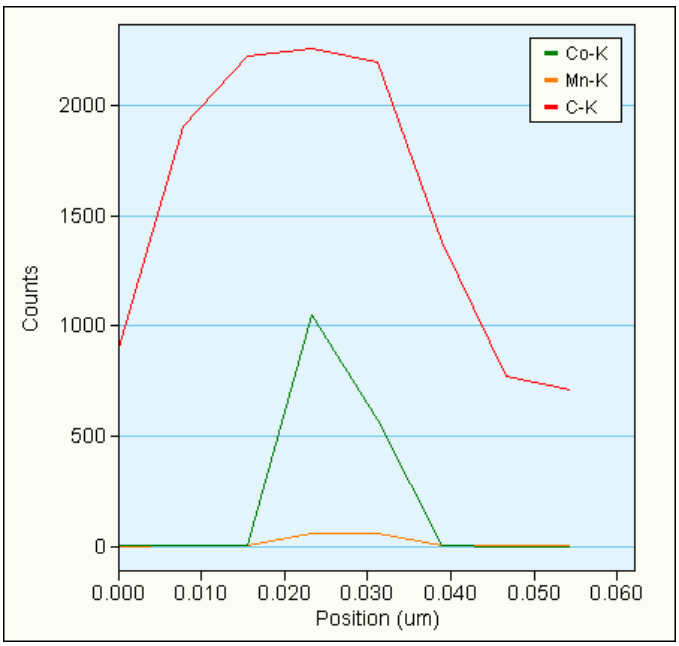

Figure 3. EDX line profile obtained with the Tecnai 20F TEM of an untreated CNT.

$$Co\ wt\% = \frac{Co\ (g)}{CNT\ (g) + \left(\frac{1}{3} * Co_3O_4\ (g)\right)} \qquad [1]$$

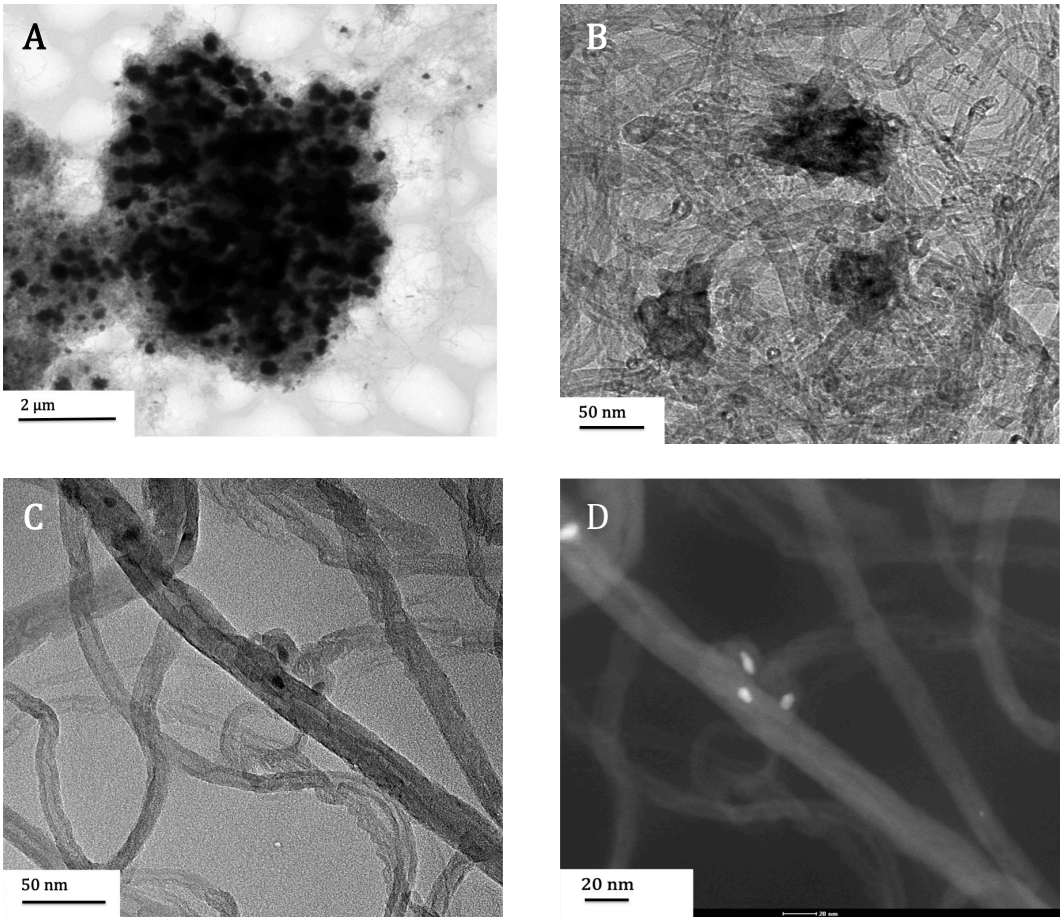

Figure 4. TEM images of catalyst INW18. A-C: bright field TEM. D: STEM-HAADF. (*dCo = 7.4 nm (XRD)).*

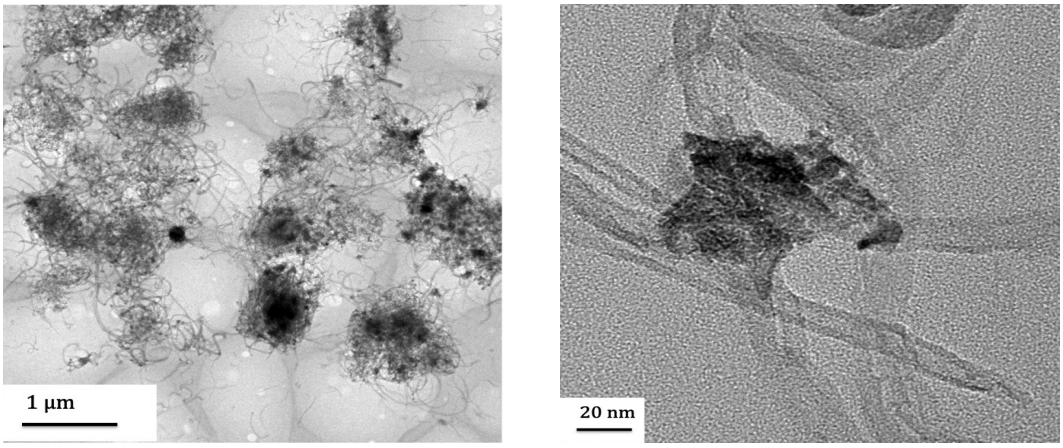

Figure 5. TEM images of catalyst L-INW18.

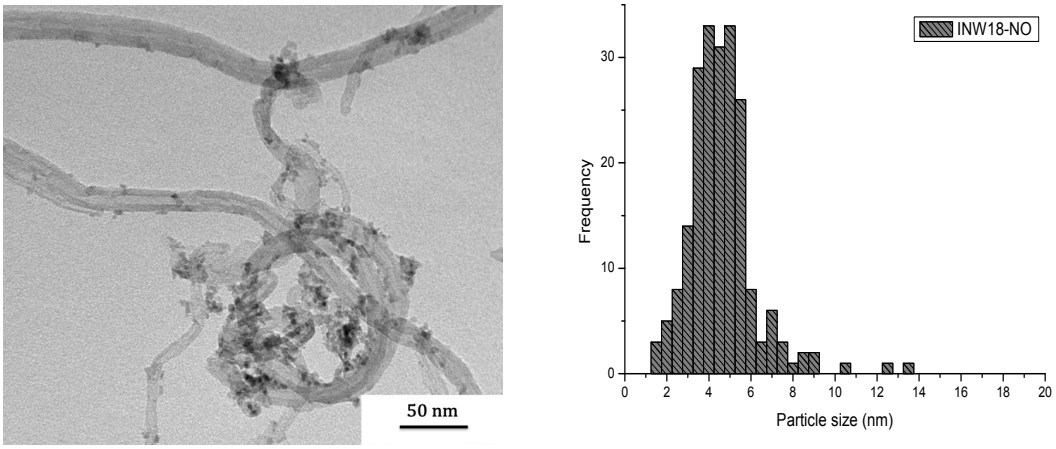

Figure 6. TEM image of catalyst INW18-NO. *(dCo_{sw} = 4.9 ± 1.7 nm).*

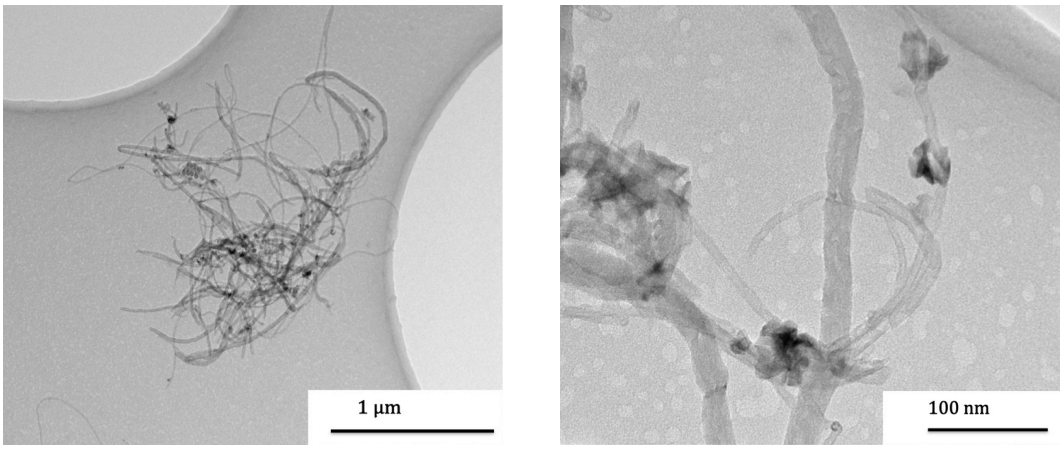

Figure 7. TEM image of catalyst INW6.

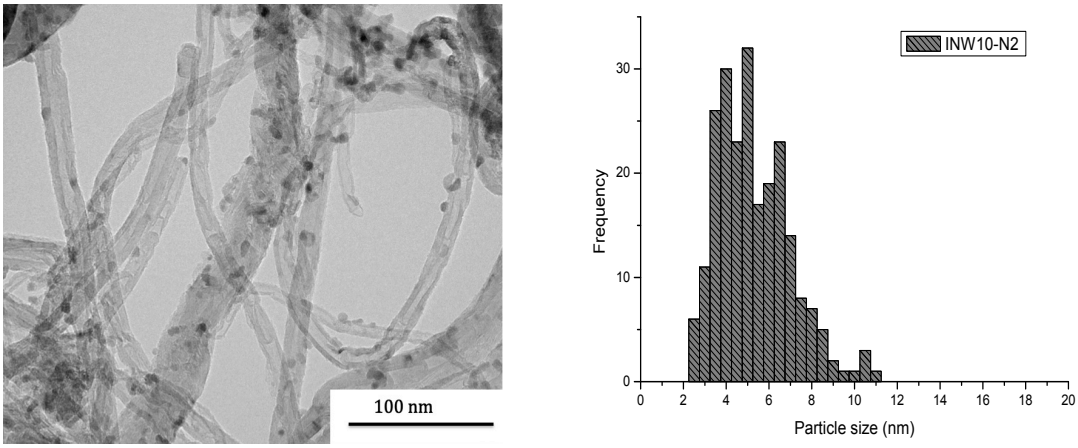

Figure 8. TEM image of catalyst INW10-N_2. *(dCo_{sw} = 5.6 ± 1.7 nm).*

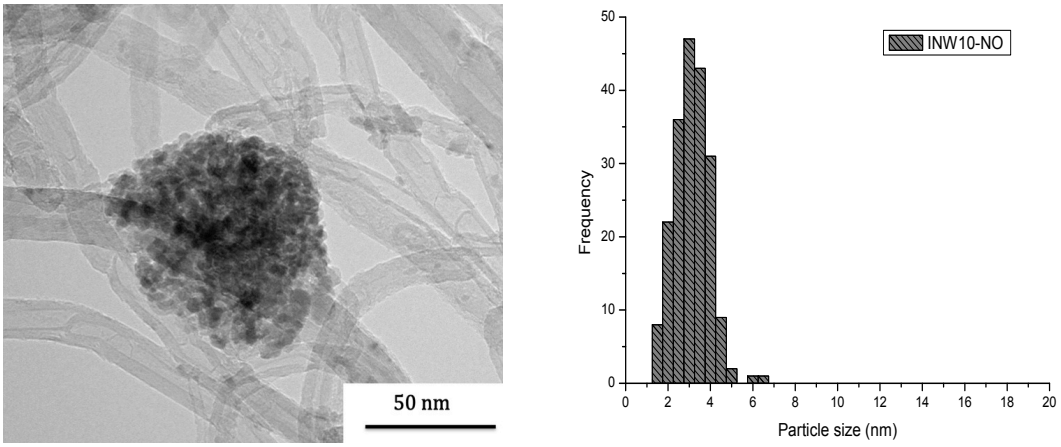

Figure 9. TEM image of catalyst INW10-NO. *($dCo_{sw} = 3.2 \pm 0.8$ nm).*

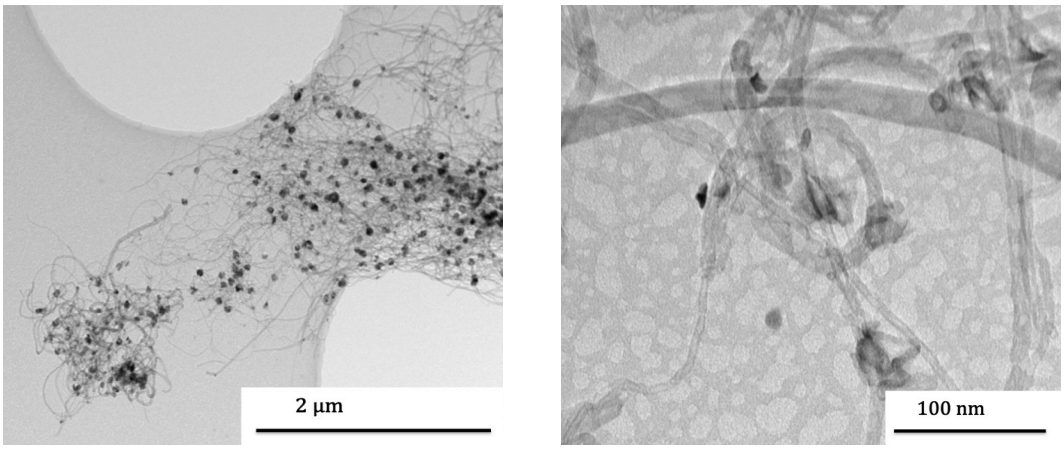

Figure 10. TEM images of catalyst INE8. (*d(Co) = 5.3 nm (XRD)).*

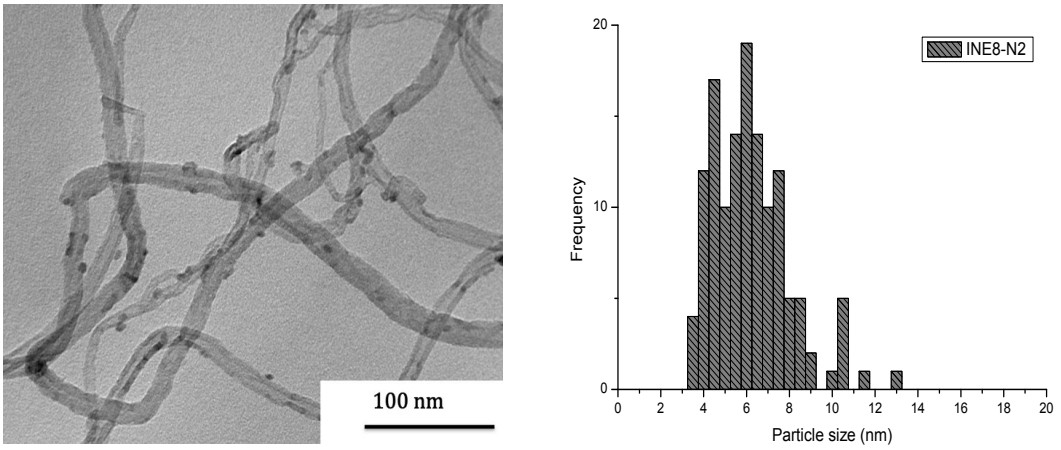

Figure 11. TEM image of catalyst INE7-N2. ($dCo_{sw} = 6.5 \pm 1.8$ nm).

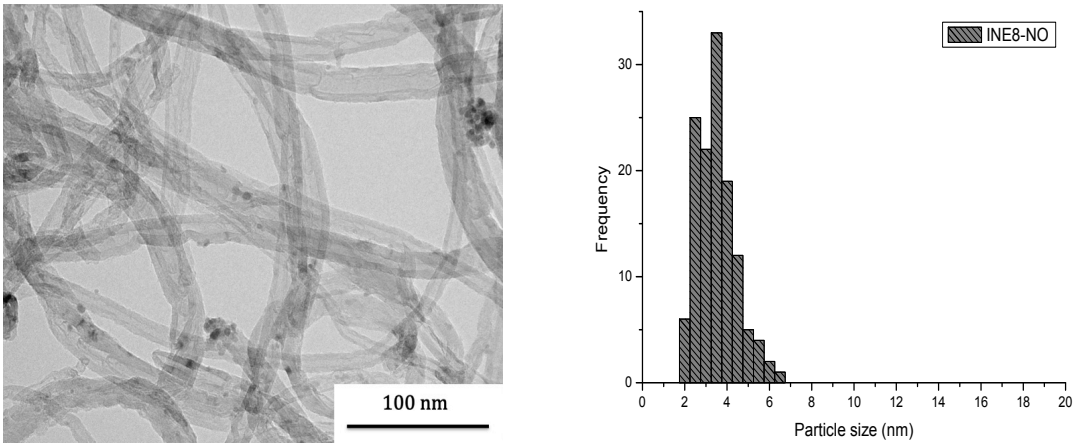

Figure 12. TEM image of catalyst INE8-NO. ($dCo_{sw} = 3.6 \pm 0.9\ nm$).

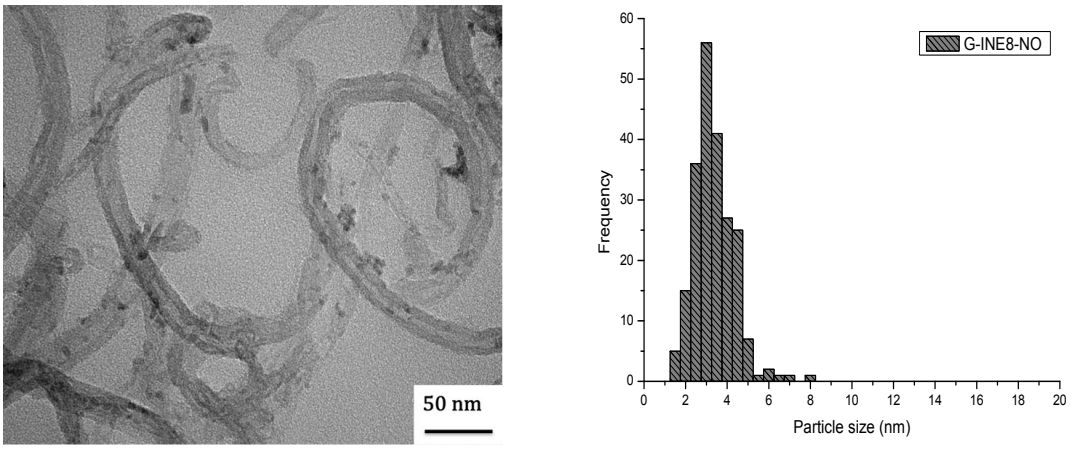

Figure 13. TEM images of catalyst G-INE8-NO ($dCo_{sw} = 3.5 \pm 1.0\ nm$).

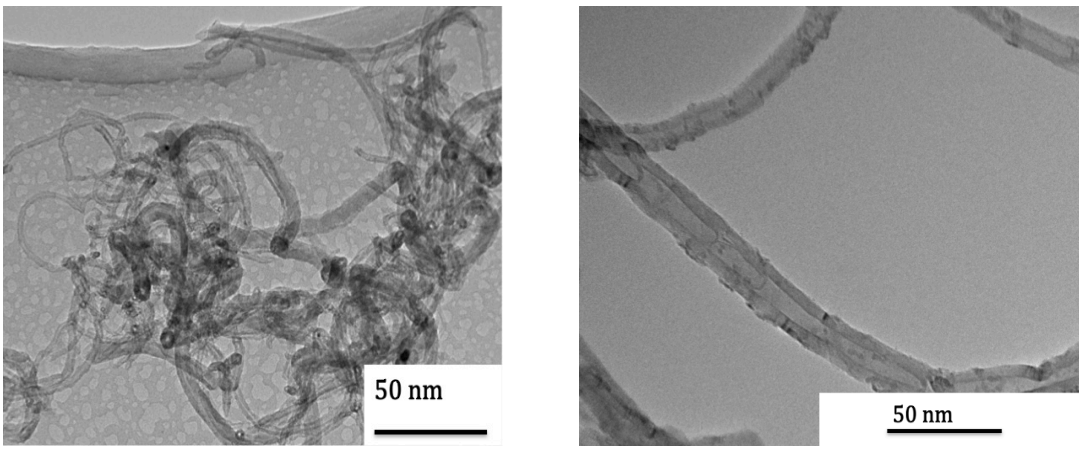

Figure 14. TEM images of catalyst IAW6.

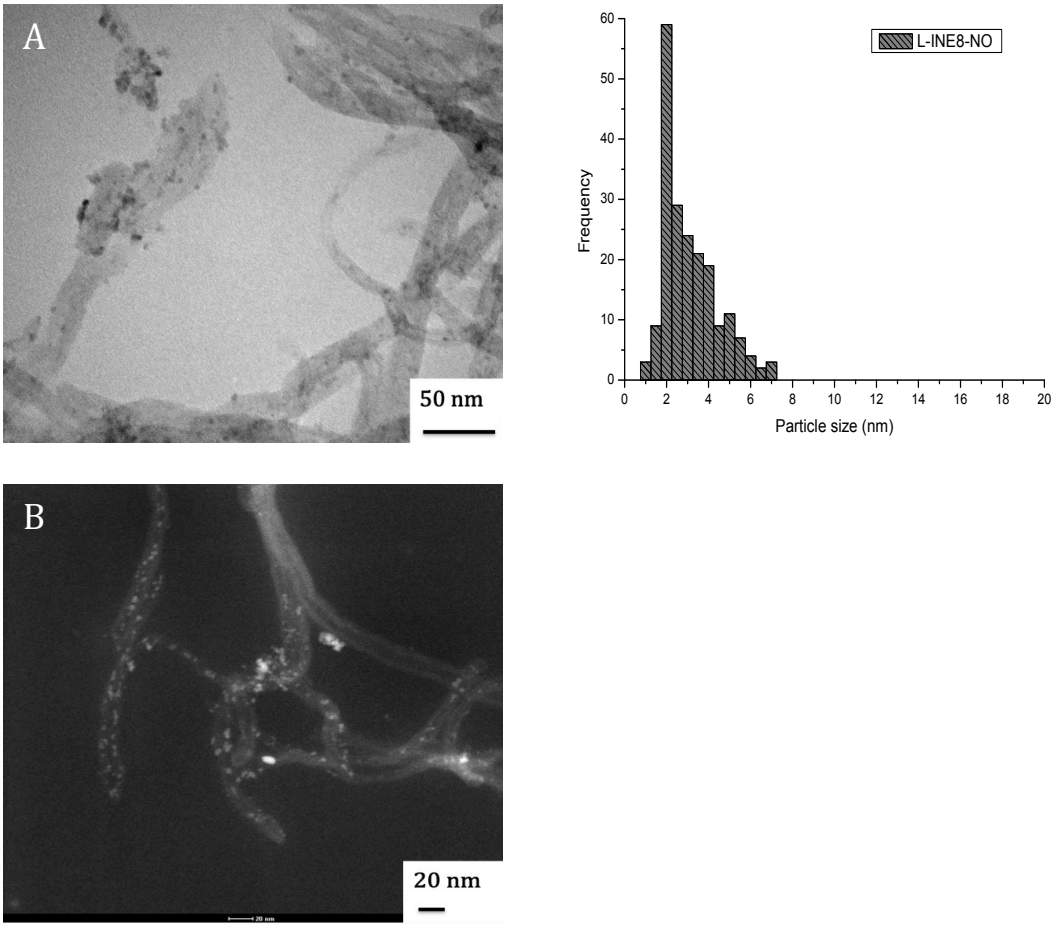

Figure 15. TEM images of catalyst L-INE8-NO. A: bright field TEM image, B: STEM-HAADF image. ($dCo_{sw} = 3.4 \pm 1.3\ nm$).

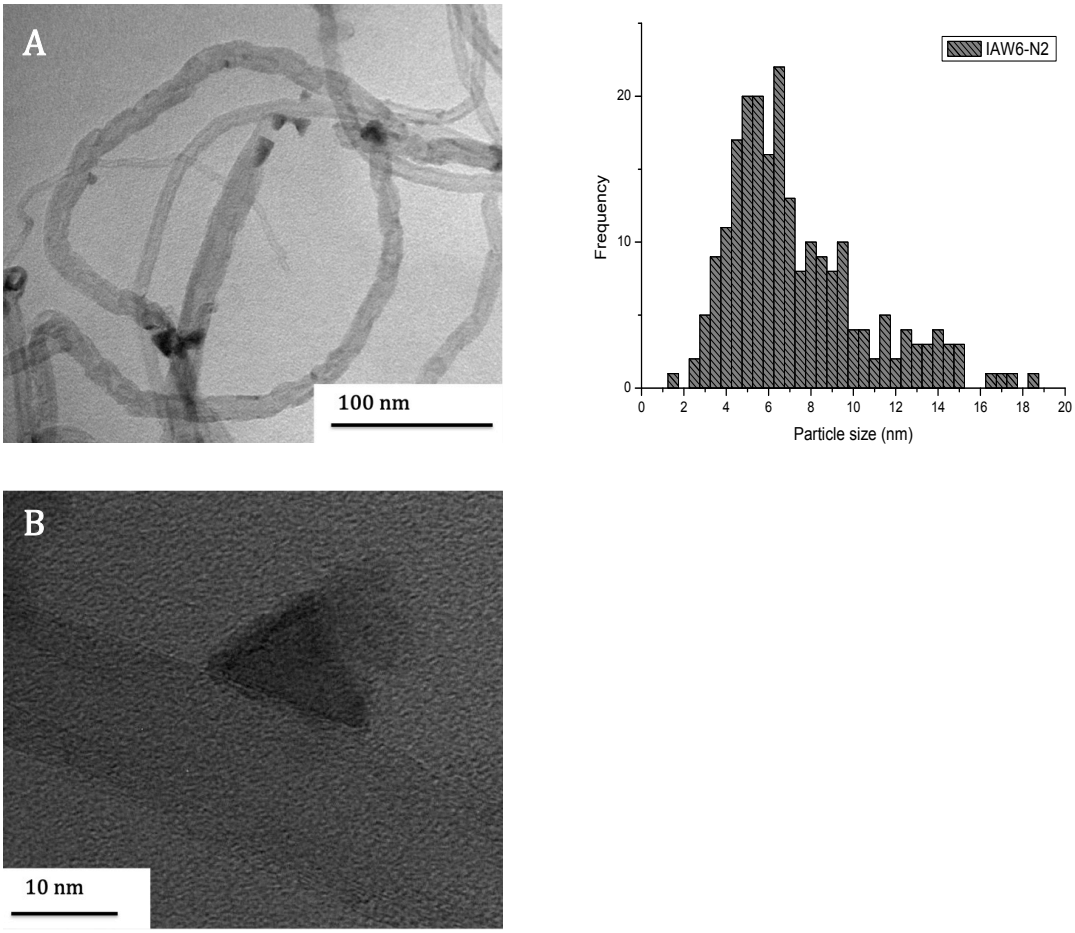

Figure 16. TEM images of catalyst IAW6-N2. A bright field image. B HR image. ($dCo_{sw} = 7.7 \pm 3.2\ nm$).

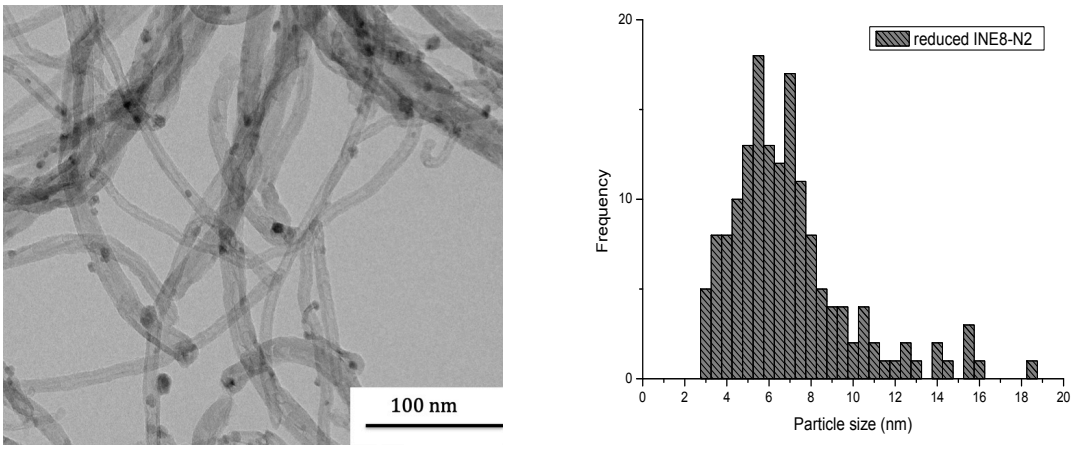

Figure 17. TEM image of catalyst reduced* INE7-N_2. ($dCo_{sw} = 8.8 \pm 4.9\ nm$).

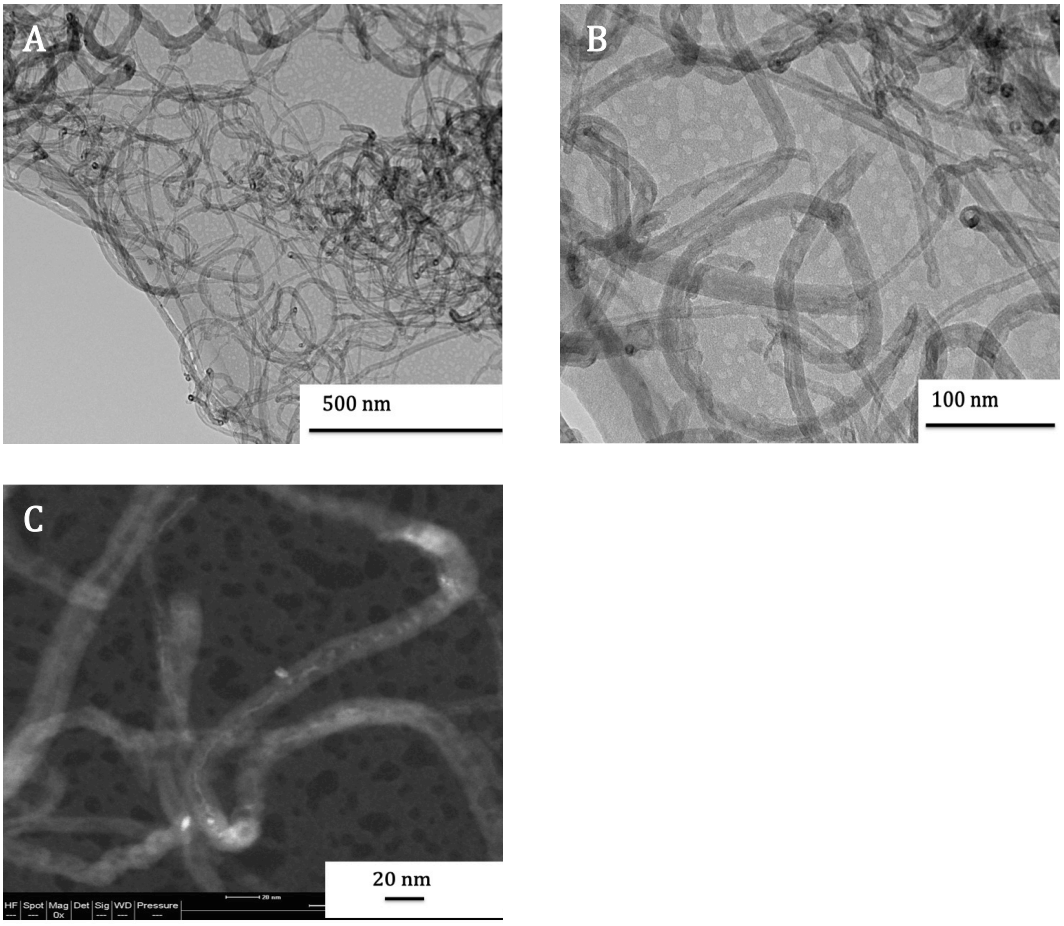

Figure 18. TEM images of catalyst L-INW6 dried at 333 K in static air. A and B: bright field images. C: STEM-HAADF image.

* The particle size histograms show counts ofparticles up to of 20 nm, however for reduced INE8-N_2 a few larger particles found as wel.

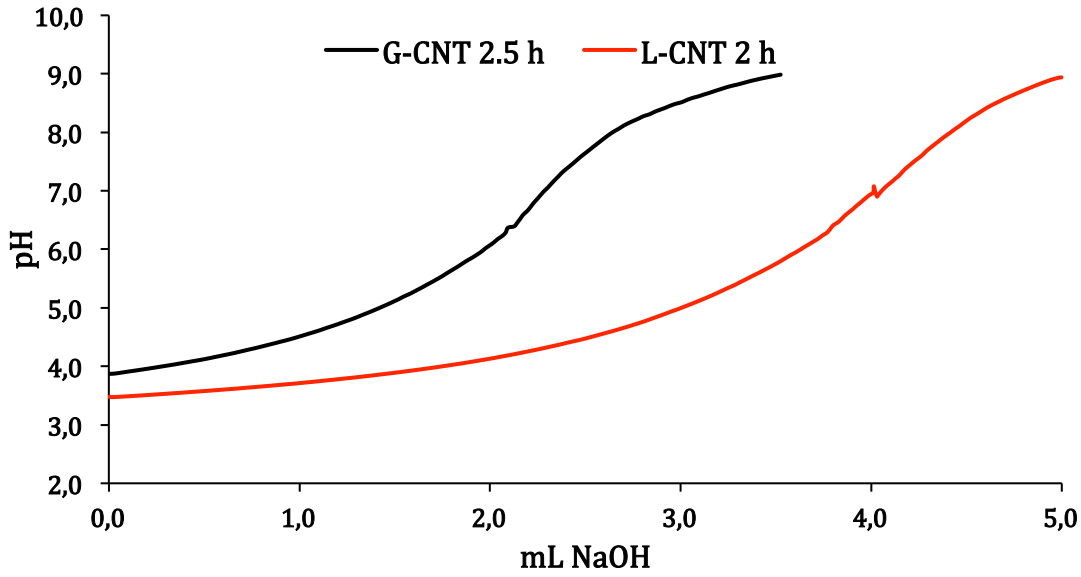

Figure 19. Titration curves of G-CNT 2.5 h and L-CNT 2h.

Appendix

Chapter Four

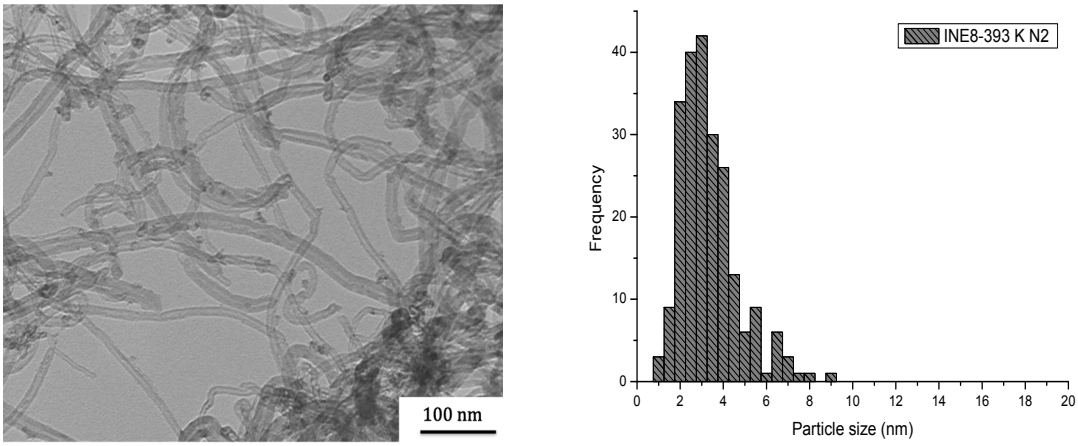

Figure 1. TEM image of catalyst INE8-393 K N_2. *($dCo_{sw} = 3.6 \pm 1.4$ nm).*

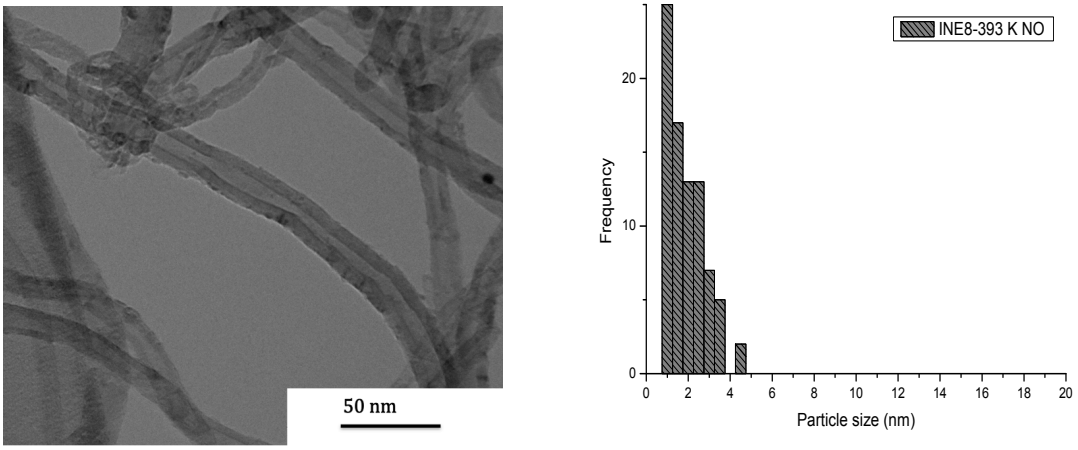

Figure 2. TEM image of catalyst INE8-393 K NO. *($dCo_{sw} = 2.0 \pm 0.9$ nm).*

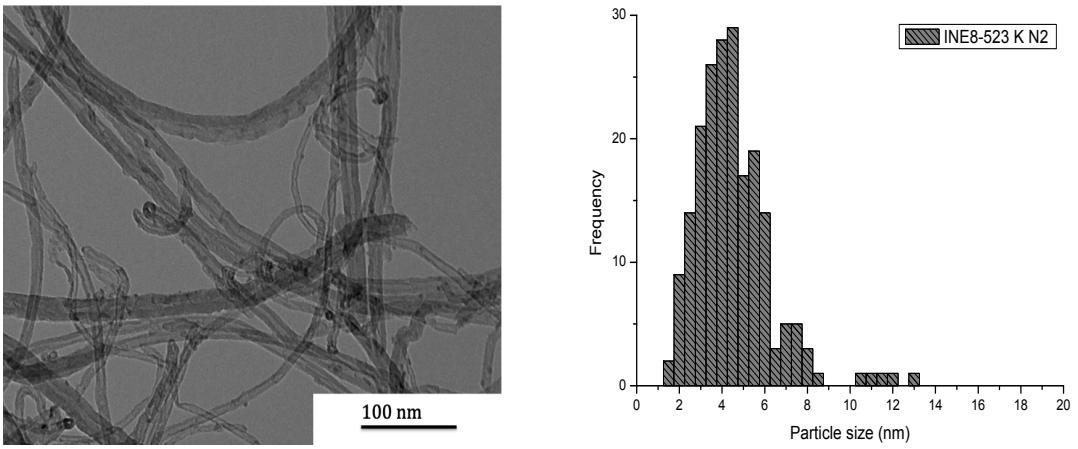

Figure 3. TEM image of catalyst INE8-523 K N_2. *($dCo_{sw} = 4.9 \pm 1.9$ nm).*

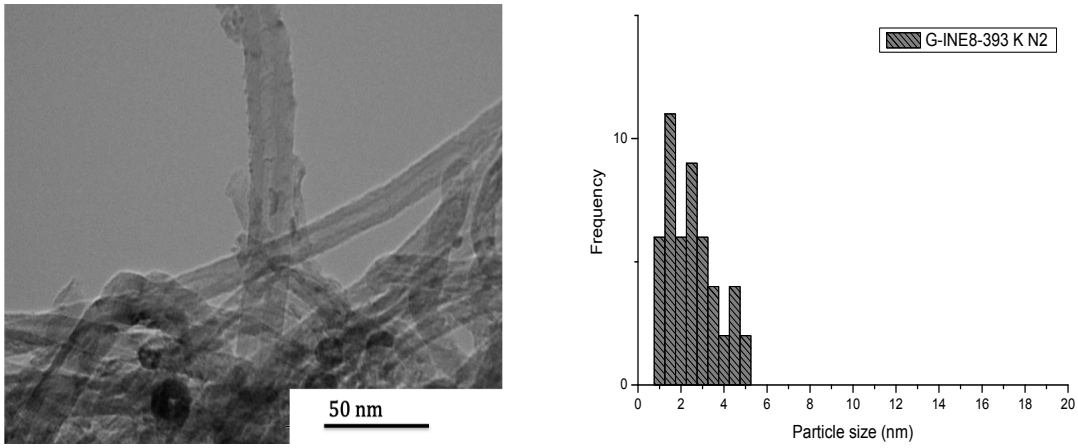

Figure 4. TEM image of catalyst G-INE8-393 K N_2. *($dCo_{sw} = 2.7 \pm 1.1$ nm).*

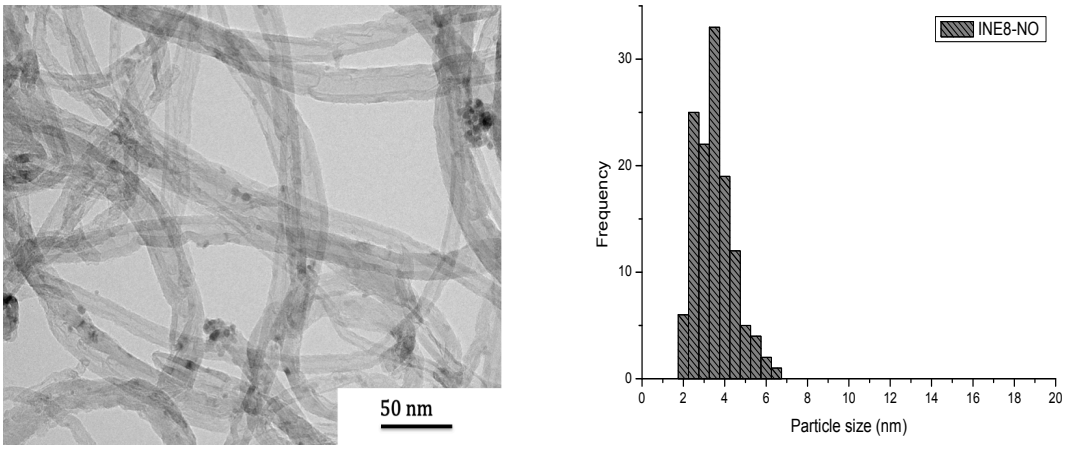

Figure 5. TEM image of catalyst INE8-NO. *($dCo_{sw} = 3.6 \pm 0.9$ nm).*

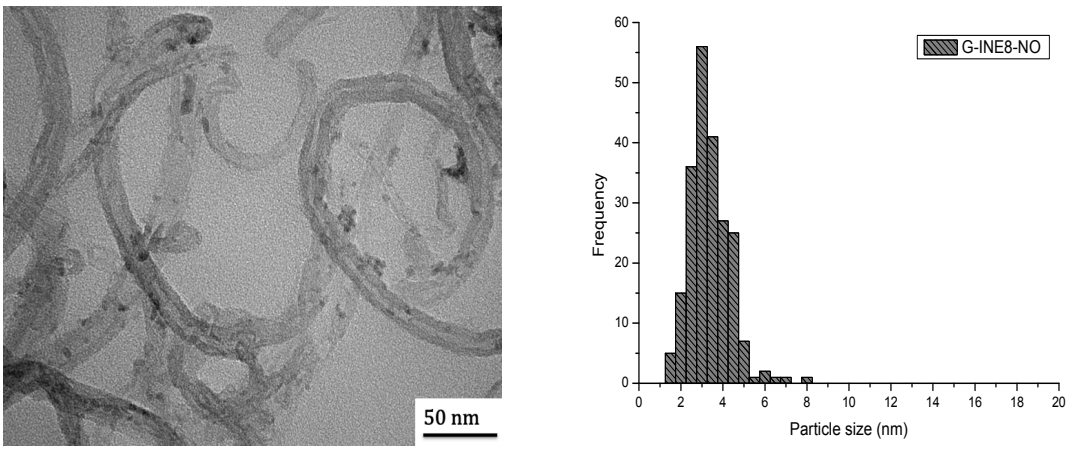

Figure 6. TEM images of catalyst G-INE8-NO *($dCo_{sw} = 3.5 \pm 1.0$ nm).*

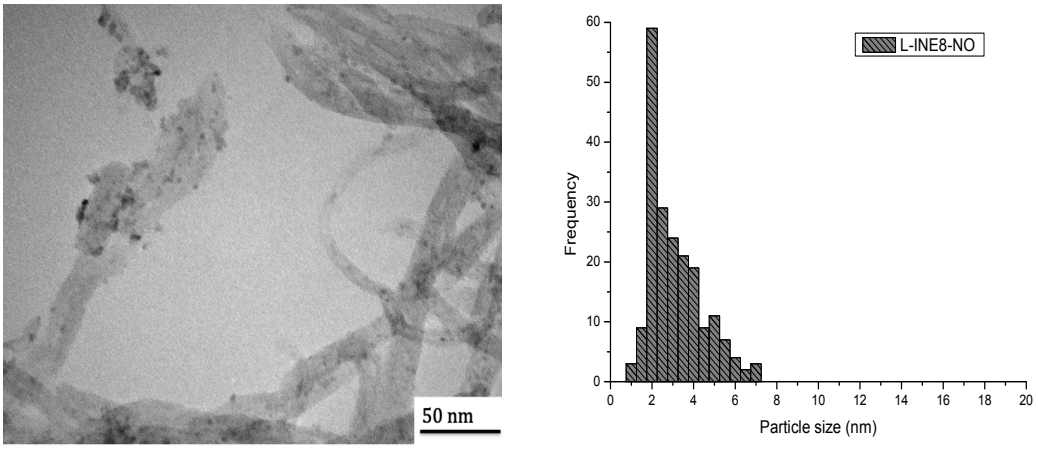

Figure 7. TEM image of catalyst L-INE8-NO ($dCo_{sw} = 3.4 \pm 1.3$ nm).

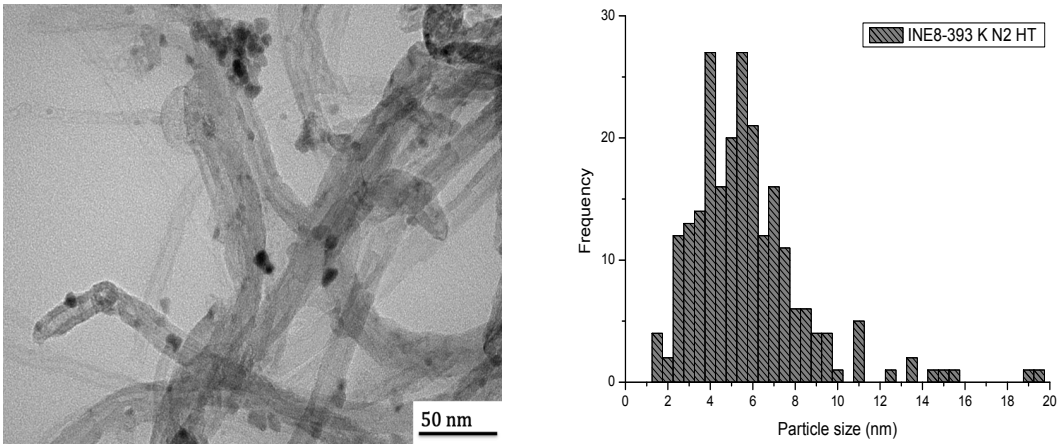

Figure 8. TEM image of catalyst INE8-393 K N2 HT. ($dCo_{sw} = 6.9 \pm 3.8$ nm).

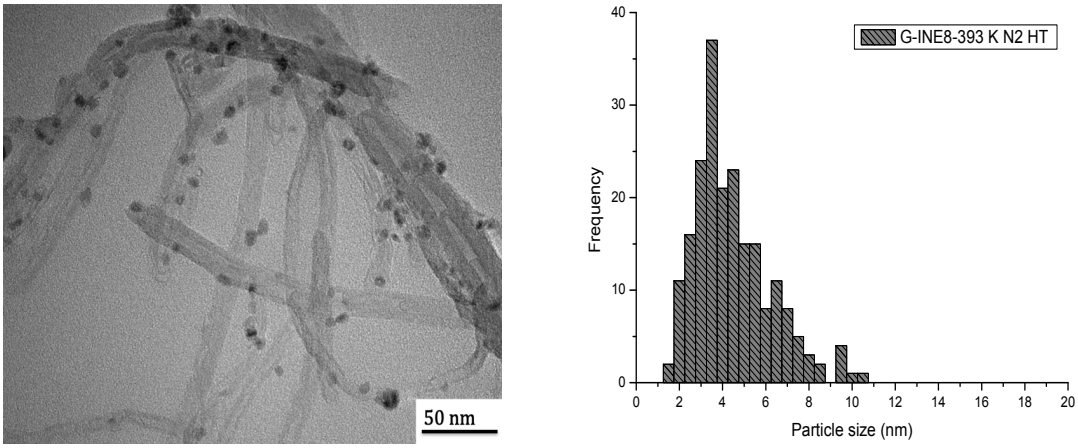

Figure 9. TEM image of catalyst G-INE8-393 K N2 HT. ($dCo_{sw} = 4.8 \pm 3.8$ nm).

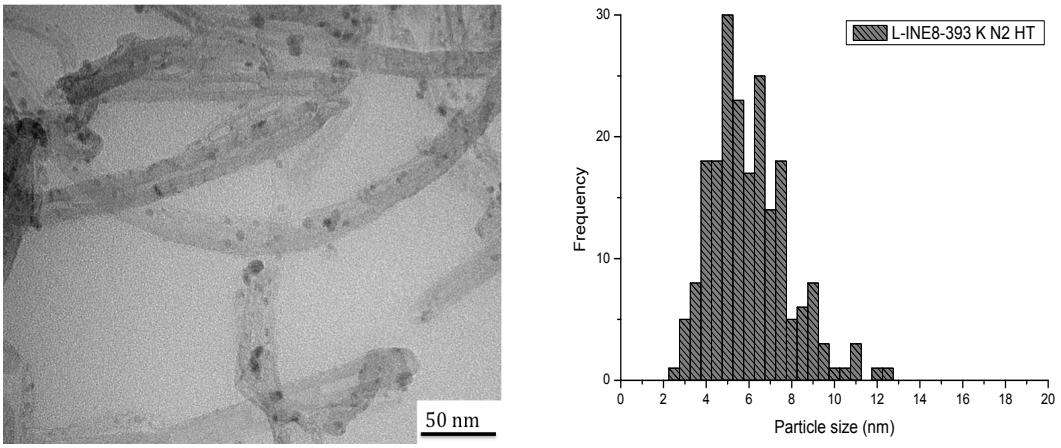

Figure 10. TEM image of spent catalyst L-INE8-393 K N_2 HT.
(dCo_{sw} = 8.5 ± 2.2 nm).

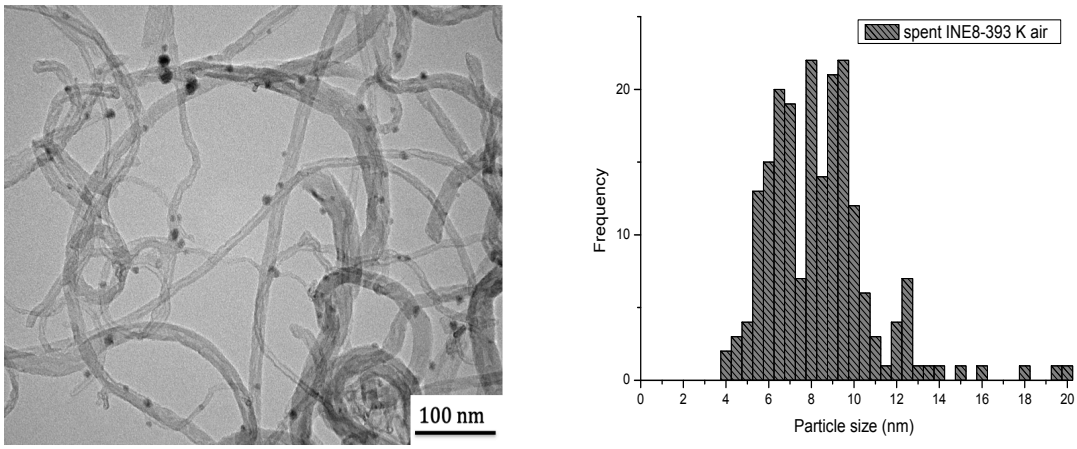

Figure 11. TEM image of spent catalyst INE8-393 K air.
(dCo_{sw} = 8.8 ± 2.5 nm).

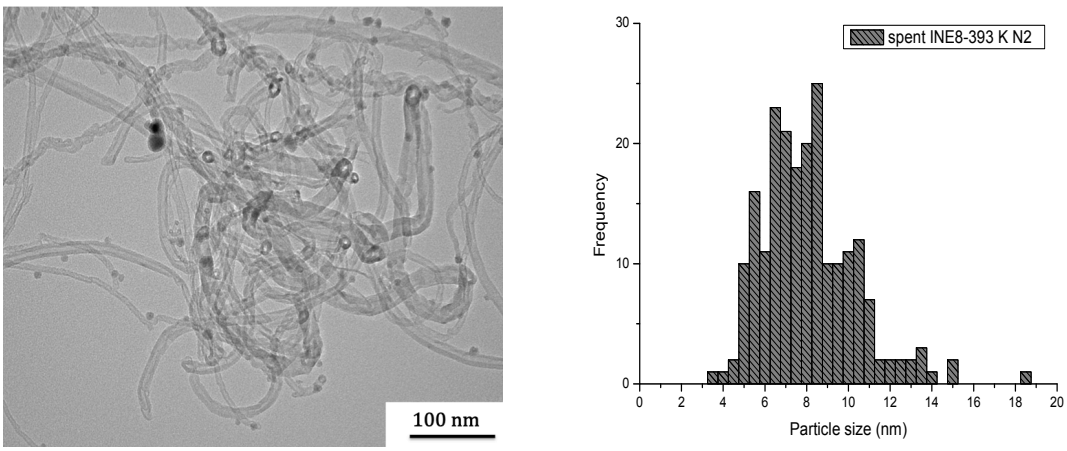

Figure 12. TEM image of spent catalyst INE8-393 K N_2. *(dCo_{sw} = 8.4 ± 2.3 nm).*

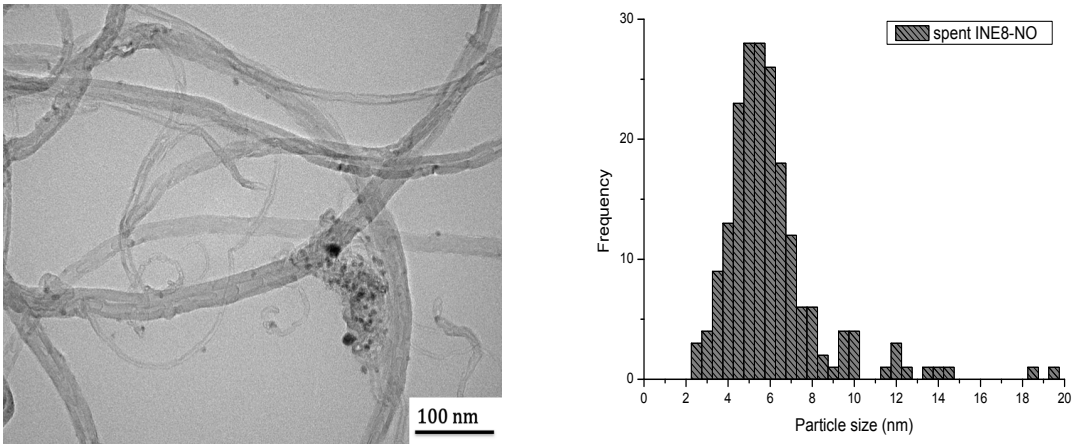

Figure 13. TEM image of spent catalyst INE8-NO. *($dCo_{sw} = 8.6 \pm 5.6$ nm).*

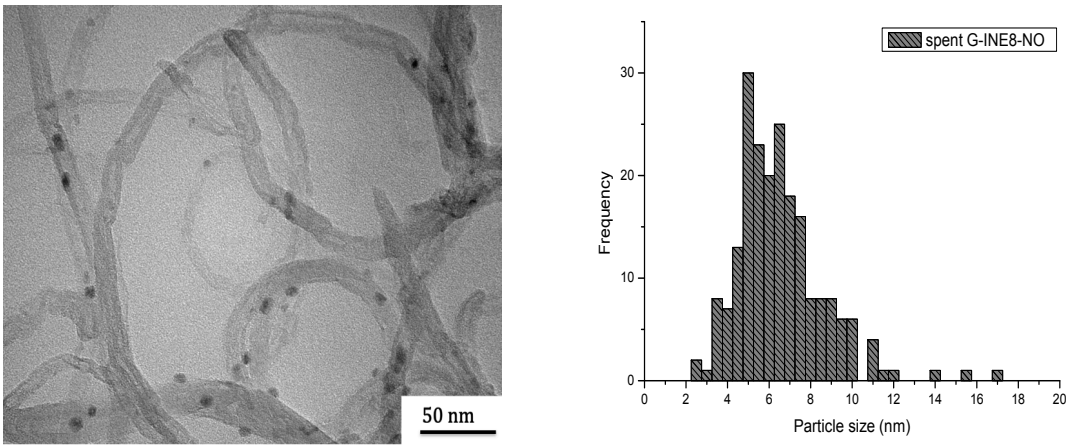

Figure 14. TEM image of spent catalyst G-INE8-NO. *($dCo_{sw} = 7.0 \pm 2.4$ nm).*

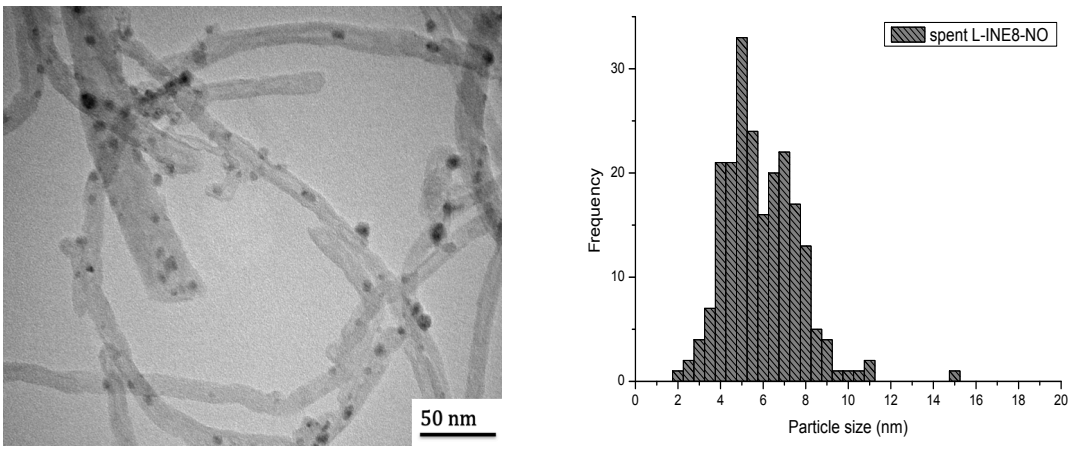

Figure 15. TEM image of spent catalyst L-INE8-NO *($dCo_{sw} = 6.2 \pm 1.8$ nm).*

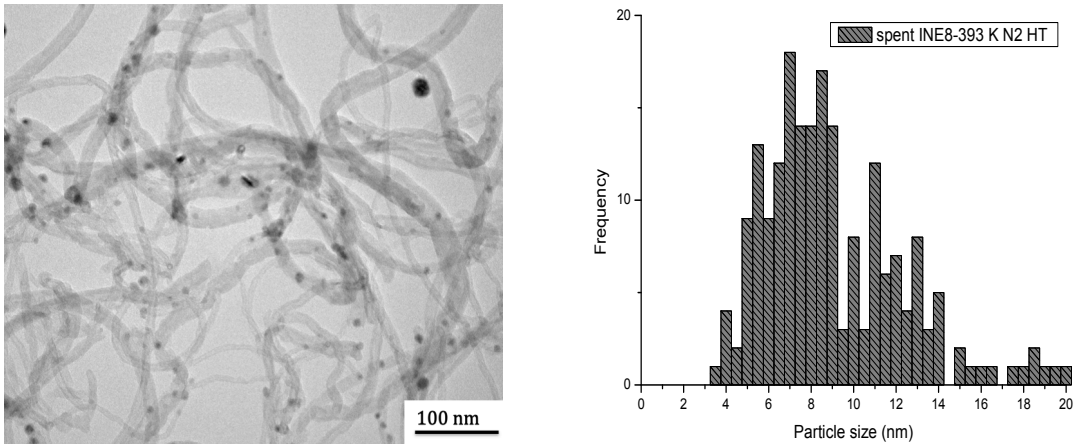

Figure 16. TEM image of spent catalyst INE8-393 K N_2 HT.
($dCo_{sw} = 11 \pm 4.7$ nm).

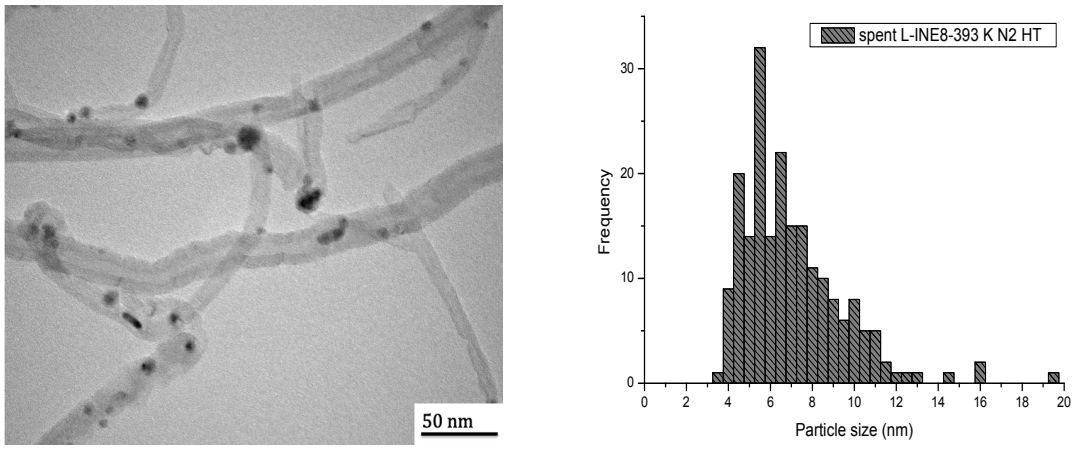

Figure 17. TEM image of spent catalyst L-INE8-393 K N_2.
($dCo_{sw} = 8.4 \pm 2.3$ nm).

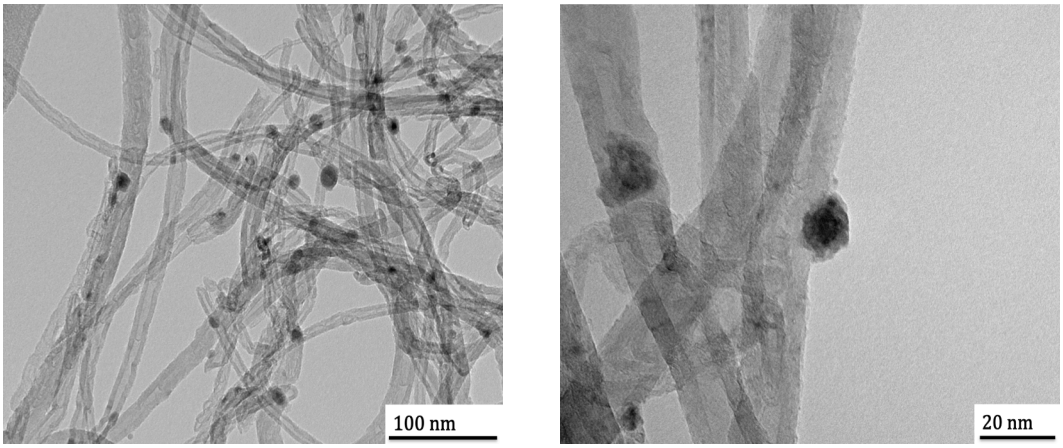

Figure 18. TEM images of INE7-N_2 4h 873 K N_2.

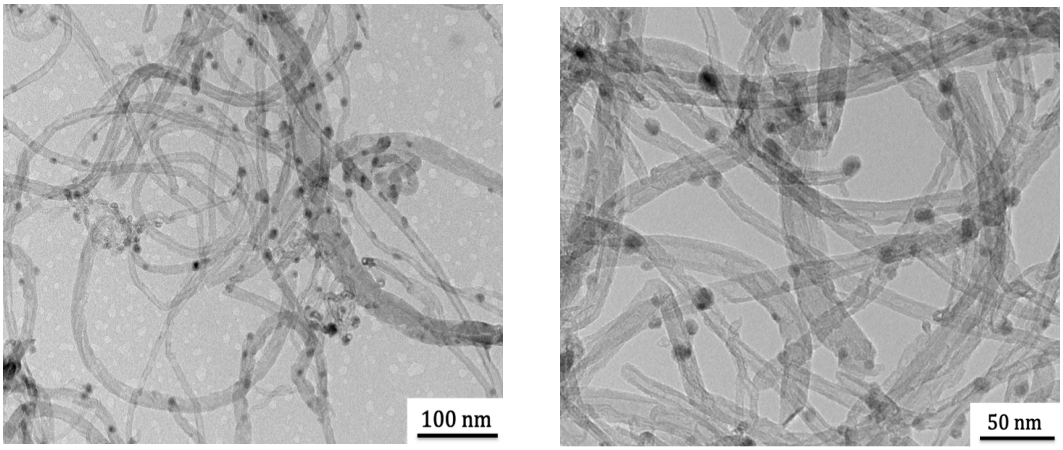

Figure 19. TEM images of INW10-N_2 4h 823 K N_2.

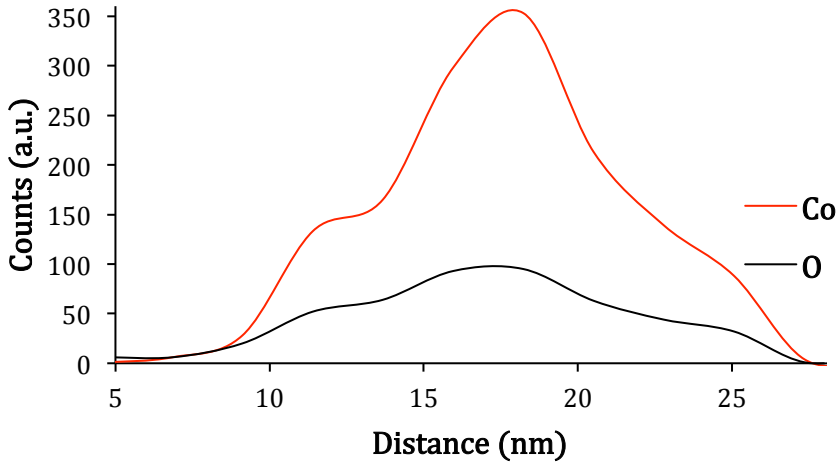

Figure 20. EDX line profile obtained with the Tecnai 20F of INW10-N_2 4h 873 K N_2.

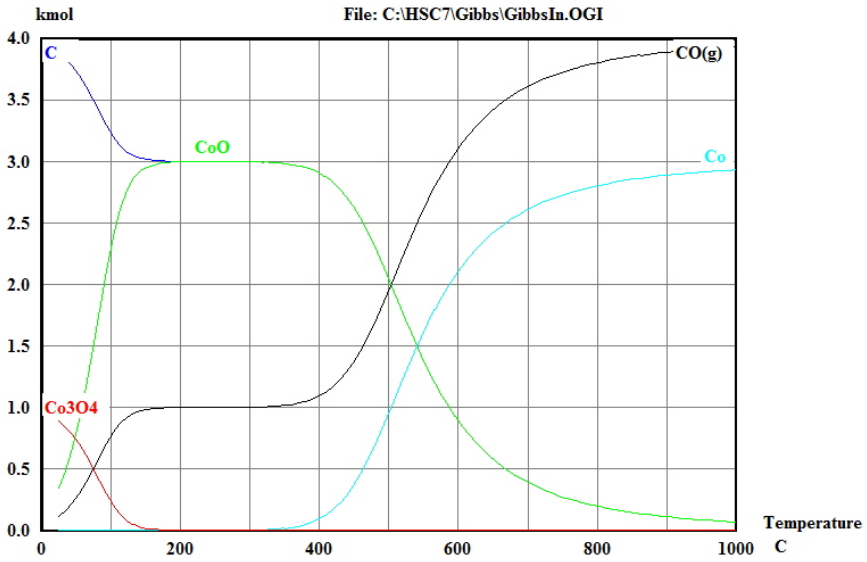

Figure 21. HSC chemistry calculations. Input: CO (g), Co, CoO, Co_3O_4, Co_2C, N_2 (1 bar).

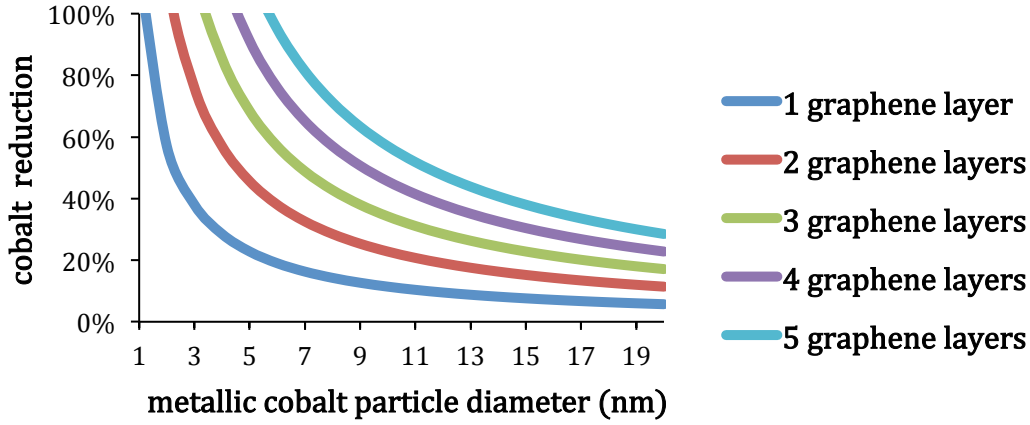

Figure 22. Stoichiometric calculations on the consumption of CNT at the interface of cobalt particles.

Assumptions Figure 23. In the calculations the assumption is made that the reduction of cobalt proceeds via equation [1] and only carbon at the interface of Co_3O_4 is oxidized and the calculations are based on 1 Co_3O_4 particle on a CNT. Furthermore the following assumptions are used: hemispherical particles with a cubic lattice structure. M_w Co_3O_4 = 0.408 kg.mol^{-1}, M_w graphene = 0.012 kg.mol^{-1}, density graphene = 1.40.103 kg.m^3, interparticle spacing = 0.142 nm, graphene layer spacing = .355 nm and atomic radius carbon = 0.170 nm.

$$Co_3O_4 + 4\,C \longrightarrow 3\,CoO + 4\,CO \qquad [1]$$

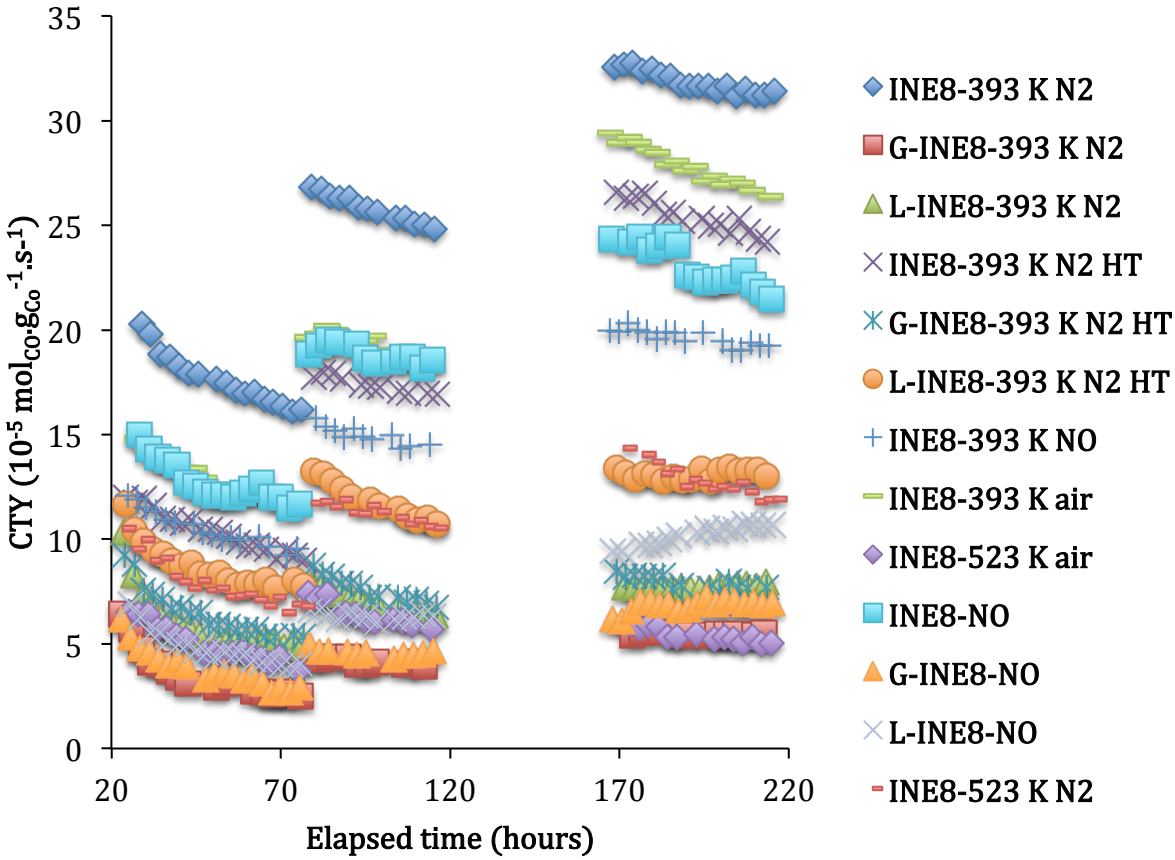

Figure 23. Overview CTY measured at 493 K (22 h – 78 h), 503 K (79 h – 167 H) and 513 K (168 h – 216 h), H_2/CO v/v 2:1 at 20 bar syngas pressure.

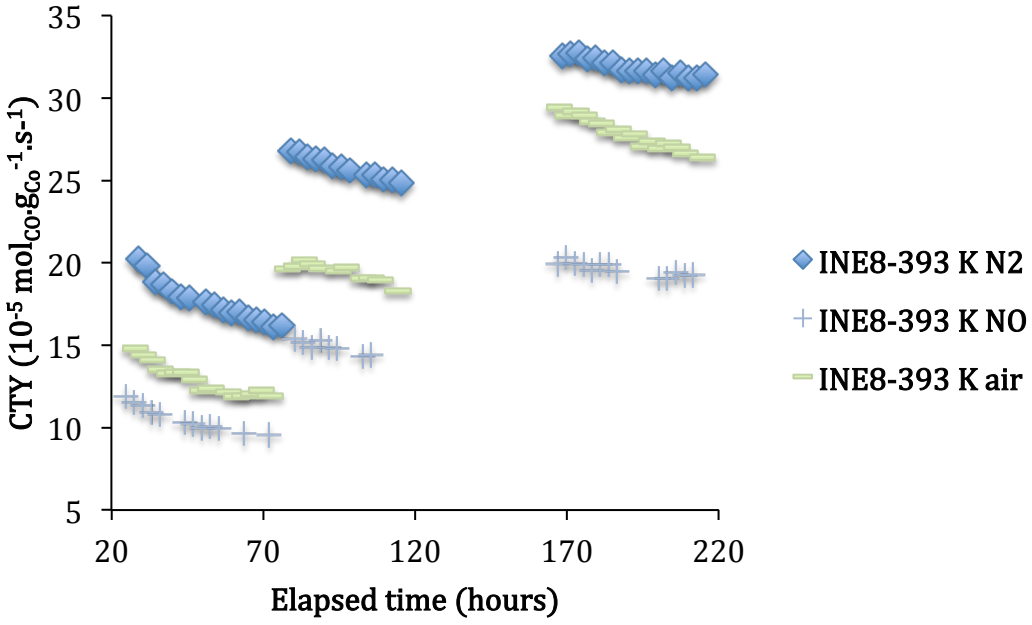

Figure 24. CTY for the catalysts INE8-393 K N_2, INE8-393 K NO and INE8-393 K air measured at 493 K (22 h – 78 h), 503 K (79 h – 167 H) and 513 K (168 h – 216 h), H2/CO v/v 2:1 at 20 bar syngas pressure.

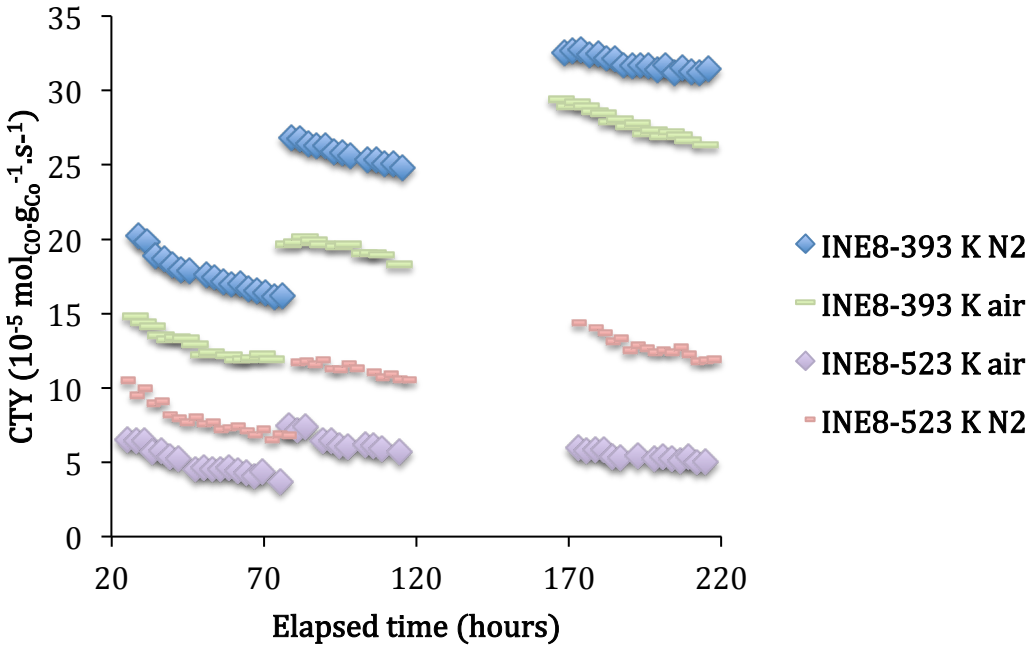

Figure 25. CTY for the catalysts INE8-393 K N_2, INE8-393 K air, INE8-523 K N_2 and INE8-523 K air and measured at 493 K (22 h – 78 h), 503 K (79 h – 167 H) and 513 K (168 h – 216 h), H2/CO v/v 2:1 at 20 bar syngas pressure.

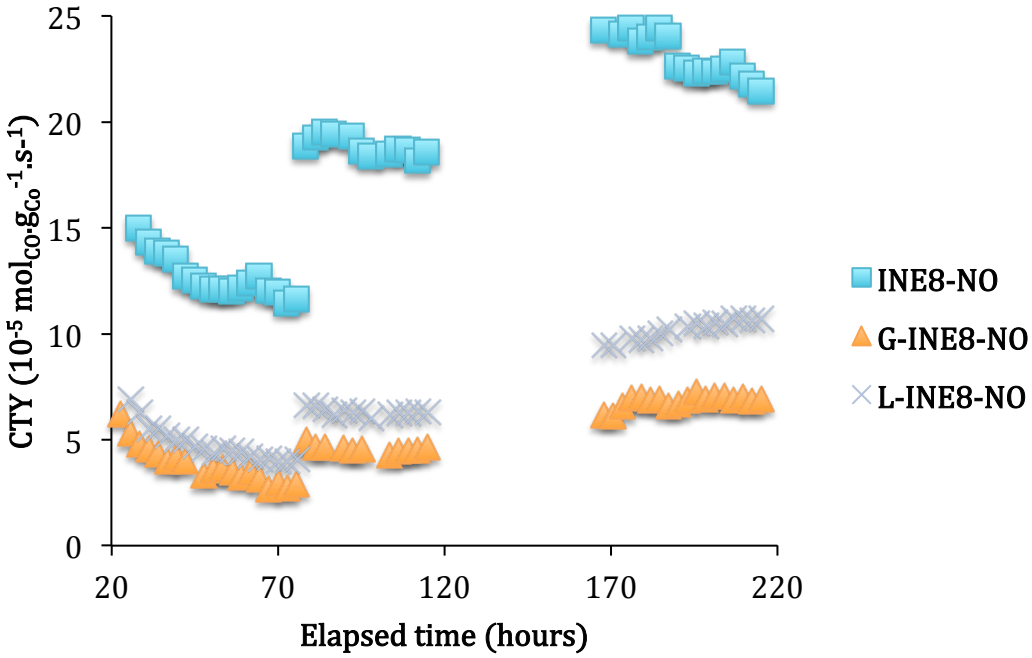

Figure 26. CTY the for catalysts INE8-NO, G-INE8-NO and L-INE8-NO and measured at 493 K (22 h – 78 h), 503 K (79 h – 167 H) and 513 K (168 h – 216 h), H2/CO v/v 2:1 at 20 bar syngas pressure.

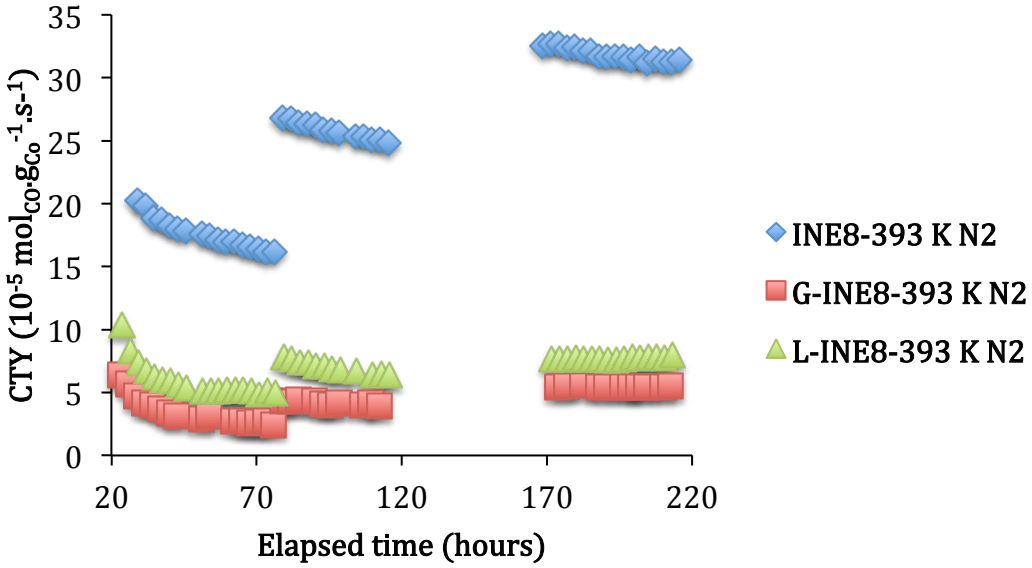

Figure 27. CTY for the catalysts INE8-393 K N_2, G-INE8-393 K N_2 and L-INE8-393 K N_2 measured at 493 K (22 h – 78 h), 503 K (79 h – 167 H) and 513 K (168 h – 216 h), H2/CO v/v 2:1 at 20 bar syngas pressure.

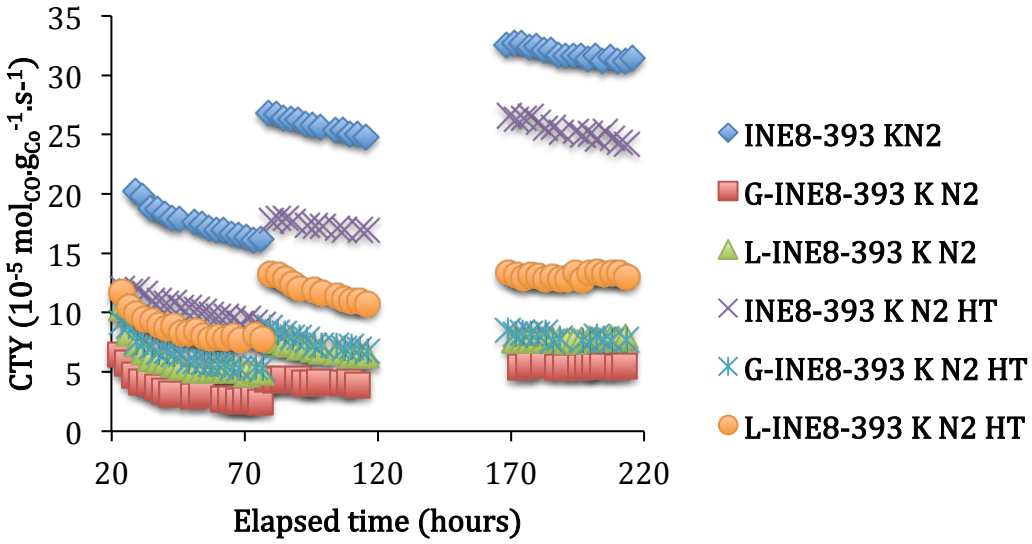

Figure 28. CTY for the catalysts INE8-393 K N_2, G-INE8-393 K N_2, L-INE8-393 K N_2, INE8-393 K N_2 HT, G-INE8-393 K N_2 HT and L-INE8-393 K N_2 HT measured at 493 K (22 h – 78 h), 503 K (79 h – 167 H) and 513 K (168 h – 216 h), H2/CO v/v 2:1 at 20 bar syngas pressure.

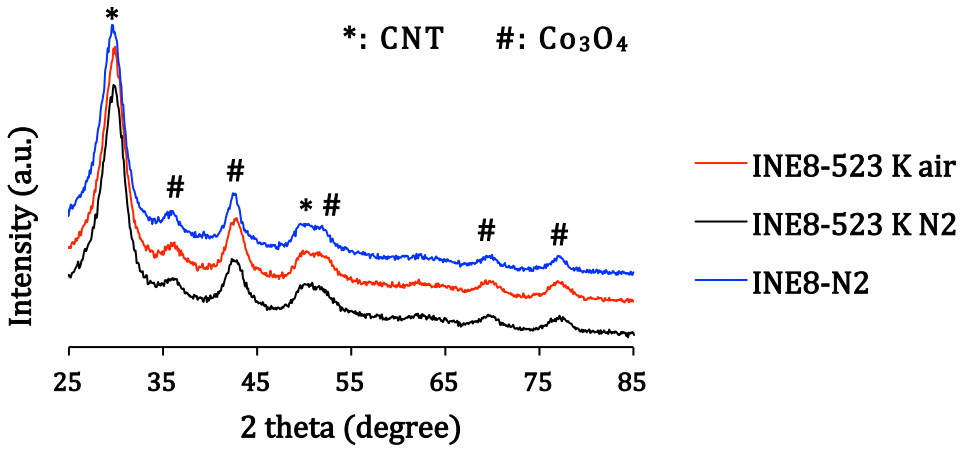

Figure 29. XRD patterns of samples INE8-523 K air, INE8-523 K N_2 and INE8-N_2.

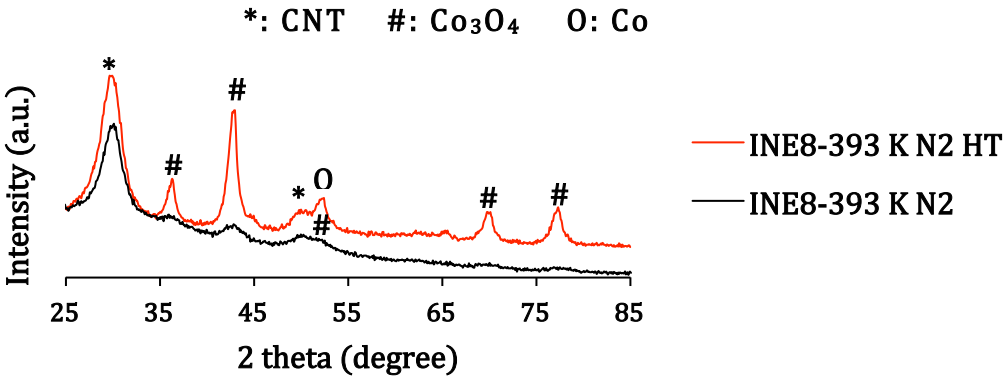

Figure 30. XRD patterns of samples INE8-393 K N_2 and INE8-393 K N_2 HT.

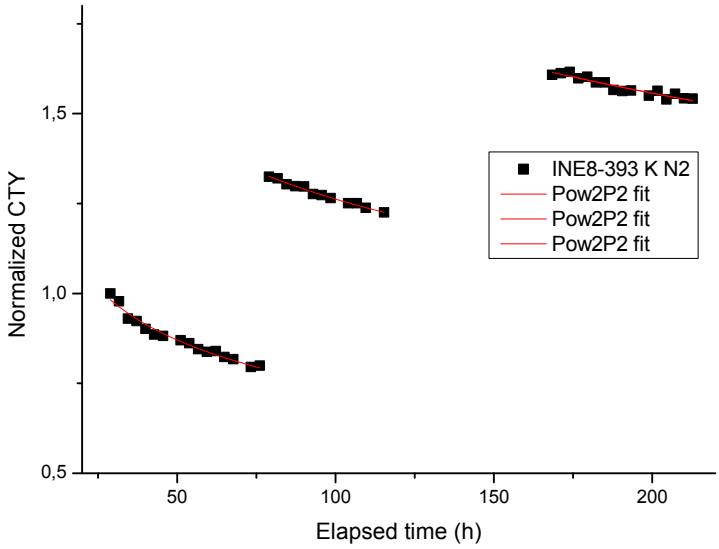

Figure 31. Curve fitting with Origin 8 using a PowP2 function for catalyst INE8-393 K N_2.

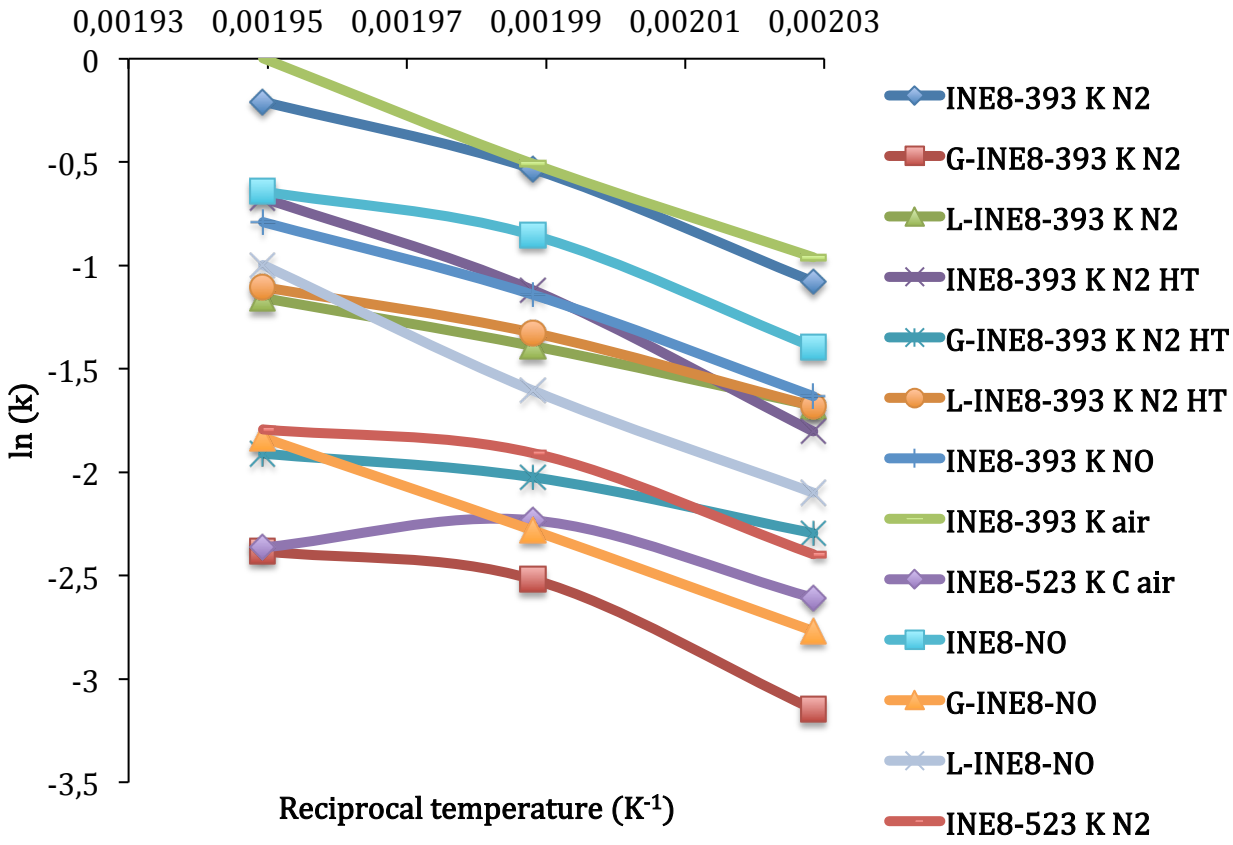

Figure 32. Arrhenius plot for high pressure tested catalysts with k ~ ln (1 – X_{CO}) measured at 493 K, 503 K and 513 K, H_2/CO v/v 2:1 at 20 bar syngas pressure.

Table1. Curve fitting constants obtained with Origin 8 using a PowP2 function.

	493 K			503 K			513 K		
Catalyst	**a**	**b**	**Adjusted R-square**	**a**	**b**	**Adjusted R-square**	**a**	**b**	**Adjusted R-square**
INE8-393 K N_2	2.12±0.09	-0.23±0.01	0.97	3.31±0.11	-0.21±0.01	0.99	4.86±0.47	-0.21±0.02	0.90
INE8-393 K air	2.20±0.14	-0.24±0.02	0.93	4.45±0.67	-0.27±0.03	0.89	18.8±2.35	-0.44±0.03	0.95
INE8-393 K NO	2.12±0.09	-0.23±0.01	0.97	3.55±0.67	-0.23±0.04	0.75	4.88±0.91	-0.21±0.04	0.72
G-INE8-393 K N_2	13.0±3.03	-0.83±0.06	0.92	2.10±0.59	-0.26±0.06	0.65	0.93±0.24	-0.02±0.05	-0.10
L-INE8-393 K N_2	5.74±1.42	-0.60±0.07	0.80	8.87±1.25	-0.56±0.03	0.97	0.44±0.09	0.10±0.04	0.24
INE8-393 K N_2 HT	2.36±0.11	-0.26±0.01	0.96	3.19±0.25	-0.17±0.02	0.91	15.4±2.74	-0.38±0.04	0.89
G-INE8-393 K N_2 HT	4.74±0.48	-0.50±0.03	0.95	15.9±3.35	-0.65±0.05	0.94	8.66±4.20	-0.44±0.09	0.62
L-INE8-393 K N_2 HT	2.72±0.29	-0.34±0.03	0.88	13.9±1.68	-0.57±0.03	0.98	0.87±0.27	0.05±0.06	-0.03
INE8-523 K N_2	3.35±0.30	-0.39±0.02	0.93	4.28±0.80	-0.30±0.04	0.82	85.1±34.9	-0.81±0.08	0.87
INE8-523 K air	5.46±0.59	-0.51±0.03	0.95	26.7±10.6	-0.72±0.09	0.87	40.4±22.1	-0.74±0.10	0.79
INE8-NO	2.18±0.21	-0.24±0.02	0.84	2.28±0.41	-0.13±0.04	0.48	25.0±8.63	-0.53±0.07	0.80
G-INE8-NO	6.71±0.93	-0.63±0.04	0.94	1.07±0.34	-0.08±0.07	0.05	0.18±0.11	0.34±0.11	0.33
L-INE8-NO	4.75±0.55	-0.50±0.03	0.93	1.55±0.38	-0.11±0.05	0.22	0.08±0.02	0.56±0.04	0.94
equation	**y=a*(1+X)^b**								

Acknowledgements

Acknowledgements

Just over a year a go, on the 31st of October 2011 to be precise, I started my Master Thesis project in the Inorganic Chemistry and Catalysis group of the Utrecht University. Before starting this adventure at the Nanoscale, I took quite some time to talk to different people within different University research groups. Since this research within my Master program, Chemistry and Physics, is a project of one year and entails have of the Master's program, I wanted to be confident that the project fitted my interest and goals, but especially a good chemistry between the supervisors and me, was an essential criterion in my decision making. Looking back at this year I can wholeheartedly say that choosing for the Co/CNT FT project under the supervision of Thomas Eschemann and Krijn de Jong was an excellent choice.

Thomas, I would like to thank you for having a great year! Working together with you has been more than a pleasure. Not only have you been a great supervisor in this project, but also nice person to be around with. You're punctuality, openness, profound interest (in science and people) and patience, is something I have learned from and I think many of us still can learn from. Supervising someone next to your own research must be a challenging and time-consuming task. Nevertheless, I always had the feeling that you took the time to help me within this project. The numerous discussions we've had on our research or other business while drinking a coffee is something I will definitely miss. However, I'm confident we will meet again, be it in a personal or professional setting.

Krijn, thank you very much for having me in your group. This year has been an interesting and challenging year. To call myself 'Master of the tubes' would be an exaggeration, however, I do feel that I have learned a significant deal on the different aspects of setting up and conducting a research project, and in particular, in the catalyst preparation and Fischer-Tropsch catalysis. Being able to attend the syngas meetings once in a while was an interesting experience. I can definitely recommend other Master students to do so as well.

Furthermore I would like to thank the technical staff for their support. All the colleagues for taking the time to explain their research and for the 'Mexican Fiesta' of course. Let's hope this becomes an annual event. Marjan Versluis, thank you for the TGA measurements. Anne Mette and Selvedin Telalović thank you for the H_2 chemisorption and N_2 physisorption

measurements. Hans Meeldijk, thank you for all the TEM sessions. We've spent quite some time together this year. Never in my life, have I been in a dark room, together with someone else, during the day, hours at a time, in such a frequent basis. This has however definitely been beneficial for this project, since the TEM-images have been a great contribution to this research.

I wish you all the best of luck and pleasure within in your research!

René Manchester
Utrecht, November 2012